Norwegian University
of Life Sciences

Master's Thesis 2019 30 ECTS
Faculty of Science and Technology

Evaluation of water flow behavior and water velocity distribution in aquaculture tanks using Computational Fluid Dynamics (CFD)

Andrés Castro Herrera
Master of Science in Aquaculture

Table of Contents

1 Abstract

The hydrodynamic design of aquaculture tanks is a very complex task where many biological and technological factors should be considered simultaneously. The use of Computational Fluid Dynamics (CFD) is a rapidly expanding technological trend which provides an effective way to evaluate and optimize the hydrodynamic design of aquaculture tanks.

Nevertheless, the study of flow dynamics in aquaculture tanks has until now relied on sophisticated computational tools and time-consuming complex methodologies. This work investigates the use of Flow Simulation as a fully integrated, user-friendly and more economical software alternative for this purpose. By also using simplified simulation settings, the aim is to reduce the human and computational efforts while still achieving reliable flow predictions.

The selected settings and the accuracy of the simulations were validated by replicating the simulation work from two scientific papers; in the papers the authors have validated their CFD simulations against experimental measurements.

A series of experiments were also performed at the university's aquaculture laboratory in order to further validate the simulation set-up and evaluate the accuracy of the simplified approach. Water velocities were measured at different locations in a fish-rearing tank and compared against the predictions from the CFD simulations. For this experimental validation two different positions of the water inlet pipe were investigated.

Additionally to the main settings, other simulation parameters were also evaluated; such as turbulence properties, meshing strategy, wall roughness and criteria for stopping the calculation process. This was done as variation cases for some of the simulations and provided means for fine-tuning of the simulation set-up.

It was found that the selected simulation methodology generated satisfactory flow patterns comparable to those of the literature cases studied. The accuracy of the water velocities estimated in the CFD simulations was found to be not as precise as those from the literature validation, but still within the acceptable accuracy thresholds proposed by different scientist in the field.

For one of the validations against the literature, an overall difference in water velocities of around 16% was found between the CFD prognosis and the presented laboratory measurements. The overall relative error of the estimations reported in the paper was of about 7%.

For the other validation against literature, the CFD-estimated water velocities were approximately at two standard deviations of the measured velocities in experiments. The predicted water velocities reported in the paper were close to one standard deviation of the measurements.

It is considered that the simplified methodology on this work should represent a much lesser burden for the creation of representative simulations than the ones presented in literature.

The simplified simulation set-up, while partly sacrificing on accuracy, offers a valuable alternative in terms of the high amount of useful information obtained from the simulations and the reduced computational resources required for their elaboration.

2 Introduction

The aquaculture industry, is one of the fastest-growing industries in the world (Lekang, 2007 p.xi), where the global production of farmed aquatic organisms has doubled every decade in the last 60 years, sometimes even in the lapse of few years (FAO, 2019). Aquaculture allows, particularly on development countries, to supplement their food needs and to acquire resources due to exports. It has been proven that the aquaculture industry has the potential to create more job opportunities and promotes the creation of other collateral industries, improving the socioeconomic aspects of a region (Holtschmit M, 2000). Aquaculture thus can contribute to achieve some important goals from the Sustainable Development Goals set by the United Nations, specially: *No Poverty* and *Zero Hunger*; and also in an indirect way to others such as *Clean Water and Sanitation; Industry, Innovation and Infrastructure* and *Sustainable Cities*.

Aquatic organisms have the ability of converting almost entirely all their feed uptake into body weight and exhibit fast growing rates when raised in an optimal environment. This makes aquaculture a highly energy-efficient way of producing quality protein and healthy fats when compared to other ways of animal production (Holtschmit M, 2000). Therefore allowing and facilitating modern aquaculture to take a bigger role in producing food for the world population could even contribute in tackling Climate Change.

A raising tank is one of the basic infrastructure components of modern and intensive aquaculture facilities, such as recirculating aquaculture systems (RAS). Compared to ponds, the water in tanks is renewed at higher rates, something that helps ensure adequate oxygen levels and effective removal of fecal particles and uneaten feed. This provides improved water quality and a better farming environment for the organisms, allowing also for higher stocking densities (Lekang, 2007).

It is of particular interest for farmers to utilize optimally the available water volume in the tank by stocking as much fish as possible and maximize the economical return of the operation. Nevertheless, the design and optimization of an aquaculture tank is not a straight forward process, on the opposite, many biological and hydraulic variables must be considered simultaneously in order to fulfill a satisfactory design.

It has been observed that the fish distribution inside the tank depends, among other factors, on the water velocities at particular locations within the tanks (Duarte et al., 2011). This may be adjudicated to the fact that adequate water velocities and flow patterns promote the good mixing of water and a better distribution of oxygen inside the tank, as well as a reduction in the local concentration of biological waste, such as ammonia (Holtschmit M, 2000; Lekang, 2007). Fish have also displayed increased growth and resistance to diseases when exposed to a particular training regime by controlling the water velocities in the rearing unit (Castro et al., 2011).

A flow pattern that promotes homogeneous water quality and water velocities optimal for the wellbeing of the farmed species is therefore the ultimate goal in hydrodynamic design of aquaculture tanks.

In addition, other factors affecting the system boundaries of the tank, such as water velocity inside outlet pipes that avoid sedimentation or fragmentation of particles (Lekang, 2007) or inlet pipe and nozzle sizing which do not represent an unnecessary burden for the available pressure in the system, make this a very complex task. It is therefore that the use of advanced tools such as Computational Fluid Dynamics to aid the design process is of increasing interest in the industry.

The optimizations of water flow patterns and water velocity profiles have been studied and optimized by the use of diverse methods, from laboratory studies to mathematical approaches (Oca & Masalo, 2013). Nevertheless, until recent times, the design and optimization of aquaculture tanks have relied heavily on experience, and the use of modern tools such as CFD to aid this process has been very limited (Gorle et al., 2019).

The few scientific studies found where CFD simulation tools have been used to optimize tank, inlet and/or outlet designs, are performed and presented in a very complex way; relying on advanced mathematical and simulation tools which are probably out of the economical reach and beyond comprehension for many actors in the aquaculture industry.

This thesis work tries to provide a more practical approach to the CFD simulations, with methodologies which are of less complexity and computational tools that could be more accessible to the industry than the ones presented in the work of academics.

This work looks at a very small but basic part of the design of intensive aquaculture production units which is the tank design and its hydrodynamic behavior in terms of water velocity distribution and flow patterns. The water behavior at the inlet and outlet pipes, while observed during the evaluation, has not been the main focus of this work.

The software add-in Flow Simulation in SOLIDWORKS was used to perform the flow analyses. While the software has some limitations, as further described in this report, the possibility of having an integrated 3D modelling, meshing, equation solving and results visualization capabilities in a single software package results quite convenient from the user's point of view. Compared to the methodologies commonly practiced in the field (An et al., 2018; Gorle et al., 2019; Klebert et al., 2018; Liu et al., 2016) where the 3D modelling and flow simulations happen separately, as well as additional steps in pre- or post-processing of the data are required, the approach taken in this work is of inevitable interest for the further spread of the use of CFD techniques in optimization of farm designs.

A typical method for validating the accuracy of flow pattern predictions, either coming from CFD simulations or from a mathematical approach, is to take a representative number of velocity measurements in the actual (real-life, real-size) water containment unit that has been under study (An et al., 2018; Gorle et al., 2018a; Gorle et al., 2019; Klebert et al., 2018; Liu et al., 2016; Oca & Masalo, 2013). Although some attempts have been done with scale-models to verify CFD simulations, this significantly introduces additional complexity on the elaboration of the validation experiments where all the hydrodynamic factors involved cannot be fully considered or directly extrapolated (Rasmussen & McLean, 2004).

The initial intended approach to this work was to evaluate the accuracy of the flow simulations only against literature sources due to the lack of equipment available for performing water velocity profiling at the university. Nevertheless, an opportunity came later to make use of a water velocity-meter prototype developed in collaboration with the university and set up an experimental study in order to provide additional validation tools for the simulations.

Previous to the start of the thesis work, there was no acquired experience in the use of the flow simulation software but only limited experience with other simulation tools. Nevertheless it is hoped that this could also provide insights on how intuitive the software tool may be for the unexperienced user.

Simultaneously to the thesis work, a course in the use of the simulation software was taken at the university, providing gradually useful information for the creation of representative simulations. Some of the course topics had to be read much in advance to the course progress in order to promptly acquire the necessary knowledge to build proper simulations for the thesis.

3 Methods and materials

The 3D modelling as well as the flow simulations were performed in a DELL computer running Windows 10 Enterprise supplied with an 8-core Intel® Core ™ i7-4790 3,6 GHz processor and 32,0 GB of RAM.

3.1 General 3D modelling

The 3D models where prepared using SOLIDWORKS software. Detail was put from the very beginning into building the necessary reference geometries, such as working planes, reference points and axis, sketches, part and assembly configurations, etc., in order to facilitate later the creation of the CFD simulations. The models were created with sufficiently adaptability to cope with the possibility of variations in geometry, location of measuring points for the different variables, inclusion of flow conditions, mesh creation and results visualization expected in further stages of the investigation.

The 3D model was made in a way such that the global coordinate system coincided naturally with the operational conditions of the tank. This meant the positive y-axis pointing upwards, positive x-axis pointing towards the right side of the tank (when seen from the front), and the positive z-axis pointing towards the front of the tank. The origin was situated at the center of the tank and at the inner surface of the outlet pot's bottom.

2D drawings were also created in order to assist the measurement and sampling activities and to provide an organized and clean way of documenting and presenting the findings.

3.2 General CFD simulation settings

In order to develop a CFD model which could represent in a reliable way the flow conditions in an aquaculture tank, the first step taken was to create a simple simulation model where the different flow condition parameters where adjusted until a satisfactory flow pattern was achieved. A total of 19 simulation cases were developed for this purpose and the resultant flow patterns were visually evaluated against the expected flow behavior in real life.

Additional variations cases were also performed for fine-tuning of the simulations set-up. These explore other parameters besides the main flow condition parameters of the first 19 simulation cases. These are described in each of the individual chapters on the validation against literature and experimental data, see chapters 3.3 and 3.4.2.

3.2.1 Analysis type

An Internal analysis type was selected for all of the cases of this work, meaning the computational domain is restricted to a fluid volume that is fully contained in a closed compartment. Modelling aids such as lids or covers were therefore applied at the open ends of the tank and outlet pipe in order to be achieve a closed system.

While an external type of analysis was considered as a possible alternative to simulate the effects of the surrounding atmosphere on the tank and outlet system simultaneously, this alternative was not further investigated.

3.2.2 Gravity

Gravity was considered in all simulations in the -y direction with a magnitude of 9.81 m/s^2. Care was taken in the elaboration of 3D models in order to account for the direction of gravity to be correct in relation to the resultant axis of each modelled tank and its operation position.

3.2.3 Evaluation of main flow condition settings

This sub-chapter explain the simulation settings selected and the process in detail of determining the appropriate flow condition settings through 19 simulation cases created for this purpose.

For these 19 simulation cases made to evaluate the main flow condition settings, a simple tank geometry similar to the one presented by Lekang (2007) was used.

For all the evaluated cases, unless noted otherwise, a water flow of 18 liters per minute (l/min), equivalent to 0,0003 cubic meters per second (m^3/s) was used as the Inlet Volume Flow. The flow condition was applied simultaneously to all of the seven equally distanced Ø8 mm nozzle holes of the inlet pipe which were distributed along the whole water column.

Case 1

The outlet pipe in this case extended from the bottom of the tank for approximately 1 m after a 90 degrees elbow. This in order to provide sufficient pipe length for the flow to stabilize after exiting the bottom of the tank. The diameter of the outlet pipe was maintained at 250 mm for the whole length of the pipe.

Two additional conditions were applied: an Environmental Pressure (1 atm) at the water surface and one Static Pressure of 950 mm of water representing the water column above the center of the outlet pipe.

With this flow condition settings the simulation displayed two warnings: one stating that a vortex crossed the pressure opening (water surface) and another warning regarding negative pressure (outlet opening). The resultant non-satisfactory flow pattern is shown in Figure 1.

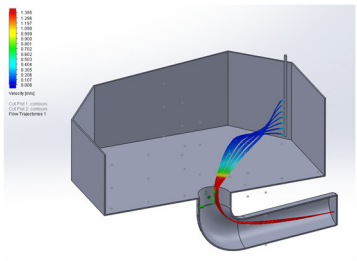

Figure 1 Resultant flow pattern – Evaluation of main flow condition settings, Case 1

Case 2

The same outlet pipe configuration with as in Case 1 was used also this time. The flow condition settings were the same as in Case 1 with the exception of that The Static Pressure magnitude was modified to 1 atm + 950 mm of water to account for the ever-present environmental pressure surrounding the tank.

Only the warning of a vortex crossing the pressure (at water surface) opening was reported in this case. The resultant non satisfactory flow pattern is shown in Figure 2.

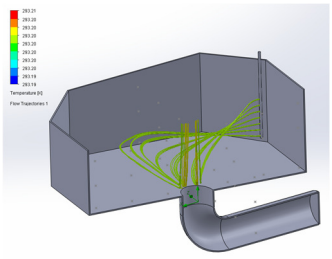

Figure 2 Resultant flow pattern – Evaluation of main flow condition settings, Case 2

Case 3

This simulation case had the same outlet pipe configuration as the previous two cases. The environmental pressure at the water surface was maintained while the Static Pressure at the outlet was replaced by an Outlet Volume Flow with an equal magnitude of that of the Inlet Volume Flow.

The recurrent warning of vortex crossing pressure opening was also experienced this time. The resultant flow was also considered not satisfactory as seemly the effect of gravity was not enough to keep the water contained in the tank and an ascending tornado-like flow pattern was displayed, see Figure 3.

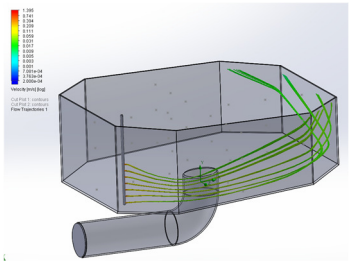

Figure 3 Resultant flow pattern – Evaluation of main flow condition settings, Case 3

Case 4

For this and the following cases, unless otherwise specified, a different outlet pipe configuration was used. This consisted of a second 90 degree bend and pipe extension in order to make the end of the outlet pipe reach the same level of the tank water level, thus trying to simulate an external water leveling arrangement in the outlet pipe which is typical of aquaculture tanks.

The Environmental Pressure condition at the tank water surface level was maintained, while the Static Pressure on the outlet pipe opening (now at same level as tank water level) was substituted with an Environmental Pressure of 1 atm.

The warning of a vortex crossing the pressure opening was also display for this case. It raised at this time the hypothesis that this warning, as an indication of a vortex at the water surface or possible waves, resulted in computational difficulties for the software.

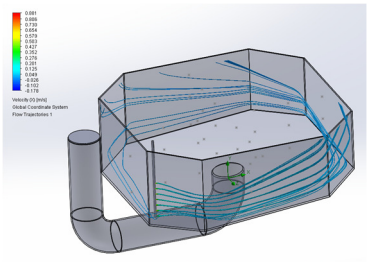

Figure 4 Resultant flow pattern – Evaluation of main flow condition settings, Case 4

Case 5

In order to test the previously stated hypothesis of the meaning of a vortex crossing the pressure opening, the Environmental Pressure condition at the water surface level was removed for this case.

While keeping the other settings unaffected, the warning was not displayed and the flow pattern seemed to represent reality for the first time, see Figure 5.

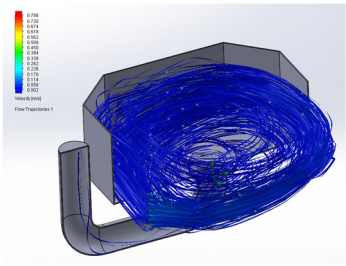

Figure 5 Resultant flow pattern – Evaluation of main flow condition settings, Case 5

Case 6

For this case the Environmental Pressure at the water surface level was included again and the Environmental Pressure at the outlet pipe replaced by an Outlet Volume Flow of equal magnitude as the Inlet Volume Flow.

As expected, the warning regarding vortex on the pressure opening was shown again and the flow did not represent once more the expected behavior expected in reality, see Figure 6.

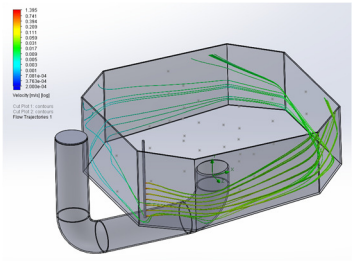

Figure 6 Resultant flow pattern – Evaluation of main flow condition settings, Case 6

Additional information was displayed in the warning indicating the Inlet/Outlet flow ratio was =1. While this was later understood as a local flow variation at the water surface level, initially there were doubts about if this could represent a situation where a difference in inlet flow vs. outlet flow was causing the warning.

Case 7

This simulation case was created in order to evaluate if the Inlet Volume Flow represented a flow of 0,0003m^3/s equally distributed among all the inlet nozzles or the flow was being multiplied by the number of nozzles. This in order to evaluate the effect on the displayed inlet vs. outlet ratio.

The Inlet Volume Flow was then applied to only one of the inlet nozzles, while the Environmental Pressure at the water surface and Outlet Volume Flow at the outlet pipe opening were maintained.

The warning about vortex at the pressure opening was displayed as expected, but it was useful to confirm that the flow pattern was similar to that of Case 6 and the Inlet/Outlet flow ratio was also equal to 1. The resultant non-satisfactory flow pattern is shown in Figure 7.

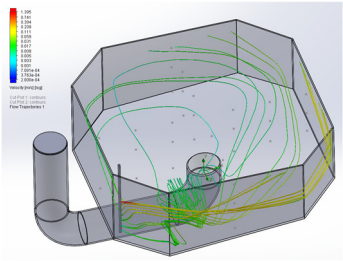

Figure 7 Resultant flow pattern – Evaluation of main flow condition settings, Case 7

Case 8 and case 9

In order to further test the hypothesis of the vortex/waves at the water surface and the effect in the distribution of flow in the nozzles resulting from a single Inlet Volume Flow, Case 8 and Case 9 were created. In case 8 the total flow was divided by the number of nozzles (seven) resulting in a flow per nozzle of 0,00004 m3/s applied individually to each of the inlet nozzles.

In case 9, an inlet flows of 0,0003 m^3/s were applied to each individual inlet nozzle. The resulting flow patterns were similar but contrasted in the intensity of the flow visualized by the water velocity, as seen in Figure 8 and Figure 9. This confirming that the way of interpreting and applying the Inlet Volume Flow was correct from the very start.

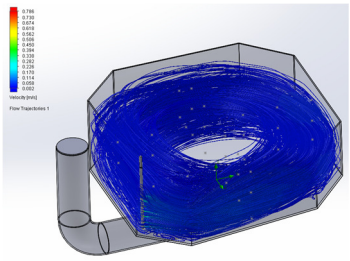

Figure 8 Resultant flow pattern – Evaluation of main flow condition settings, Case 8

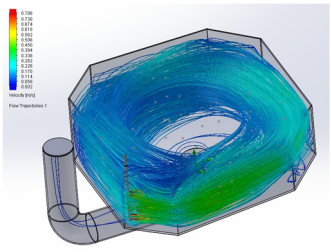

Figure 9 Resultant flow pattern – Evaluation of main flow condition settings, Case 9

Case 10 and Case 11

These cases was created to evaluate if a lower outlet pipe would affect the water level inside the tank. The outlet pipe was therefore shortened after the last bend to approximately the half of the tank wall height.

An Environmental Pressure was applied to the outlet pipe opening and the Inlet Volume Flow was maintained at 0,0003 m^3/s. For case 10 no Environmental Pressure was applied at the water surface, while for Case 11 this condition was applied. The resultant flow patterns are presented in

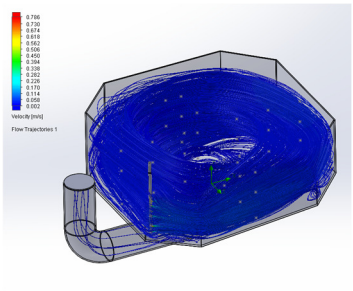

Figure 10 Resultant flow pattern – Evaluation of main flow condition settings, Case 10

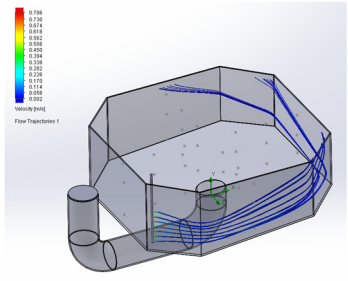

Figure 11 Resultant flow pattern – Evaluation of main flow condition settings, Case 11

No change in the water level inside the tank was experienced, thus raising the hypothesis of a hydraulic or air lock happening inside the tank volume; something that prevented the water from adjusting its level. Please note that this hypothesis and the one presented in case 4, are hypotheses on how the software may understand the flow conditions applied to the model and not about the understanding of the author on hydraulic phenomena.

For case 11 the warning of vortex crossing the pressure opening was displayed, with an Inlet/Outlet flow ratio of 0,922.

Case 12

Case 12 introduces a thin Ø1 mm inside-diameter pipe at the center of the tank lid in order to "vent" the volume inside the tank. Other settings were identical to Case 11 with the difference that the environmental pressure at the water surface is now applied at the end of this small venting pipe. The resultant flow pattern is shown in

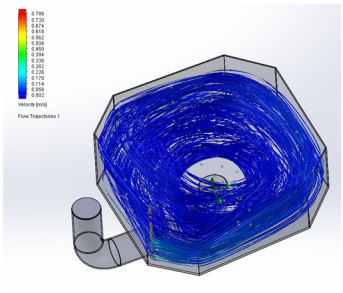

Figure 12 Resultant flow pattern – Evaluation of main flow condition settings, Case 12

While the resulting flow pattern may actually seem satisfactory, the main purpose of adjusting the water level to the outlet pipe level was not achieved, therefore triggering the more complex investigations of Case 13, Case 14 and Case 15.

Case 13 – Free Surface

The use of the Free-Surface option was investigated for this simulation case in an attempt to satisfactory represent the interaction between air and water that occurs at the water surfaces. For this purpose two Fluid Volumes were created; one representing the water and one representing the air in the tank. While no information was found regarding how to model a basin open to atmosphere, some other examples of water-air interface and the use of Free-Surface were found online in the form of instructional videos and that knowledge extrapolated for use in these three simulation cases (*HOW TO*, 2018; *SOLIDWORKS Flow*, 2017).

Environmental Pressure was applied at the end of the outlet pipe. The vented lid from Case 12 was also used in the model but no pressure-opening condition was applied to it.

The Free Surface option requires enabling of the time-dependent analysis type in the simulation. The simulation was left to run until one of the criteria to stop the simulation was satisfied; either all *goals* converged (achieved a steady value) or a maximum number of travels of the fluid across the computational domain was reached. A *goal* can be specified to evaluate a parameter at a certain location, in this case the water velocity. The maximum number of travels was 4, as automatically specified by the software.

When the maximum number of travels was achieved, only 13.98 seconds of physical (real) time had been solved. It was noted in the resultant flow pattern (Figure 13) that the water level was still at the original water level and no steady circular flow had yet been achieved.

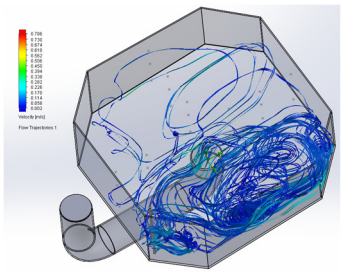

Figure 13 Resultant flow pattern – Evaluation of main flow condition settings, Case 13

Case 14 – Free Surface

It was assumed at this stage that by not having a pressure opening at the top of the vented lid and no additional air could enter to replace the water exiting the system, the water level was therefore unchanged.

A new vented lid with a larger opening at the top was included and Environmental Pressure applied to both, the venting opening and top air surface. An Environmental Pressure was also applied at the outlet opening.

A Physical Time condition to stop the simulation was set to 10 seconds, with calculation time steps of 1s. The calculation time for this case was of little over one and a half hour.

For these Free Surface cases (13 to 15), the initial fluid condition was specified to be water, as well as for the Inlet Volume Flow concentration.

The warning regarding vortex at the pressure opening was also experienced for this case. The resultant flow pattern is shown in Figure 14.

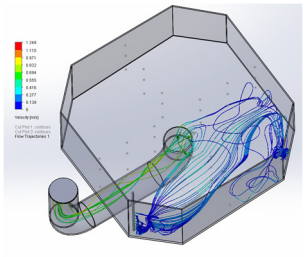

Figure 14 Resultant flow pattern – Evaluation of main flow condition settings, Case 14

Case 15 – Free Surface

The approach on this case was to remove completely the outlet pipe extension, leaving only a short vertical pipe of Ø250 mm at the bottom of the tank. An Outlet Volume Flow was applied at the pipe's end, with a volumetric flow equal to the inlet flow.

The vented lid at the tank's top was replaced with an unvented lid and an Environmental Pressure condition (1 atm) was applied at the air's top surface.

A Physical Time setting to stop the simulation was set to 2 s, with calculation time steps of 1 s. The calculation time required for this simulation was of approximately 30 minutes.

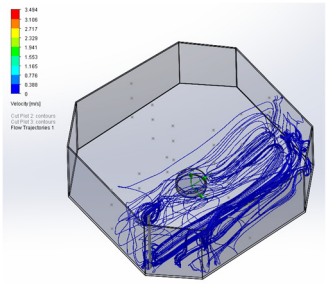

Figure 15 Resultant flow pattern – Evaluation of main flow condition settings, Case 15

Case 16

Based on the results from cases 13 to 15, the time-dependent analysis was considered not suitable due to the long time to solve the simulations, see further explanation in section 3.2.4.

Case 16 was done without the Free Surface option enabled, therefore returning to a steady state type of analysis. A frictionless condition was then applied at the tank water level. An Environmental Pressure condition was still applied at the outlet pipe end. The outlet pipe was set back to the configuration where it reached to the same level of the tank's water level.

The criteria to stop the simulation was set to One Satisfied, either achieving a specific number of travels (four) *or* convergence of the goals. 36 Velocity Goals were included at similar positions to those of the measuring points for velocity profiling on an idealized tank presented by Lekang (2007). The calculation process ended by reaching first the maximum number of travels. The flow behavior, as seen on Figure 16, was satisfactory.

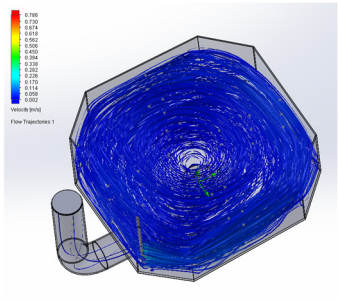

Figure 16 Resultant flow pattern – Evaluation of main flow condition settings, Case 16

Case 17

This case was created in order to investigate the effect on the results depending on the criterion to stop the calculation. The same flow settings as in Case 16 were used, but the criteria to stop the simulation was set to All Satisfied (goals convergence *and* maximum number of travels).

While it was expected that the goal convergence reached 100%, it was noted that the calculation stopped at the same number of travels (and iterations) as Case 16 and the progress of convergence was not complete for all of the goals. The resultant flow pattern is shown in Figure 17.

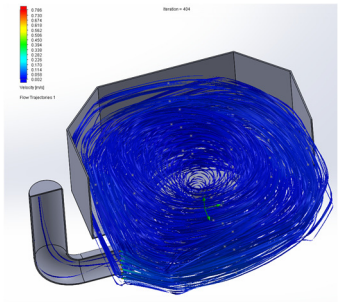

Figure 17 Resultant flow pattern – Evaluation of main flow condition settings, Case 17

Case 18

Case 18 was used to simultaneously investigate the use of goal convergence as the only criteria to stop the calculation combined with a simplified design of outlet pipe. This outlet pipe design was the short Ø250 mm pipe at the bottom of the tank's center used previously on Case 15.

An Static Pressure of 1 atm + 620 mm H_2O was applied at the outlet pipe end, aiming to simulate the hydraulic pressure conditions at this point but using a simplified model which may result in reduced computational efforts.

The calculation stopped at 337 iterations (vs. 404 of Cases 16 and 17), and the average of the velocities in the tank was reduced by 10,7% and 6,6% against Cases 16 and 17, respectively.

The resultant flow pattern is shown in Figure 18.

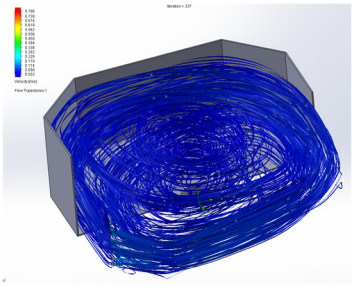

Figure 18 Resultant flow pattern – Evaluation of main flow condition settings, Case 18

Case 19

Case 19 was created to evaluate the impact of the frictionless (slip) condition at the water surface against a no-slip condition. Case 5 accounted for this no-slip condition but at the time no Velocity Goals were included to aid the convergence of the solution, it was therefore necessary to create a replica of that case with the Velocity Goals included, namely Case 19, in order to compare it against Cases 16, 17 and 18.

The average of the water velocities when using a no-slip condition was reduced in 23,6%, 20,2% and 14,5% when compared against the cases with a slip condition at the water surface; Cases 16, 17 and 18 respectively.

There was no difference in the average velocities between Case 5 and Case 19.

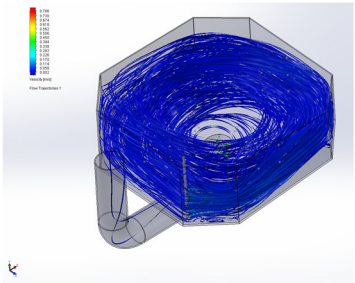

Figure 19 Resultant flow pattern – Evaluation of main flow condition settings, Case 19

3.2.3.1 Selected main flow condition settings

Based on the evaluations in the previous 19 simulation cases, it was decided to incorporate in the 3D models a complete outlet pipe system and not use any modelling simplifications for the simulations. The flow condition settings chosen to be further use in the cases for validation against literature and experimental data were the volumetric flow at the inlet nozzles, an environmental pressure condition at the outlet end and a shear-free condition at the water surface level.

3.2.4 Steady flow vs. transitional (time-dependent) flow

The time-dependent or transitional analysis was considered not to be adequate for evaluating the general characteristics of the flow (stable patterns and water velocities) in a timely manner and with the computational resources available. A steady-state (steady flow) analysis was therefore chosen. See further explanation in the Discussion.

3.2.5 Criterion to stop the calculation

The criterion to stop the calculation was decided to be set to One Satisfied, representing the convergence of all the representative Velocity Goals for a particular simulation.

3.2.6 Turbulence model

Flow Simulation was used to solve the time-dependent form of the Navier-Stokes equations, which are formulations of mass, momentum and energy conservation for fluid flows. The Favre-averaged Navier-Stokes equations were used to predict the turbulent flow and consider the time-averaged effects of turbulence. Furthermore, the k-epsilon (k-ε) turbulence model was used to close the Navier-Stokes equations, accounting for the appearance of Reynold stresses in the formulation (SOLIDWORKS-Corp., 2018b).

Flow Simulation has in-built a boundary model which uses the Van Driest's profile for the Modified Wall Functions approach; which is used to describe the laminar/turbulent flow and the transition between these in the areas near the wall, or solid surfaces. (SOLIDWORKS-Corp., 2018b).

A Two Scale Wall Function (2SWF) is used by the software to couple the boundary layer flow with the main (turbulent) flow, where according to the mesh refinement level and characteristic number of cells across the boundary layer thickness, two approaches could be taken: The *thick boundary layer* or the *thin boundary layer*. For cases falling in between this boundary layer thickness criteria a combination of the two approaches is used (SOLIDWORKS-Corp., 2018a; SOLIDWORKS-Corp., 2018b).

3.2.7 Roughness

Surface roughness was set to 0µm for all of the main flow settings investigation cases as well as for the simulation validation cases against literature and laboratory measurements. Nonetheless, the effect of roughness was investigated in an individual case as described in section 3.4.2.1.4.

3.2.8 Convergence goals

As mentioned earlier, Velocity Goals were utilized to guide the convergence of the solution. The position and specifics about these goals, such as sub-type, direction and position within the tank, are further described in each of chapters on validation against literature and laboratory measurements.

Additional goals were created to attain information regarding the overall behavior of the flow, such as additional velocity goals (at different positions within the tank, at the outlet pipe and inlet pipe nozzles), turbulence intensity and turbulence length. These additional goals were not selected to converge in the calculation, but rather used through the process of creating the simulations only as verification points for assumptions and manual calculations.

3.3 Validation of CFD simulations vs. literature

3.3.1 Validation against An et al. (2018)

The work done by An et al. (2018) was partially replicated in order to validate the way the simulations were built and the accuracy of the results between methodologies. One of the multiple tank configurations presented in their work was selected to be simulated under the flow conditions experienced at that catfish farming facility.

3.3.1.1 3D model & dimensions

A tank with a concentric outlet and a single vertical inlet pipe was chosen to be modelled with the information that was available, see Figure 20. While not all the details of the geometry were described, it was possible to build a very similar model by assuming some of the information missing.

The tank diameter was of Ø7 m with a water depth at the wall of 1,2 m, resulting in a diameter to height ratio of D/H=5,83. The tank bottom was considered horizontal. At the center of the tank's bottom, a conical part of Ø1,5 m in diameter and 250 mm in height connected to a Ø200 mm outlet pipe extending from the bottom of the tank downwards. This outlet pipe was then connected to a 90 degrees elbow, redirecting the flow radially towards the wall of the tank. After a second 90 degrees bend the outlet pipe extended vertically until reaching the top edge of the tank's wall. The pipe bending radius at the outlet system was assumed to be equal to the diameter of the pipe.

An inlet pipe with 6 equally spaced nozzles of Ø40 mm was positioned vertically adjacent to the wall separated by a distance to the inlet pipe centerline of 400 mm. The diameter of the inlet pipe was Ø 100 mm. The spacing between inlet nozzles was of 170 mm, while the distance from the bottom inlet nozzle to the bottom edge of the inlet pipe was assumed to be half of this separation. All the dimensions presented in their work were assumed to be internal dimensions.

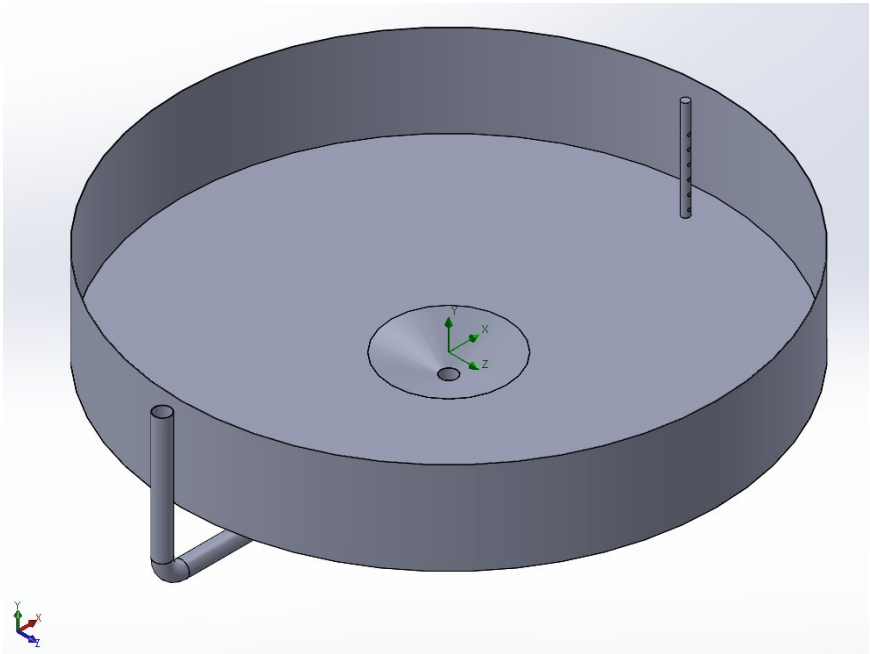

Figure 20 Resultant 3D model of tank used for the validation against An et al. (2018)

3.3.1.2 Meshing

A structured mesh of hexahedral cells was used. The global mesh was refined until a visually satisfactory basic cell size (in comparison to the overall size of the fluid domain) was achieved. The grid was further refined at the boundary layer; the area adjacent to the tank's wall, tank's bottom and around the inlet pipe.

A total of 486,806 fluid cells from which 231,387 were in contact with solids gives an indication on the overall level of mesh refinement and also of the refinement at the boundary layer. The resulting mesh is presented in Figure 21, Figure 22, Figure 23 and Figure 24.

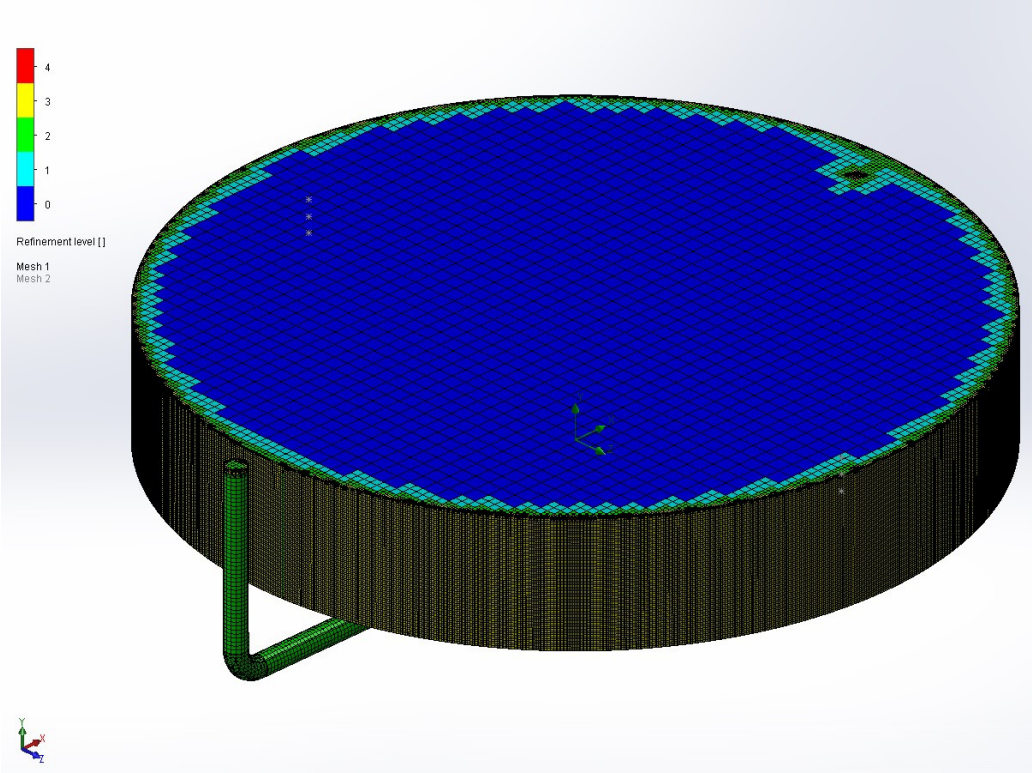

Figure 21 Mesh overview – validation against An et al. (2018)

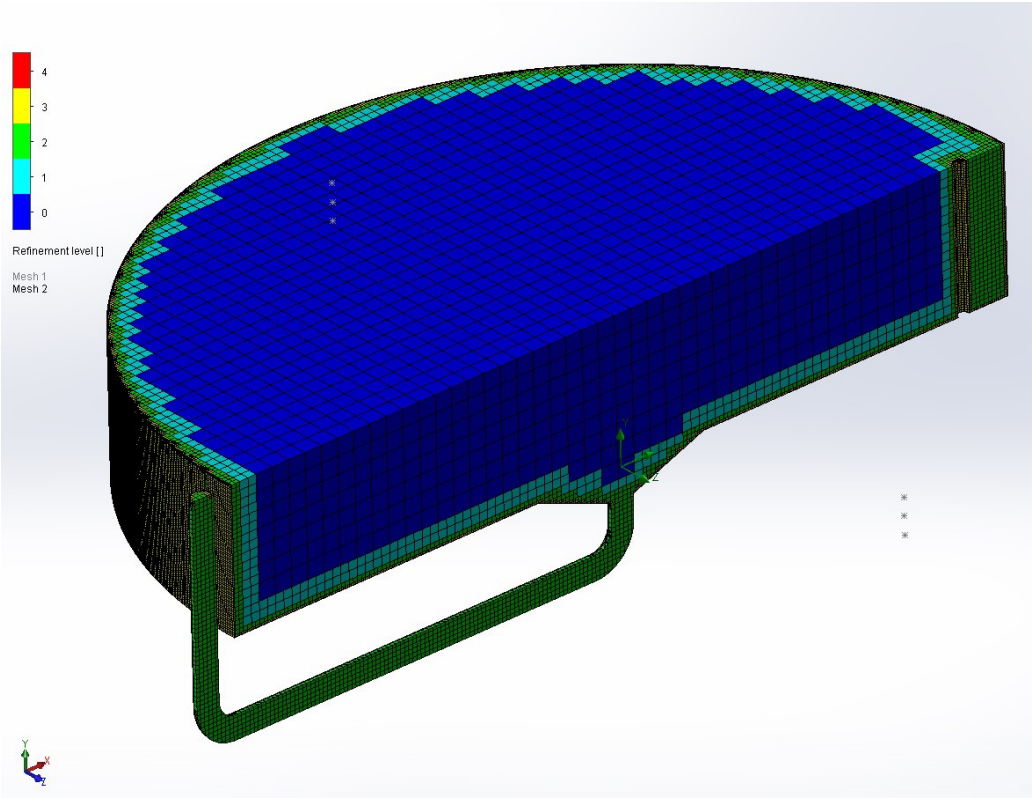

Figure 22 Mesh cut view – validation against An et al. (2018)

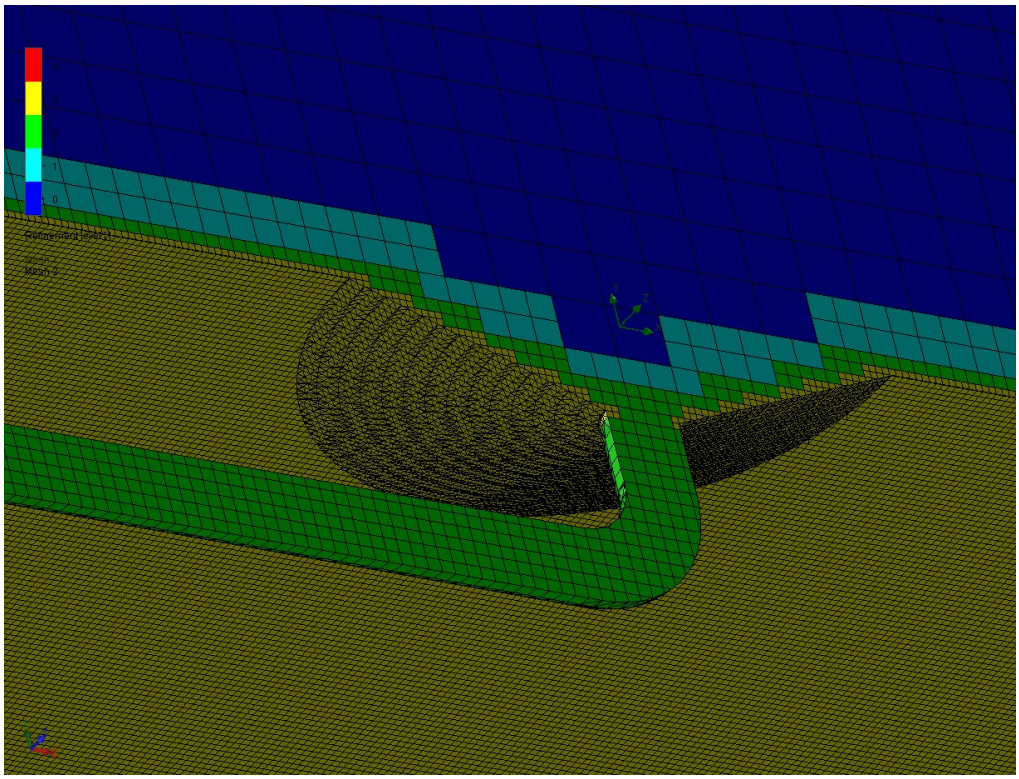

Figure 23 Mesh detail at tank bottom – validation against An et al. (2018)

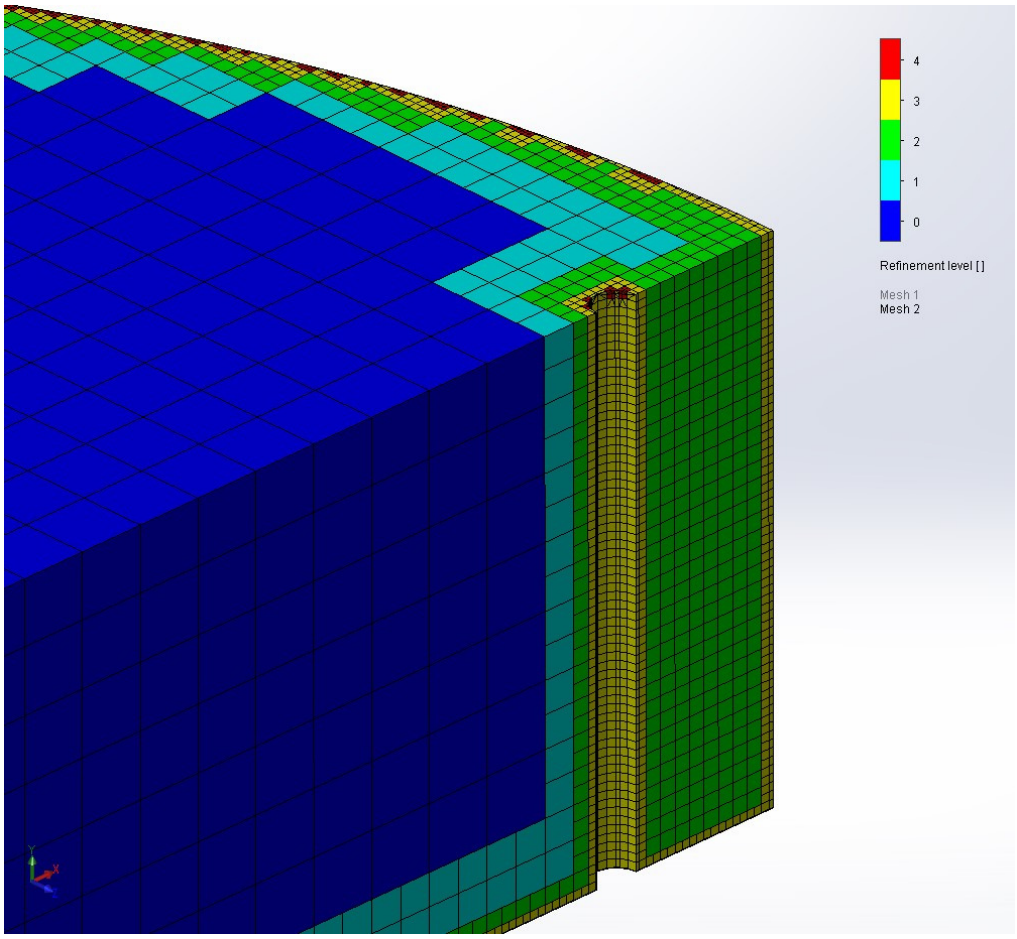

Figure 24 Mesh detail at inlet pipe – validation against An et al. (2018)

3.3.1.3 Water flow and turbulence parameters

An inlet water flow of 0,010103386 m^3/s was calculated from the given nozzle water speed of 1,34 m/s and size of the nozzles holes. The initial turbulence parameter setting were set to a turbulence intensity of 5% and a turbulence length of 0,0035 m. The same turbulence parameters were applied to the Inlet Volume Flow.

These values were selected as a starting point to investigate the effects of using values different from those recommended by Flow Simulation. This was based on information presented at the flow simulation course and confirmed by information available online from multiple contributors (*Turbulence Intensity*, 2018; *Turbulence lenght scale*, 2012).

Later in the process of this work, the turbulence intensity and turbulence length were included as reference goals in the simulations in order to determine the values characteristic to the particular tank geometry and flow conditions. This is further discussed in the results and discussion sections.

3.3.1.4 Position and type of goals

A total of 6 Goal Points were included matching the sampling positions presented by An et al. (2018). These were placed on two groups, three of them on each side adjacent to the tank wall. They were located on a radial plane perpendicular to the plane formed by the inlet pipe and outlet column. They were positioned at 0,2 m; 0,35 m and 0,5 m of water depth and at a radial distance from the center of the tank of 3 m.

The Goal Points were created as Velocity Point Goals in the x and z direction, this in order to be able to calculate later (in a spreadsheet) the resultant horizontal velocity at each location; allowing means for direct comparison against the results presented by An et al. (2018).

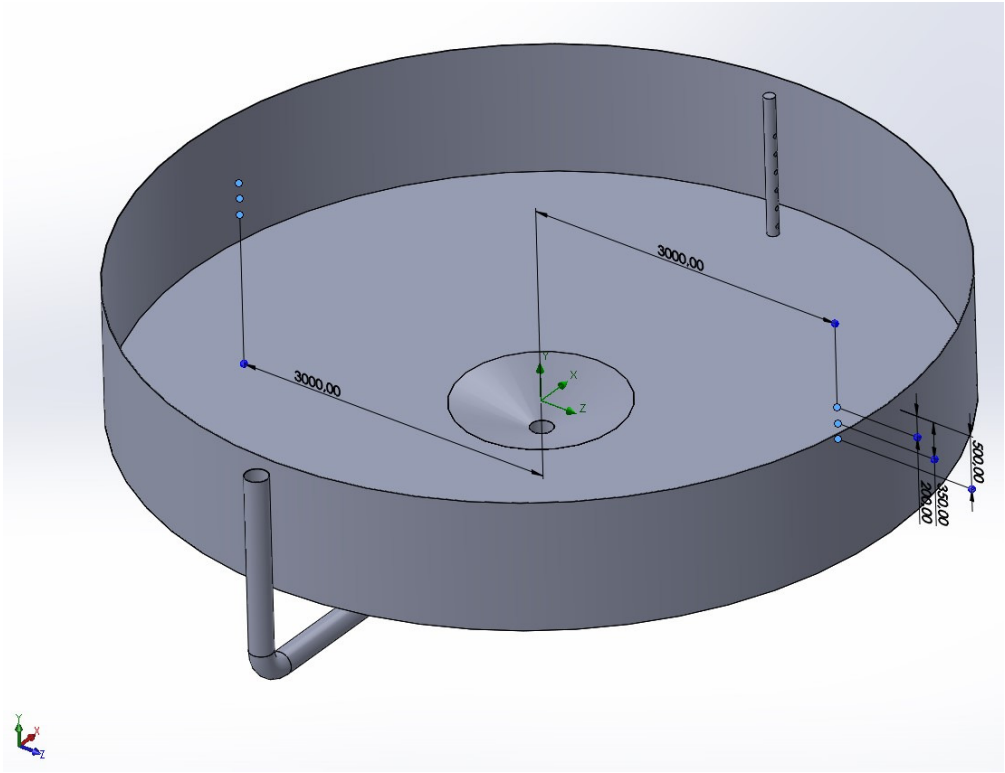

Figure 25 Sampling points - validation against An et al. (2018)

3.3.1.5 Additional simulation – Variation on boundary layer conditions

For this replication of the work presented by An et al. (2018), an additional simulation was performed where only an additional condition at the tank wall and tank bottom of the Real Wall type was applied. This in order to understand if the addition of a Real Wall condition was needed in order to take advantage of the Two Scale Wall Functions (TSWF) solving approach near the boundary layer used by the software (see section 3.2.6).

It was noted that the mesh generation was not affected, thus resulting in the same amount of total fluid cells and of fluid cells contacting solids. Additionally the effect on the overall accuracy of the results was not considered to be of significance (only ~0,02%) and therefore the use of Real Wall was not further use herein or in other simulations of this thesis work. It was assumed that the presence of a solid body at the boundary was enough to activate the TSWF and no further actions were needed.

3.3.2 Validation against Gorle et al. (2019)

It was also decided to replicate parts of the work presented by Gorle et al. (2019) to provided means of additional validation for the overall simulation set-up and accuracy of the simulations. The octagonal tank described, prior to the modifications they described, was used for this validation case. The tank was intended for culture of Atlantic salmon smolts.

3.3.2.1 3D model & dimensions

The 3D model was built as much as possible from the information presented by Gorle et al. (2019) and crossed checked against Gorle et al. (2018a) and Summerfelt et al. (2016) from the assumption that it is the same tank described by both authors, see Figure 26.

All the dimensions of the tank were not clearly indicated in their work, therefore some assumptions were made. It was unclear in the schematics of the tank where the dimension lines were pointing at. The initial assumption was that the dimensions were pointing to the inner faces of the tank walls, but when comparing the resultant volume of a tank built in such dimensions, this did not correspond exactly to the volume presented by both authors of 788 m^3 (Gorle et al., 2018b; Gorle et al., 2019; Summerfelt et al., 2016). The resulting volume if the dimensions were all considered internal would be of 836 m^3 which was considered too far off the presented volume of 788 m^3.

It was therefore later assumed that the 8,7 m dimension (center wall width) was internal, while the 2,9 m dimension (corner width) was to the outside of the tank's wall. The thickness of the tank walls was not presented but assumed then to be of 300 mm.

This combined approach to interpret the presented dimensions made the total width of the modelled tank to coincide with the overall width dimension of 14,5 m presented by Summerfelt (Summerfelt et al., 2016) of a rectangular tank at a hatchery in Steinsvik, Norway, from which a picture showed a very similar outlet configuration, therefore assumed to be the same tank.

The bottom of the tank was described as *conical* by Gorle et al. (2019), nevertheless the 3D model was made as a multi-sided prism, resembling better the shape of the figures presented in their work. A 12-sided polygon was then modelled at the bottom of the tank from which 16 flat surfaces extended towards the 8 sides of the tank. The vertical position of the bottom polygon was approximated by using the 10 degrees inclination mentioned by Gorle et al (2019) and the width of the polygon was extrapolated visually from another of the figures presented and assumed to be 2500 mm (slightly wider than the outlet casing).

The tank wall was described as 4,2 m height while the water level was maintained at 3,9m, resulting in an effective D/H ratio of 3,56. The calculated water volume of tank in the 3D model considering a water level of 3,9 m (and the volume occupied by the inlet and outlet systems) was of 777 m^3.

Two inlet pipes of Ø450 mm in diameter were included (extending from the wall's bottom level). 11 equally spaced nozzles of Ø90 mm in diameter were included in each of the inlet pipes. The spacing of the nozzles was not specified in their work, therefore a spacing of 350 mm was used; this provided an equally distributed pattern along the water column.

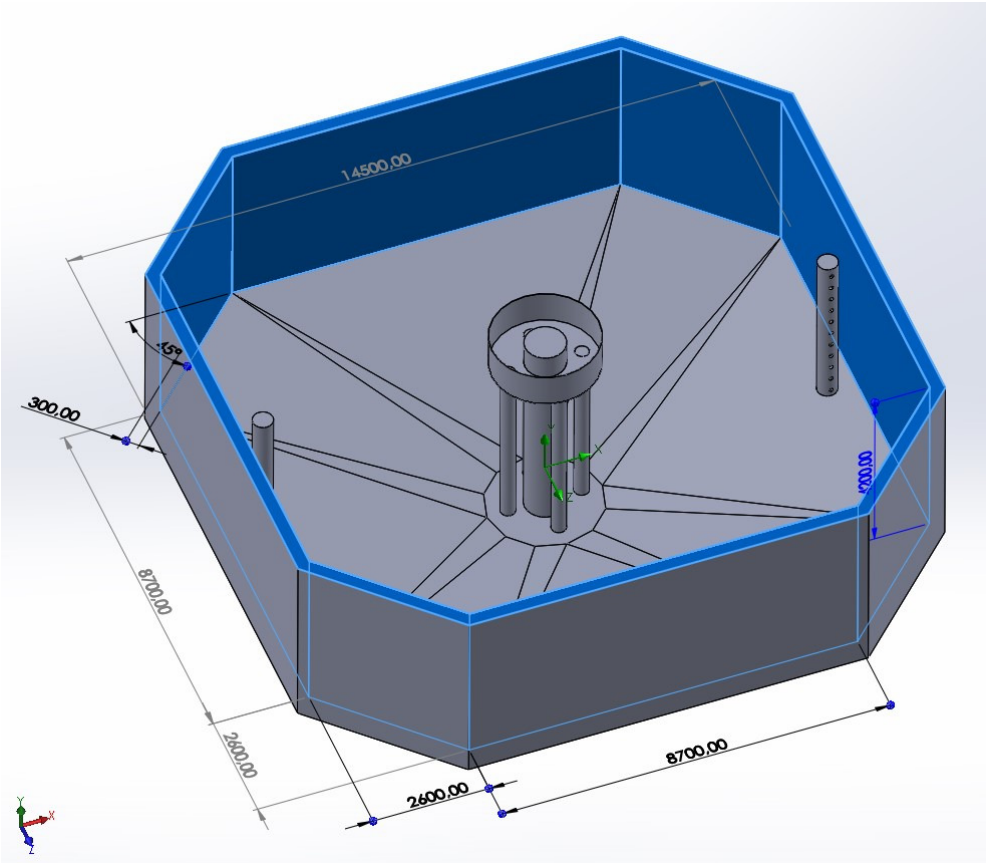

Figure 26 3D model and main dimensions - validation against Gorle et al. (2019).

3.3.2.2 Meshing

A structured mesh of hexahedral cells was used. The global mesh was refined until the largest cell size was of approximately 315 mm in width. This size was estimated based on the total characteristic number of cells across the width of the tank and the considered internal tank's width. The mesh was further refined at the boundary layer (near the tank walls and tank bottom and around the inlet and outlet pipes). A total of 205,481 fluids cell were generated from which 95,084 were in contact with solids.

The resultant mesh is presented in Figure 27, Figure 28, Figure 29 and Figure 30.

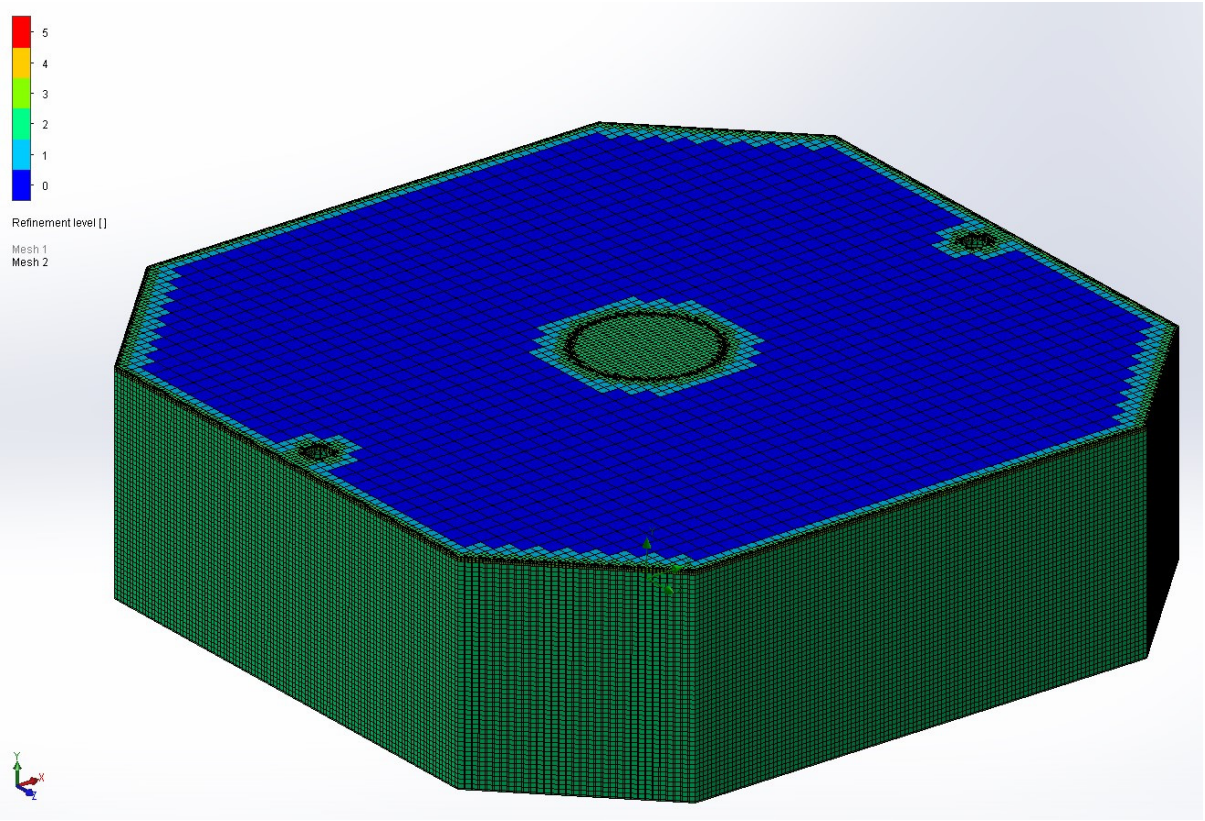

Figure 27 Meshing overview - validation against Gorle et al. (2019)

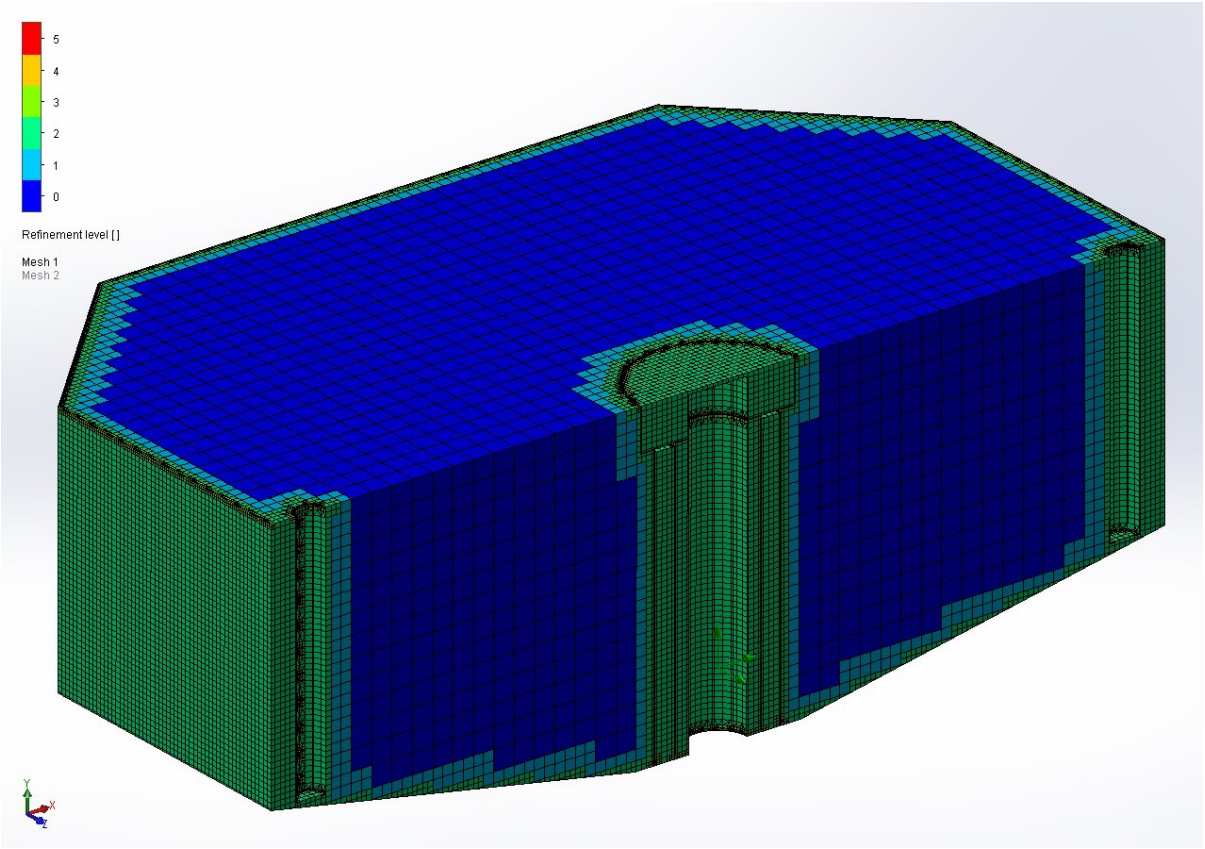

Figure 28 Meshing cut view - validation against Gorle et al. (2019)

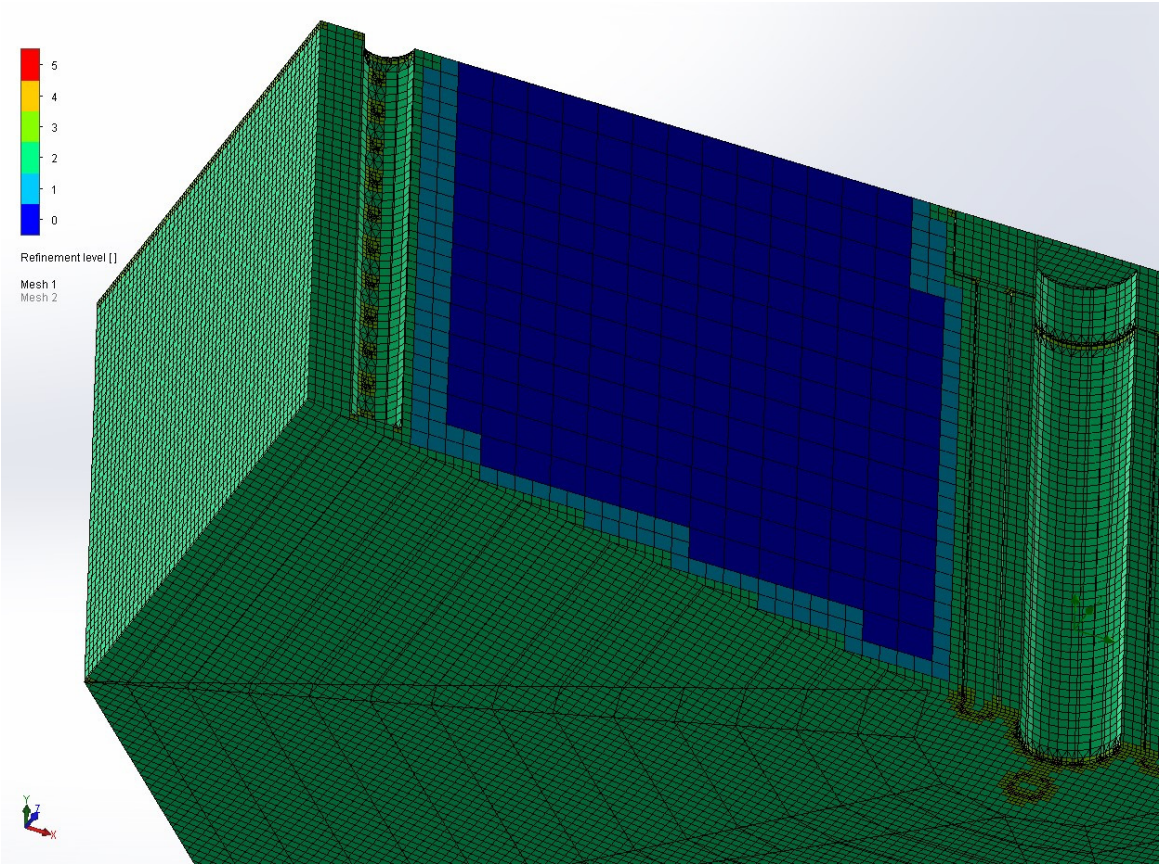

Figure 29 Meshing detail at tank's bottom, inlet and outlet pipes - validation against Gorle et al. (2019)

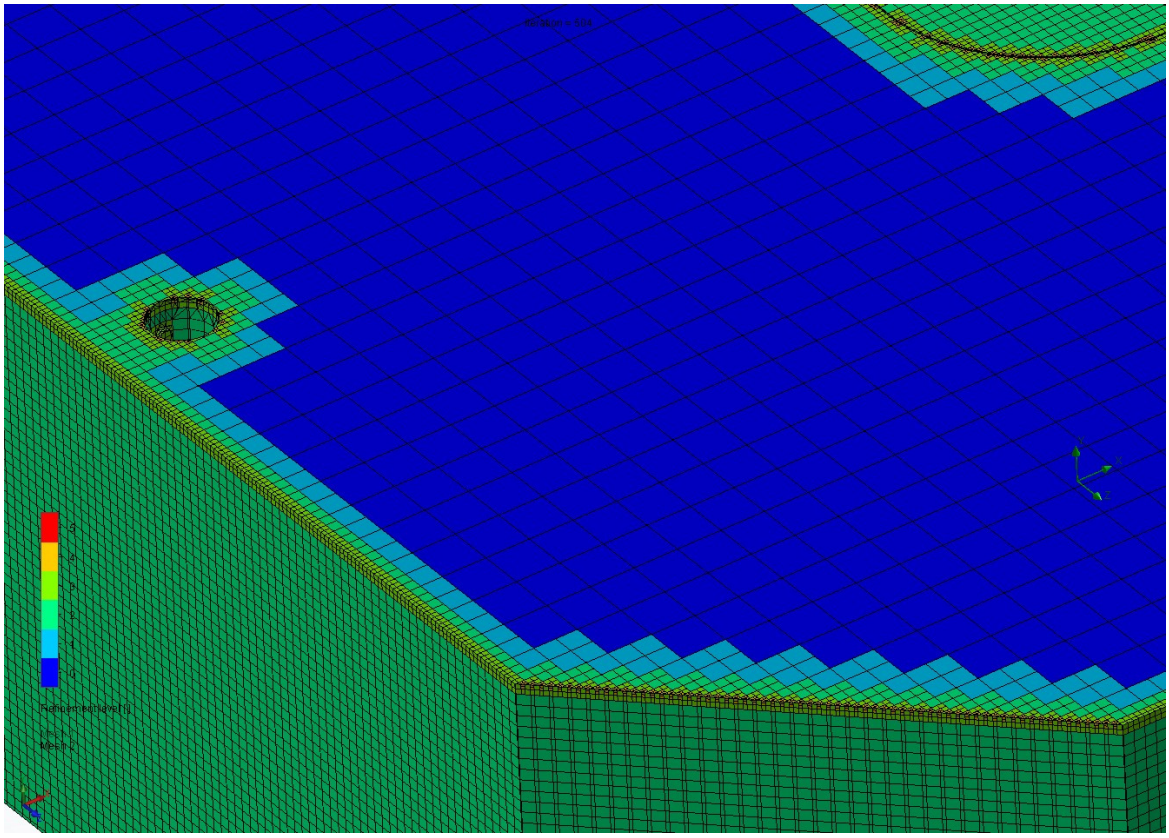

Figure 30 Meshing detail at tank's wall and water surface - validation against Gorle et al. (2019)

3.3.2.3 Water flow and turbulence parameters

An inlet water flow of 0,287777777 m^3/s was calculated from the hydraulic retention time of 45 minutes presented by Gorle et al. (2019) and the tank volume resultant from the 3D model created. It was decided to not use the presented flow rate of 292 L/min by Gorle et al. (2019), as this would represent a different retention time when using the resultant 3D model water volume.

The flow was distributed between the inlet pipes in the same way as Gorle et al. (2019) for the initial part of their work, in such a way that one of the inlet pipes (in the negative x-sector) supplied 25% more flow than the opposite inlet pipe.

The initial turbulence parameter settings were set to a turbulence intensity of 5% and a turbulence length of 0,3 m. The turbulence parameters were applied to the Inlet Volume Flow were of a turbulence intensity of 5% and a turbulence length of 0,0035m were used.

3.3.2.4 Position and type of goals

The position for the Velocity Goals was estimated from the equations presented by Gorle et al (2019), where a relationship between the *wall height (h)* and the sampling position was made. This information was later found to be contradictory, since in a figure of the same work, *h* was referred as the *water level* and used for the formulation of the sampling positions.

For the purposes of the simulation, *h* was considered to be the *water level* and not the tank wall height. The formulations for determination of the sampling positions were: y=0,17h; y=0,43h and y=0,68h. The resultant vertical positions for the velocity goals were then calculated to 0,663 m, 1.677 m and 2,652 m, see Figure 31.

The horizontal spacing of the sampling points, along a parallel plane to the xy plane, was also not fully specified in the paper. It was only mentioned that the amount of measurements along the whole width of the tank was of 15. These were assumed to be spaced from the center by 868,75 mm in order to be equally spaced along the tank's width and for some of the Velocity Goals in the simulation to coincide with the x/R positions of 0,25; 0,5 and 0,75; something that would make easier extracting and comparing the information from the results presented only in the form of graphs by Gorle et al (2019).

The sampling points were placed along a plane parallel to xy plane positioned at z=1,5m on the Global Coordinate System. Note that in the coordinate system used by Gorle et al. (2019) the positive direction of the z-axis was inversed from the engineering convention commonly used.

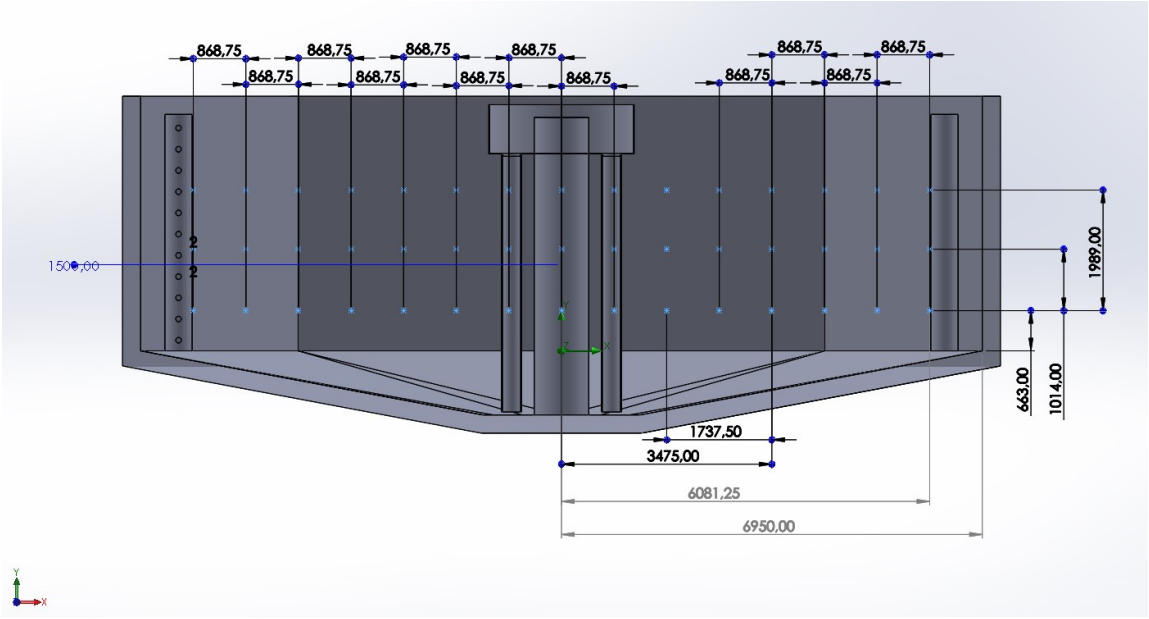

Figure 31 Position of sampling points - validation against Gorle et al. (2019)

3.3.2.5 Additional simulations – Variations on turbulence parameters

Two additional simulations were performed to test the effects of drastically changing the turbulence settings for the inlet flow. All the other simulation settings were kept unchanged.

Case 29 was made to test a large change in the turbulence intensity at the Inlet flow from 5% to 15%. The turbulence length was kept as 0,0035m.

Case 33 was made to test equal turbulence intensity and turbulence length values in both the initial conditions and the inlet flow. This meant a larger turbulence length for this simulation when compared to the base case simulation. The values used were 5% for turbulence intensity and 0,3 m for turbulence length.

3.4 Validation of CFD simulations vs. experimental data

3.4.1 Experimental data acquisition

3.4.1.1 Experimental set-up and equipment

In order to have means for a full-scale validation of the simulation settings, a rearing tank from the university aquaculture laboratory was modelled and analyzed using CFD. One of the largest tanks from the laboratory was chosen in order to minimize the effect of tank sizes when comparing towards the validations against literature, and to make the simulation of a tank as similar in size as possible to those used in commercial aquaculture facilities.

3.4.1.1.1 Tank and water outlet system

The tank used for the experimental validation was a square tank with rounded corners which has been supplied from A-Plast AS. The tank had an outlet pot located at the center and bottom of the tank. An outlet pipe exited the outlet pot from the side. The outlet pipe ran under the tank towards one of its corners where it intersected a vertical pipe. The vertical pipe extended to approximately the upper edge of the tank.

No detailed drawings of the tank were available from the supplier's website or from the building documentation at the laboratory. Details of the inlet and outlet pipes were also not available in any form of documentation, therefore a survey of these was also included in the scope of the work for the experimental validation.

Accurate measurements of the tank were performed, trying to capture all the relevant dimensions and geometrical features needed for the elaboration of a 3D model suitable for the simulations. Significant effort was put into acquiring precise data which would minimize possible uncertainties related to the geometry used in the CFD simulations. The main survey of the system was performed in a lapse of 10 days, starting on the 18. February 2019. The measuring process of the tank and outlet system is described in detail in the Appendix 1: Survey process of studied tank system.

The resultant model and the measured dimensions of the tank, as described in the following sub-sections, are presented in Appendix 3: Fish Lab Tank - As measured - Rev1.

Details of the outlet pipe resultant model and measured dimensions are shown in Appendix 4: Outlet Pipe - As measured - Rev1.

3.4.1.1.2 Water inlet system

The water inlet system was comprised of a vertical inlet pipe adjacent to one of the tank walls. The inlet pipe extended downwards from the manifold pipe above the tank. A membrane valve to control the incoming flow was installed in-line with this inlet pipe.

The position of the incoming pipe was determined by the fixed position of the manifold pipe and its supports. An inadequate position of the tank relative to the inlet manifold resulted in the situation where the inlet pipe was bended in place in order to make it go to the desired depth. Permanent deformation on the pipe was visible probably generated from sitting in a bended position for long time.

3.4.1.1.2.1 Original inlet pipe nozzles

The inlet pipe nozzles consisted of 5 holes of various sizes: 5 off Ø5,9 mm, 1 off Ø12 mm and 1 off 15,77 mm. This last mentioned hole seemed to have been modified multiple times, therefore resulting in an oval hole. The different diameters measured of this oval hole were initially averaged to the value previously presented.

It was visually obvious that the holes were not drilled along the same vertical line nor with the same angle. The spacing between the holes was also measured to be very variable, from 99 to 104 mm.

The measurements of the hole's diameters, spacing and location was measured using the Vernier. Distance between holes center was done by approximating visually the location of the holes center at the edges (furthest point of contact).

Due to the irregularities expected on the flow coming out of this inlet pipe, the original inlet pipe was considered not suitable for the replication of the tank in a CFD simulation (Figure 32). A set of new inlet pipes were therefore fabricated as substitutes.

Figure 32 Original inlet pipe

3.4.1.1.2.2 Inlet pipe nozzles modifications

The original polypropylene (PP) inlet pipe was welded to a flange which was for use specific on the existing valve. The inlet pipe was cut at enough distance below this welded connection to allow for a polyvinylchloride (PVC) slip-on pipe connection to be integrated there. Additionally the distance was calculated so the pipe would enter the tank cover from above providing enough room for the slip-on

connection to sit under the cover, facilitating the way the whole system could be put back in normal operation after finishing the experiments.

A new PVC pipe was selected to fabricate the alternative inlet pipe. By using polytetrafluoroethylene (PTFE) pipe tape between the new PVC pipe and pipe parts, it was possible to modify the inlet system in an easier way than choosing again PP parts and welding them back together. This also provided the flexibility to re-modify the system when encountering unforeseeable needed changes.

Additionally, the end-cap on the inlet pipe was changed to a smaller type which would not collide as badly with the tank's wall and bend excessively the inlet pipe.

Figure 33 Original inlet pipe configuration vs modified inlet pipe

3.4.1.1.2.2.1 Ø5,5 mm nozzles

The first modification tried on the inlet nozzles was to include 5 off Ø5,5 mm holes instead of the original sizes.

In order to be able to drill holes in a straight line parallel to the pipes length, a small aluminum angle profile was firmly supported on the pipe, providing then a fully geometrically determined reference line which was drawn on the pipe with a pencil.

In order to control that all the holes were drilled at the same angle on the pipe at the bench drill, a fixture consisting of a steel U-profile and pipe clamps was used (Figure 34).

Figure 34 fabrication fixture for drilling of nozzle holes

The steel profile was then firmly attached to the bench drill by bolt and nuts, thus minimizing the vibrations and movements of the pipe while drilling. This allowed for the holes to be drilled in a very precise way. The holes were deburred externally after drilling with a sharp blade to minimize the disturbance in the flow.

The hole-spacing in the new fabricated inlet pipes was measured by taking the maximum distance between holes edges and then subtracting the previously measured hole-diameter. It was then verified an equal spacing of 100 mm between the holes, while the hole-diameters matched the drill bit size accurately. The nozzle holes where not distributed among the whole water column, but rather concentrated at larger depths of the tank. This in contrast with the designs found in the validation against literature. Details of the inlet pipe modifications are presented in Appendix 5: Tested position of inlet pipe – Rev1.

The dimension details of the pipe connections (elbows and slip-on connection) were taken from the supplier's catalog and used in aiding to model as accurate as possible the details of the inlet pipe (GPA Flowsystem, 2018a; GPA Flowsystem, 2018b; GPA Flowsystem, 2018c; GPA Flowsystem, 2018d; GPA Flowsystem, 2018e)

A test run of the laboratory set-up was performed on the 07.03.19. The pressure loss of such small holes limited drastically the inlet flow, and the maximum flow achieved was in the range of 37 l/min with a full opening of the inlet valve. It was therefore decided to make larger nozzle holes.

Also a preliminary simulation was also performed (see Cases 23 & 24 in section 3.4.2.1.2) where the values of water velocity found were in the order of 17 times larger than the values captured by the velocity meter at the lab. This raised questions on the accuracy of the velocity meter but also helped to decide to make larger holes in the nozzles to increase the tank flow, hoping then to be able to measure larger values with the velocity meter.

3.4.1.1.2.2.2 Ø10 mm nozzles

It was indicated by the laboratory personnel that an acceptable maximum flow at the tank was in the order of 50 l/min. A larger flow than this would generate problems of air being sucked in at the outlet pipe and trapped further down the outlet system.

It was therefore decided to drill holes which would provide the equivalent area of the holes in the original inlet pipe. It was calculated that these equally sized holes should had a diameter of Ø9,97 mm. A Ø10 mm drill bit was then used, following the same measurement and fabrication method as before. The holes were drilled concentric to the Ø5,5 mm holes on the same inlet pipe, thus reducing the amount of work.

This larger holes gave a maximum flow of approximately 74 to 81 l/min with 3 opening turns on the valve (measured with the in-line flow meter). At the velocity meter an almost constant reading of 00,00 l/min was displayed, indicating the water velocities achieved with this nozzle configuration were so little that the equipment was not able to measure them.

With this such large water flow it was observed the formation of a large free-vortex, which occurs when the threshold of flow for an specific tank geometry is exceeded (Oca & Masalo, 2013). This threshold value was not investigated since it was of greater interest to investigate the forced-vortex-induced water velocity pattern and the effect of inlet design on it. Thus in order to have higher water velocities which the meter could register, and a smaller free-vortex, it was decided to modify the nozzle sizes again for a smaller hole size which could provide higher water velocities with lower total water flow.

3.4.1.1.2.2.3 Ø6,5 mm nozzles

In order to maximize the torque generating the forced-vortex with the maximum allowed flow on the lab system (50 l/min), the impulse force of the nozzle streams was calculated from the approximation to the impulse force equation, previously seen on Lekang (2007), presented by Masalo (2013). In this simplified approach, the nozzle velocity is assumed to be much larger than the average water velocity in the tank, giving the resultant equation:

$$F_i \cong \rho Q V_{in}$$

The velocity calculated at the inlet nozzle was in the order of 5 to 6 m/s, thus considered sufficiently higher than the water velocities inside the tank (in the order of few cm/s) to use this simplification in the formula. For the solely comparison of magnitude of the resultant force for a particular flow but with different nozzles sizes, the density was taken out of the equation and only the product of *water flow x inlet velocity* was considered. It was assumed an achievable flow of 50 l/min (0,00083 m^3/s). The inlet nozzle velocity was calculated using the cross sectional area of the nozzle hole which would result from the next available drill bit sizes at the laboratory above Ø5,5 mm; these being Ø6 mm and Ø6,5 mm.

Table 1 Impulse force magnitude factors for different inlet nozzle sizes

Case	Flow [m^3/s]	Inlet pipe diam of holes [mm] (size 1)	Area of hole [mm^2] (size 1)	Nozzle velocity [m/s]	Impulse force/rho ~=QV
Test	0,0008333333	10	78,54	2,122060946	1,76838E-06
Test	0,0006166667	5,5	23,75835	5,191157355	3,20121E-06
Test	0,0008333333	6	28,2744	5,894613738	4,91218E-06
Test	0,0008333333	6,5	33,18315	5,022629457	4,18552E-06

The Ø6 mm hole diameter was considered still too small to make a difference in the amount of losses due to friction at the nozzle reduction. This was later confirmed in the lab where a maximum flow of around 46 l/min (in-line meter reading) was achieved at full opening of the valve with the Ø6,5 mm holes.

It could be seen that the new impulse force (magnitude-factor) was more than twice than with the Ø10 mm holes (for the same flow) and around 30% larger than with the Ø5,5mm holes (due to the limited flow of ~37 l/min in that case).

3.4.1.1.2.3 Inlet pipe positions

Two different inlet pipe positions were evaluated. One consisted on including two 90 degrees PVC slip-on elbow adaptors to bring the inlet pipe further away from the tank's walls and evaluate the effect of changing the position of the inlet pipe towards the center of the tank, see Figure 33.

The second position investigated was actually the original position of the inlet pipe, but using the newly made inlet pipe with equal nozzle holes of Ø6,5 mm. Since the modified inlet pipe was provided also with a smaller end-cap, it was possible to position the pipe closer to the wall without bending it. While it was still not possible to bring the pipe fully vertical at its original position, only a small adjustment of few millimeters (~4mm) was necessary to achieve this: the header pipe had to be moved one position up in its mounting brackets (+26mm). This at the same time changed slightly the angle of the inlet pipe relative to the vertical and move the end-cap a few millimeters away from the tank's wall.

Another alternative was to empty the tank and move it these few millimeters in order to achieve a full clearance of the end-cap and the tank's wall. This option was deemed too complicated and it was decided to accept a small out of verticality of the inlet pipe for this configuration. It was not possible to visually see this out of verticality, only with the use of the water level.

The inlet pipe was then positioned in place by using two straight slip-on sockets and an intermediate piece of pipe. The length of the sockets and pipe was checked against that of the previously used elbows in order to achieve the same overall height of the inlet pipe, Figure 35. Details of the positioning of the inlet pipe are presented in Appendix 5: Tested positions of inlet pipe – Rev1.

Figure 35 Inlet pipe positioned adjacent to the wall

3.4.1.2 Water velocity meter

The equipment used to measure the water velocities in the tank (herein "velocity meter") was provided in the form of a prototype by LEDO AS. This prototype consisted of a *flow meter* attached to an aluminum pole. The flow meter was of the type intended to be used as flowmeter mounted in-line in a piping systems. The flow meter consisted of a section of pipe with a propeller mounted at the center of it. By counting the number of turns in the propeller the flow meter is able to calculate the water flow passing through the pipe.

The velocity meter specifications were not available or inexistent from the supplier. The type and model of the flow meter used was not possible to be checked on the equipment itself. The area where this information was displayed was covered and sealed in order to protect the meter from water ingress. It was therefore unable to confirm the model, but assumed to be the same component as the flow meter used for measuring total flow win the water tank described in section 3.4.1.3.1. The range of measurements of this flow meter was from 10 to 200 l/min.

A control box, was mounted at the top of the aluminum pole. The box was not secured for water ingress.

The properties of the plastic used for fabricating this box and the mounting part attached to the flow meter were not possible to be confirmed by the supplier. Their adequacy of the materials for use in fish farms was therefore not possible to be verified.

Both the control box and the flow meter were fixed in place by means of plastic strips (zip-ties).

The control box included of a set of electronics inside (two electronic boards) and a digital screen pointing outwards through an opening in the box. Parts of the electronics inside were not firmly attached to the control box. Cables between the two boards were connected using simple cable connectors without a firm locking mechanism.

A cable coming out of a second opening on the control box provided means to supply power to the electronics from a 9V (6LR61) battery. The control box had externally a smaller box for allocating the battery. No means for securing the battery inside its dedicated box were provided.

The exterior of the whole equipment was painted in black. The type of paint used was also not know and unable to be verified if this was adequate or harmful for fish.

The screen displayed initially the water flow readings in liters per minute with a resolution (displayed value step) of 0,22 l/min.

3.4.1.2.1 Requested modifications to the water velocity meter

The meter was first available on the 18.02.19 but it was initially equipped with a short pole which was not long enough for reaching the desired water depths at the tank. It was therefore requested to be changed for another longer pole. The equipment was received the same day with the extended pole.

After only being able to take one measurement on the test run (Case 23), the velocity meter unfortunately fell from a height of approximately 1 m and stopped working. It was noticed that some of the internal cables were unplugged. The velocity meter was taken back on the 26.02.19 to the supplier for repairs / reconnecting.

The equipment was collected back on the 04.03.19. Based on input previously given to the supplier, all of the electronics were now securely attached to the control box and no more cable connections between the electronic components were visible.

Non-requested additional modifications were also performed on the velocity meter. These included the inclusion of an ON/OFF switch and a permanently connected battery located loose inside the control box. This battery seemed to be of the same type as the ones used in old mobile telephones.

After using the equipment for measuring on Case 23, it suddenly stopped working again. It was taken again back for repair on the 11.03.19 The reason why the meter had stopped working this last time was that it became too low in power.

The velocity meter was collected fixed on the 15.03.19. The battery had been removed and instead a short USB cable connection was provided in order to directly connect it to a 5V power supply. A mobile telephone adapter to convert from 240V AC to 5V DC was also supplied.

Due to the electric shock hazard of having a 240V cord extension above the water tank, an extension cable for USB was also requested that day and provided immediately. This allowed for the AC current supply to not be above water level and instead to be in the vicinity of the tank at the floor level.

It was informed that the velocity meter was now made to display instead of water *flow* values in l/min, to display *velocity* values in m/s. The diameter used for this calculation was of 43mm.

The own measurements taken on the equipment were an inlet diameter of Ø46,26 mm and Ø43,80 mm at the outlet side (both measurements taken at the outer most edge). The plastic enclosure of the flow meter is apparently fabricated be injection molding, therefore having partition lines

characteristic of the molding process and draft angles to aid the expulsion from the mold. Due to these draft angles, the interior of the flow meter is not of a constant diameter. This represented an additional source of inaccuracy for the conversion of units from flow to velocity units (l/min to m/s).

The inside diameter at the center of the meter (where the propeller is located) was not possible to be measured with the available measuring tools.

The diameter used by the supplier to convert from flow to velocity units was considered not sufficiently accurate and only an unnecessary source of error in the measurements. Also since (as experienced in Case 23) the measurements displayed were very low in magnitude (ranging from 0,44 to 0,89 l/min), it was requested to set back the meter to display again water flow but now in liters/hr. By doing this it was possible to gain one decimal in the readings when converting manually to l/min; for example 0,222 l/min instead of 0,22 l/min originally displayed. No improvements were really attained in the resolution of the measurements by doing this: the values displayed had the equivalent value steps than before. This raised the suspicion that the equipment was not designed to measure such small flow regimes.

3.4.1.2.2 Own modifications to the water velocity meter

Some modifications on the velocity meter were made by the author in order to suit better the needs for the experiments. These are described in the following sub-sections.

3.4.1.2.2.1 Assembly clamps

In order to provide a firmer grip which could guarantee the position (vertically and angle-wise) of the meter when facing the water flow and possible misalignments due to handling, the plastic strips (zip-ties) were replaced with two stainless steel hose clamps, see Figure 36. Some pieces of plastic hose were also included under the clamp in order to provide an adequate diameter for the clamp, improve the grip on the aluminum pole and to avoid damage on the equipment when tightening the clamps.

3.4.1.2.2.2 Water depth markings

In order to determine the water depth at which the velocity meter was placed, the pole was marked with red electric tape every 100 mm from the center of the meter and upwards to a total of 800 mm. The tape was applied two times because it was noted the paint on the aluminum pole peeled off easily with the first tape application. This method of applying the tape over the bare aluminum pole increased the visibility of the markings.

Figure 36 Self-made modifications to the water velocity meter

3.4.1.2.2.3 Mounting clamps

Mounting clamps were also provided with the equipment. These were of the type used for wood construction to keep parts together temporarily under construction. These have been previously modified with a hole along the slider part. A pipe clamp was attached at this hole. These clamps were used to design a new mounting method for the equipment and keep it in a fixed and stable position while taking measurements inside the water tank.

The two clamps were installed along the aluminum pole. The lower clamp provided a tight grip against the aluminum pole, while the upper clamp provided a slightly looser fit, allowing it to slide up and down while still providing a sufficient support sideways.

3.4.1.3 Preparations for measuring the tank's water flow

3.4.1.3.1 In-line arrangement with flowmeter

A flow meter, assumed to be of the same type that the one used in the velocity meter, was also later provided under request for the experiments. The manufacturer of the flow meter was Sea. The meter was a YF-DN50 model, with a specified working range of 10-200 l/min and a water pressure rating of P≤ 1,75 MPa.

The flow meter was supplied with a factory control and display unit. This box displayed the water flow in l/min. A 19V +/- 8 V DC power supply was needed to operate unit. A computer adaptor of suitable power output was modified by the supplier and connected directly to the power supply of the unit.

Due to the associated risks of working with 240V AC near water measurements, a large plastic box was used as a shield and platform solution. In here were allocated most of the AC connections while serving also the function of support surface for the control and display unit.

A pipe arrangement starting from the upper T-pipe connection (described in section 0) was included in order to place this flow meter and have live readings of the tank's water flow.

The threaded connections on both ends of the flow meter were connected to thread-to-pipe adaptors, making it possible to build the rest of the system with only slip-on adaptors and pipe segments.

Due to the nature of the outlet system design, air is constantly introduced into the outlet system at the upper T-pipe connection. In order to minimize the effect of the air in the flow readings, the flow meter was mounted on a positively inclined section of this arrangement at 45 degrees.

A secondary air-venting pipe configuration was included after the flow meter in order to avoid an air-lock situation at the crest of the siphon shaped arrangement.

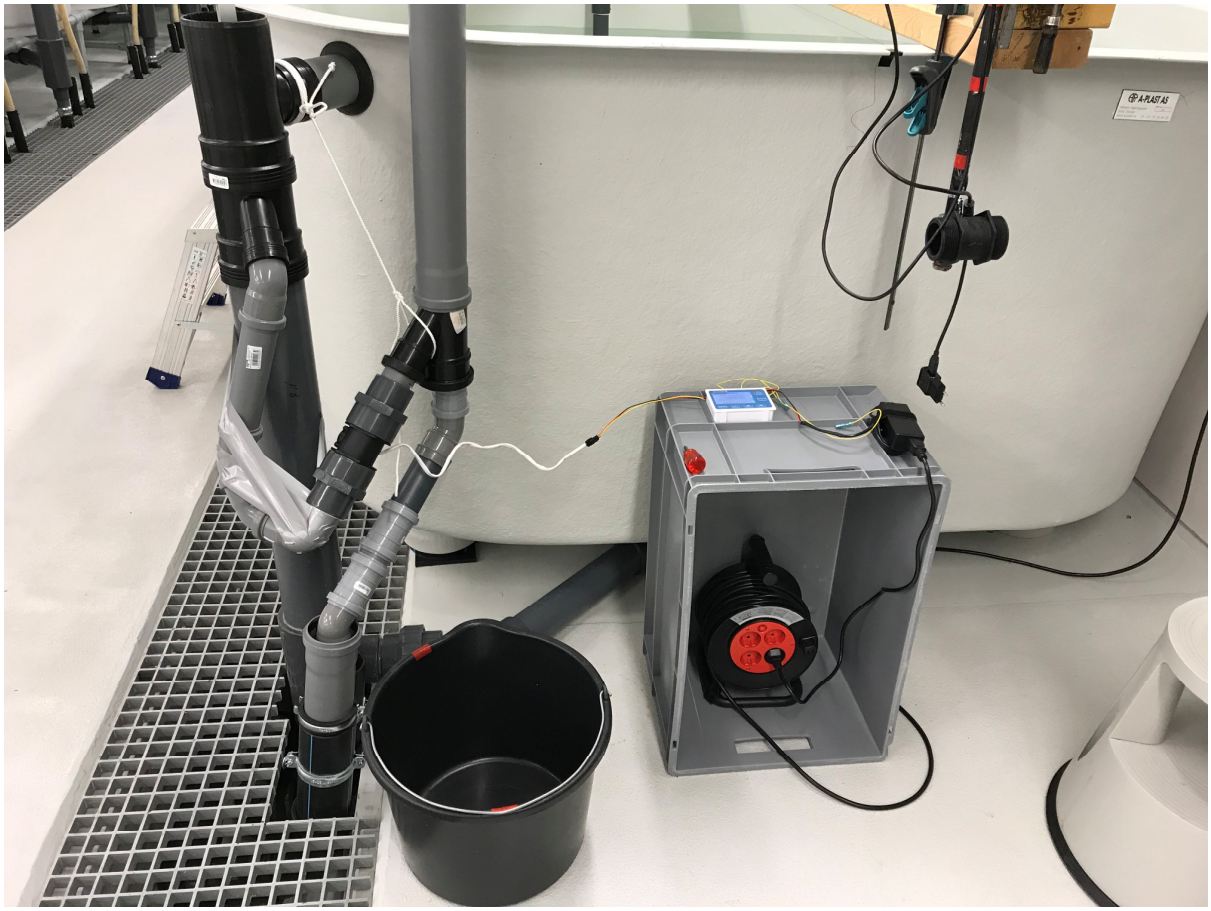

Figure 37 In-line flow meter set-up

3.4.1.3.2 Arrangement for manual flow measurements

The manual flow measurements were taken following the well-known bucket and stop-clock principle. This method has been previously used by the author while taking laboratory courses at the university and recommended also by the laboratory personnel as an accurate enough, reliable and convenient method.

The in-line flow meter arrangement was made in such a way that the locations of the pipe connections would allow for easier manual flow measurements. It was possible to redirect the flow from going into the main outlet header and into the bucket rapidly, with ease and minimizing the water splashing. This is believed to have provided reliable measurements as well as a safer working environment.

Figure 38 Demonstration of the manual water flow measurements

3.4.1.4 Data sampling

3.4.1.4.1 Tank flow samplings

The data sampling for the validation against experimental data was performed in two periods. The first period consisted of three days, where measurements at 6 different positions within the tank were done each day. The dates of the measurements from the first period were 15.03, 16.03 and 18.03 of the year 2019.

The second period was used to evaluate the alternative inlet nozzle size with the inlet pipe positioned at its original position. The second period consisted of four days, where between 4 and seven measurements were taken per day. The dates of the second sampling period were from the 05.04 to the 08.04 of the same year.

While the inlet configuration and valve opening were the same among the days in each period, small variations in the flow measured (and water level on the tank) were observed.

The RAS system of the laboratory can provide a constant flow and pressure determined by the height of the main inlet tank. Nevertheless the measurement of the flow in the experimental tank was performed every day of the experiments period in order to register possible changes in the flow due to different operational scenarios at the laboratory; including possibly changes in the amount of tanks operating, changes in valve opening at each of the other tanks sharing the same RAS system, etc.

Before starting the measurements of water velocity inside the tank, the total water flow was measured using the two means of flow measurement: in-line meter and bucket with stop-clock.

The first day of experiments the inlet valve was slowly fully opened (to avoid damage on the pipe or valve itself) and then allowed 1 hour for the water level and flow to stabilize before performing the measurements. The valve was left open for the consecutive days.

First the in-line flow meter display was observed and the minimum and maximum values displayed in the lapse of a minute were registered. The difference in the values was divided in half and added to the minimum value to find the median value. This method was selected due to the high variations observed in the flow displayed by the meter. A different value was displayed approximately every second with no apparent trend. It was nevertheless decided to continue to use and register the in-line meter in order to have two references for flow and to evaluate the performance of this flow meter arrangement at the outlet.

It was then proceeded to perform the bucket and stop-clock. A 20 liters bucket was previously calibrated with 20 kg of water measured at the laboratory balance. Red electric tape markings were applied at the water level at two locations along the circumference of the bucket.

Figure 39 Bucket calibration for manual flow measurements

The bucket was then placed in a location besides the outlet pipe where the modified outlet preparation could be easily and rapidly moved from its operational position to redirect the flow into the bucket. The edge of the bucket was placed almost in contact with the outlet pipe so the transfer time and splashing were minimized.

The stop-clock from a mobile phone was used for the measurements. The phone was positioned on top of one of the low step-on ladders to have easy access to it. The stop clock was started and let it to progress until 10 seconds were reached. At this moment the outlet pipe was redirected into the bucket.

The stop-clock was stopped when the water reached the markings on the bucket. The outlet pipe was then repositioned to its original position returning the water flow into the main outlet header.

The water from the bucket was returned to the tank by using a smaller bucket to minimize the weight to be lifted on each occasion. The remaining water in the bucket was then returned to the tank and the measuring bucket shaken empty and let facing down for a minimum of a minute before starting a new measurement.

The registered value on the stop-clock was written down in the sampling sheet and verified two times before proceeding with repeating the measurement. Each of the time measurements was registered in both the total time (as displayed in the clock) and the actual filling time by subtracting the initial 10 seconds waited before redirecting the outlet flow.

The measurements were repeated 5 times. The average (filling) time from each day was used to calculate the tank flow (in liters per minute) considered for that day. This flow measurements was the one used in the CFD simulations.

The calculations of average time and resultant flow from this method as well as the flow median calculation for the in-line meter were performed in an XL spreadsheet.

3.4.1.4.2 Water level measurements

The water level at the tank varied according to the water flow going through the tank. Four measurements from the tanks edge to the water level were taken; one at each tank wall on its middle part.

The measurements were taken by using the 90 degrees angle tool and introducing it slowly into the water until the other end became in full contact with the tank's top flange, thus taking a vertical measurement towards the water surface. The measurements were read from the downstream side of the tool by looking at the level where the tool became wet on that side.

The values were averaged to determine the current water level for that day and later used in the simulations.

3.4.1.4.3 Velocity readings

After the water flow measurements were performed, the velocity meter was positioned at the sampling location following the methodology described in Appendix 2: Methodology for positioning of the water velocity meter at the desired sampling points. It was then allowed for the system to run for a minimum of 62 minutes in order for the flow to stabilize. This waiting time was based on the first calculated hydraulic retention time of the tank given the specific water level and water flow.

The waiting time between re-positioning of the velocity meter for a different location on the same day was of minimum 30 minutes. This considering that the re-positioning of the meter, slowly and cautiously done every time, did not disturb the flow pattern as much as when returning the water from the buckets into the tank.

Measurements were registered every 15 seconds for each sampling position. The first day this of sampling this was done for a lapse of 2 minutes for a total of 9 measurements at each position. For the consecutive days the samplings were taken every 15 seconds for a period of 4 minutes, thus increasing the statistical sample size from 9 to 17 readings at each location.

The previously prepared sampling sheets contained empty fields to register the total amount of readings of each water flow displayed. The range of values experienced went from 0 to 106,56 l/hr (1,776 l/min). The value step displayed (resolution of the velocity meter) was of 13,32 l/hr (0,222 l/min), resulting in a manageable number of columns in the sampling sheet and values to be

monitored. The total number of readings of each magnitude was used to find the average value between the readings.

An additional column to register any displayed error in measurements was also included. While during the actual measurements no errors were displayed, previously the meter had displayed the warning “error” in the preliminary evaluations (case 23) and therefore included in the sampling sheet.

Three columns for registering the time of repositioning, time of start of sampling and time for ending of sampling were also included. Additional information such as location and name of the sampling position, fields and aids for taking the flow and water level measurements and space for notes were also included in the sampling sheet and presented in Appendix 6: Sampling Sheet – Rev2.

The velocity meter displayed a reading approximately every second. The magnitude among consecutive readings did not show any apparent trend, but instead seemed to jump from one value to another very different one every time. For example, it could go from 0 to 39,96 (l/hr), then back to zero again, to later display 26,64, jumping up to 79,92 and returning immediately to zero. This early indicated the meter was operating far below its design range and therefore not able to capture the water flow in a correct way.

The approach taken of taking multiple readings at same time intervals was in an attempt to try to take as much readings as manually possible, while at the same time randomizing the effect of the highly variable values.

3.4.1.4.4 Access and safety

Access for positioning the velocity meter at the measuring points was achieved by placing a wooden beam at the corner of the tank from which the measurement location was more accessible. This beam was secured in place by a tightening clamp.

Two short step-on ladders were used to climb onto the tank and on top of the access beam. Care was taken to use slow and controlled movements and to avoid carrying tools or equipment while climbing or descending. This allowed to use both hands for ensuring a good grip towards the adjacent solid structures, such as tank edges, pipe support mounting brackets and wall. Pipes, valves, center section of the adjacent tank cover, electrical connections, cable channels and other non-sturdy structures were avoided as means of support or balance, Figure 40.

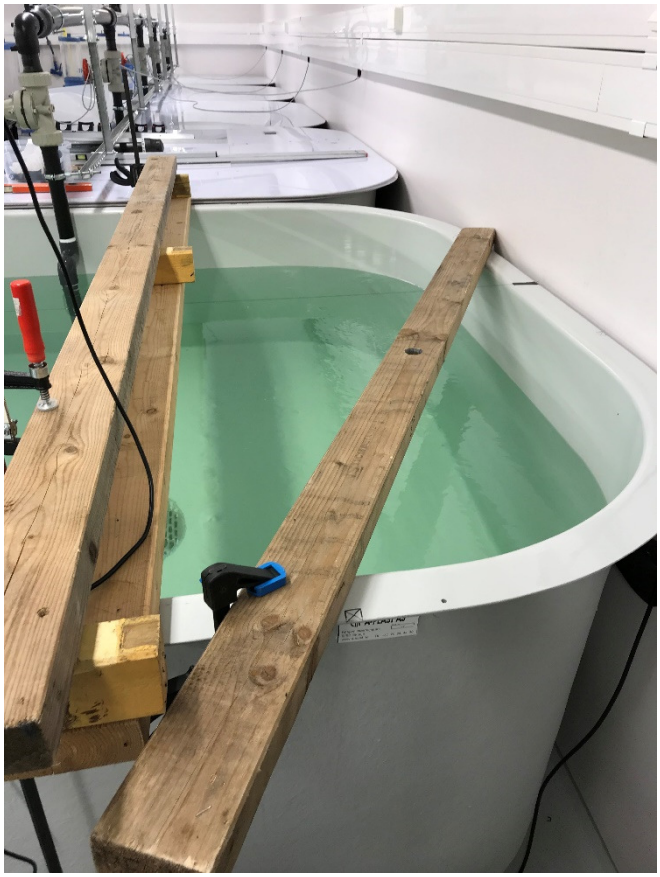

Figure 40 Access beam

As mentioned previously, the AC current electrical connections were protected by a plastic box from water splashing from above and from the sides, while also providing an elevated surface to avoid any water contact of possible spilled water on the floor. This proved to be of a useful precaution when, during taking manual water flow measurements, a pipe became loose and water was splashed over the top and sides of the box, leaving the electrical connections fully dry (see Figure 37).

3.4.2 CFD model

3.4.2.1 Preliminary simulations for fine tuning of the simulation parameters

3.4.2.1.1 Case 21 and Case 22 – Idealized flow/ 3D geometry check

Case 21 was used to simulate preliminary the modelled laboratory fish tank with an idealized water flow of 50 l/min and evaluate the selected simulation settings, such as the selected flow condition settings applied on the laboratory tank 3D geometry.

A warning regarding a vortex crossing the pressure opening was experienced this time but at the outlet opening. The outlet pipe was terminated at the tank water surface level, something that was understood could trigger the warning due to the relatively complex flow pattern at this location combined with short pipe distance above this point.

The 3D model was therefore modified to include a longer section of pipe above the water surface level, while still maintaining the environmental pressure setting at the water level.

Case 22 was run to confirm this geometrical solution with positive results, meaning the warning was no longer displayed and the simulation displayed the expected flow behavior.

The total number of cells with the selected mesh refinement settings was of 788,627.

3.4.2.1.2 Case 23 and Case 24 – First laboratory measurement / inlet nozzle Ø5,5 mm

Case 23 considered the water flow measured on the 07.03.19 of 33,749 l/min when using the Ø5,5 mm nozzle holes. Only one position (1HT) was measured with the velocity meter because, as previously mentioned, the low velocities registered and displayed by the velocity meter triggered modifications on the inlet nozzles.

The meshing was more refined that in cases 21 and 22. The total number of cells with the selected mesh settings was of 2,029,383 from which 1,071,772 were in contact with solid surfaces.

While running Case 23, the computer at the classroom stop responding due to high processing efforts and the software crashed. The result files automatically stored in the project folders were checked but it was found that almost no progress had been achieved at the goal convergence.

Case 24 was created to run Case 23 again in its totality. Case 23 and Case 24 settings are therefore identical.

The time it took for the software to create the mesh and solve the simulation was of 4 hours and 53 minutes.

The average *flow* readings from the velocity meter were of 0,6675 l/min. By considering the cross sectional area of the meter, this value was converted to a *velocity* reading of 0,6619 cm/s.

For this preliminary simulation the velocity meter was included as part of the 3D model. It was observed that the aluminum pole, as well as the velocity meter itself deformed the water flow pattern around and inside them.

The total velocity found in the simulation at a point located at the center of the modelled velocity meter was found to be 11,571 cm/s, while the velocity in the z-direction was of 11,566 cm/s.

While the ratio of magnitudes between the simulated velocity against the laboratory measurement was of 17,4812 (a difference of 1648%), it was useful to know that the total velocity simulated inside the flow meter was very much the same as the velocity in the z-direction, something that confirmed the simulation represented what could be expected in reality inside the velocity meter.

3.4.2.1.3 Case 25 – Test of laminar flow settings

Since the velocity estimations in CFD compared to the measured velocities were considered disappointing from Case 24, Case 25 was created to test the use of Laminar & Turbulent Flow as compared to Turbulent Only previously used. This in order to asses if the laminar component in the simulation settings would improve the results due to some concerns that the k-epsilon turbulent model used by the software (SOLIDWORKS-Corp., 2018b) “could not be integrated all the way to the wall” as previously discussed by An et al. (2018) (making reference to a work from Moukalled et al. (2016) which was not possible to find from the university library resources).

The simulation took 4 hours and 45 minutes to be solved, meaning the inclusion of the laminar component was not a significant factor in the computational efforts. Nevertheless the CFD/laboratory measurements velocities ratio was further increased to 17,83. It was then decided to continue with Turbulent Only settings for the main simulations.

3.4.2.1.4 Case 26 – Test of roughness settings

Case 26 was created identical to case 24 but with the addition of roughness at the solid surfaces. A value of 2,5 µm was used for this purpose.

The computational time to solve the simulation was of 4 hours and 42 minutes, also indicating not significant additional computational efforts to solve for roughness.

The ratio between velocities from CFD and laboratory measurements was of 17,4894,

3.4.2.1.5 Case 27 – Adjustment of turbulence settings

Due to the high difference ratio between the CFD estimated velocities against the laboratory measurements, it was decided to modify the initial turbulence parameters from the software-suggested values (2% in turbulence intensity and 0,015125 m of turbulence length) to the values used in the validation against An et al. (2018), which were already performed at the time and had proven to result in a better prediction of the water velocities (turbulence intensity: 5%, turbulence length: 0,0035 m).

Additionally a mesh refinement around the velocity meter was included for this case which was not included from Cases 23/24 to 26. The mesh refinement previously included at the nozzles holes was removed for this case while the boundary layer refinement was increased.

The computational time to solve the simulation was of 6 hours and 46 minutes. The resulting simulated velocities on Case 27 (for position 1HT) showed a decrease in the order of 1 cm/s., something that at the time was considered significant but unsure if should be attributed to the change in turbulence parameters or the mesh settings.

It was therefore decided to continue with the modified turbulence settings for the final calculation but it was decided to include again the mesh refinement at the inlet nozzles.

3.4.2.2 Final simulations

In both of the sampling periods, the flow measurements showed variations among the different days. Initially it was considered to make one simulation for each sampling day in order to account for the variations in the water flow at the laboratory.

On Case 23 it was observed that the inclusion of the velocity meter was properly described by the simulation with regards to the deflection in the flow pattern. Nevertheless, accounting for how much the velocity meter would disturb the flow for each sampling configuration meant that, the number of simulations should equal the number of samplings; making the simulating and processing of data a very complicated, time-consuming and an extenuating task.

Nevertheless, in order to be able to evaluate the velocity profile along the whole width and depth of the tank, it was later decided to make instead one simulation for each period (and inlet pipe configuration). They were performed considering the average water flow from the flow measurements performed at each day of the sampling period.

The nomenclature of the simulations reflects the initial plan of having one simulation for each sampling day. Each sampling day corresponds to a simulation case number. For the first period, Cases 30, 31 and 32 represent the 3 days of sampling in this period. For the second period, Cases 34, 35, 36 and 37 represent the 4 days of sampling.

3.4.2.2.1 3D models & dimensions

Two simulations for day 1 of the first sampling period were created, one including the velocity meter and one without it. These were named “Case 30” and “Case 30 without velocity meter”. This would provide the basis to evaluate how much the inclusion of the velocity meter affected the resultant simulated velocities when compared against a simulation were the velocity meter was not included. For all the other final simulations the velocity meter was not included.

3.4.2.2.2 Meshing

An automatically-generated structured grid model of hexahedral cells was used. The mesh settings used for the final simulations were readjusted trying to provide a good balance between computational time and enough refinement at boundary layer. Note that the amount of cells differs from the one including the velocity meter and the rest of the simulations where this is not included.

The total amount of fluid cells, for the single simulation considering the velocity meter, was of 2,114,024 from which 1,072,450 were in contact with solids.

For the rest of the simulations (not including the velocity meter) the resultant total number of fluid cells was of 2,057,365 and the number of cells contacting solids of 1,045,030, see Figure 41, Figure 43, Figure 44, Figure 45 and Figure 46.

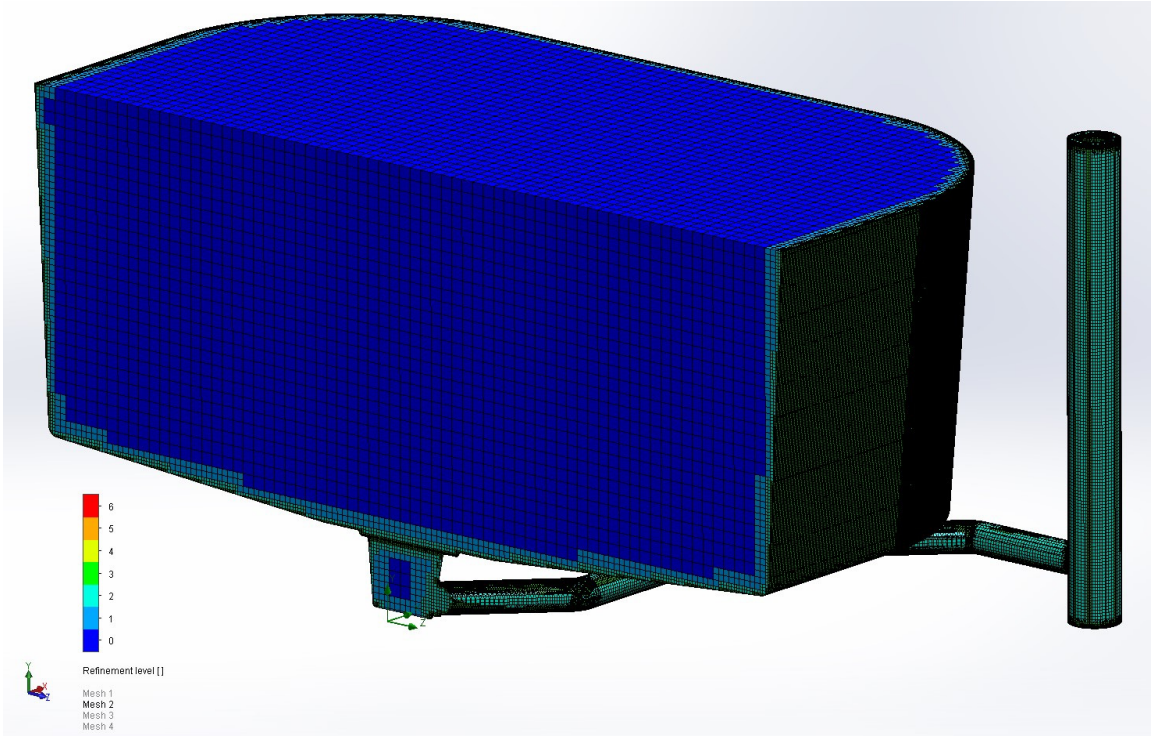

Figure 41 Meshing cut view – Cases without velocity meter – all cases

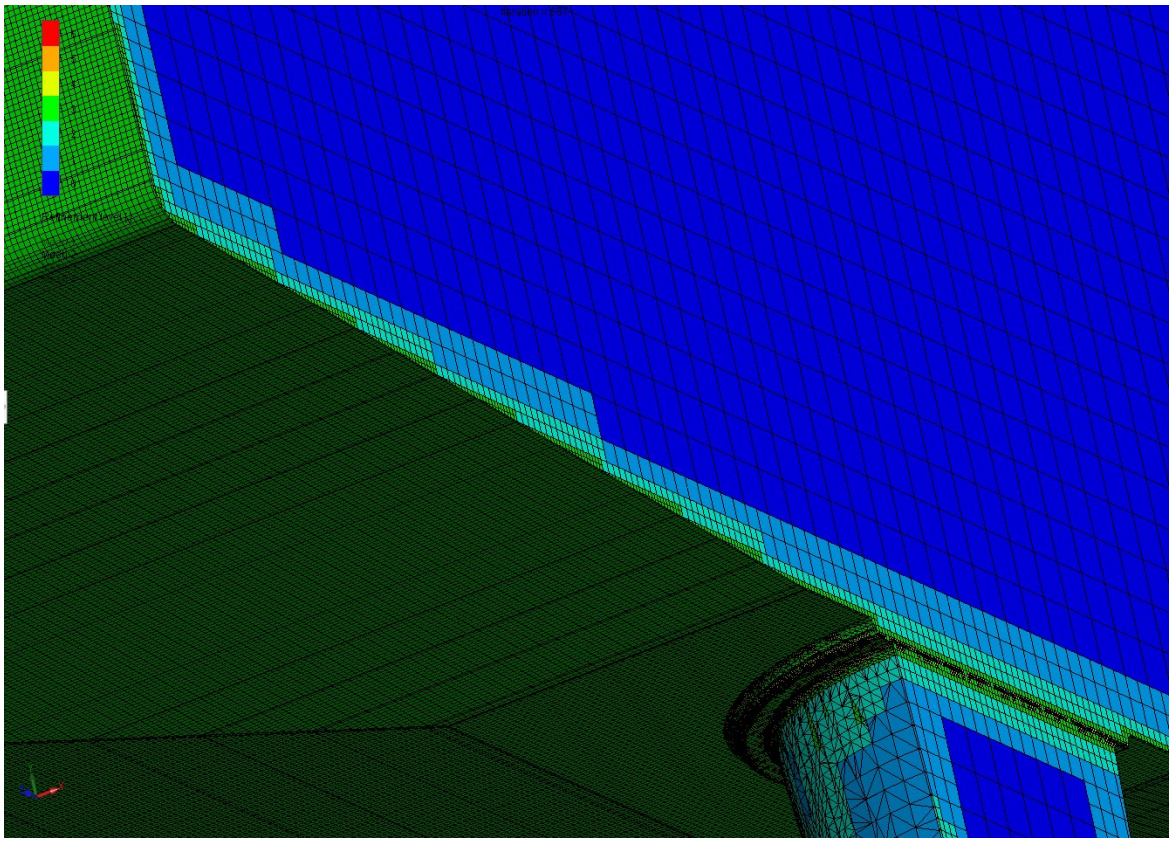

Figure 42 Meshing detail at tank's wall and bottom – all cases

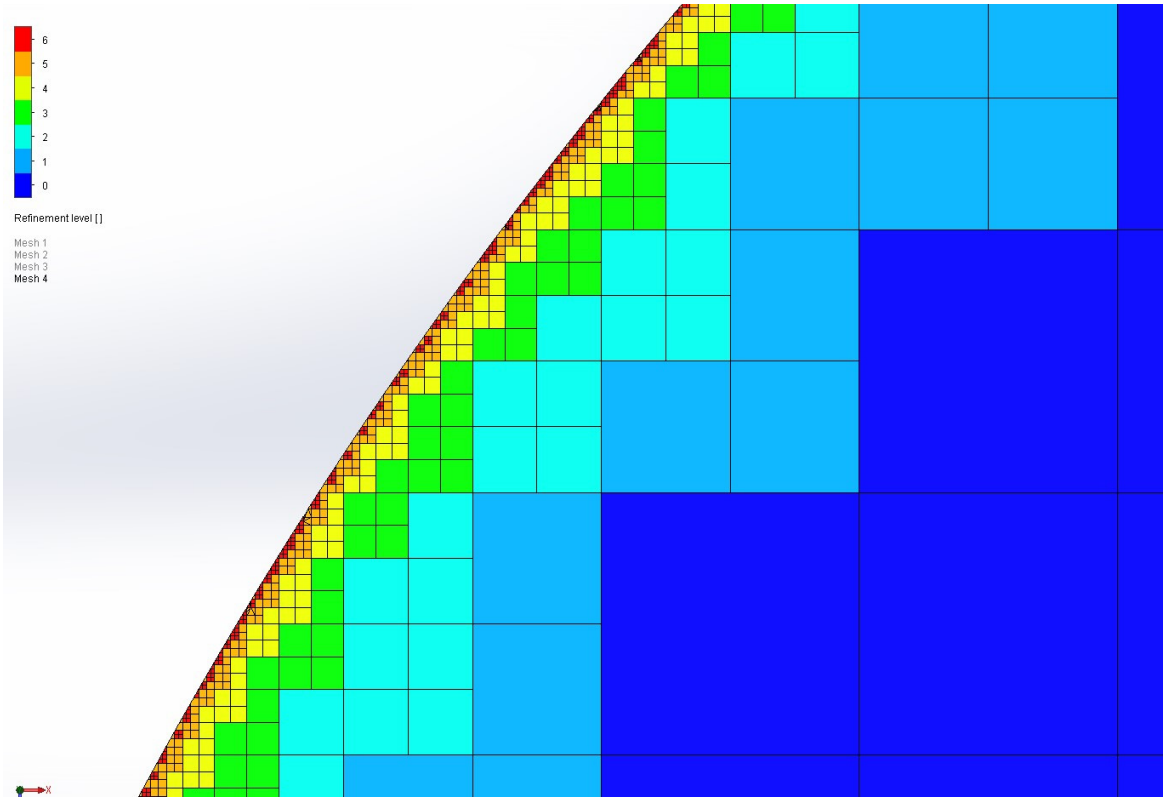

Figure 43 Meshing details at tank's corner at water surface level – all cases

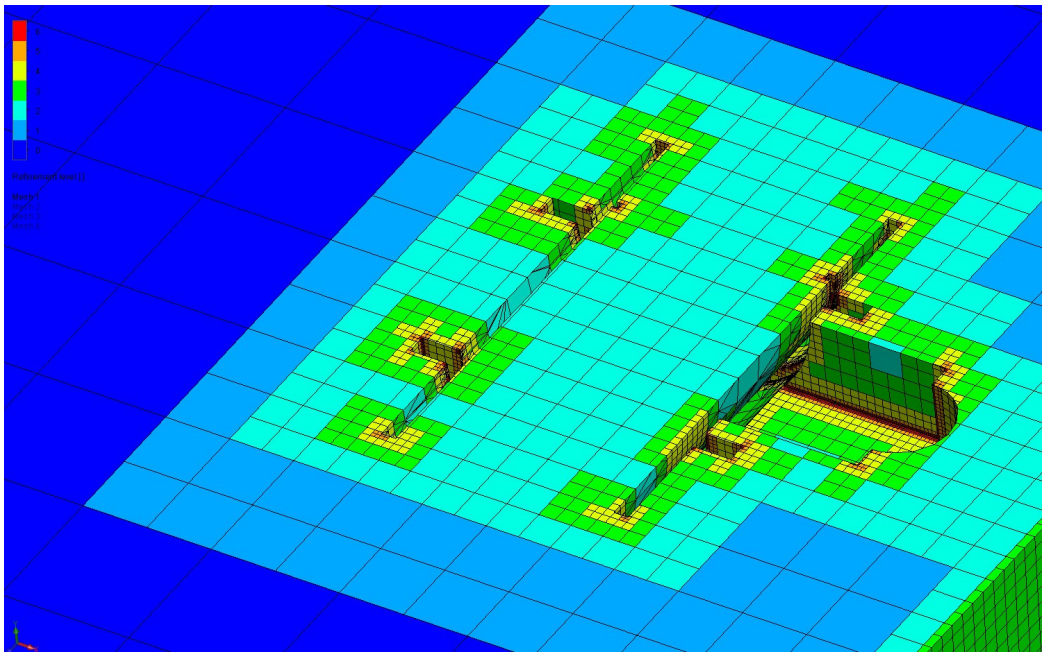

Figure 44 Meshing details at velocity meter – Case 30 with velocity meter

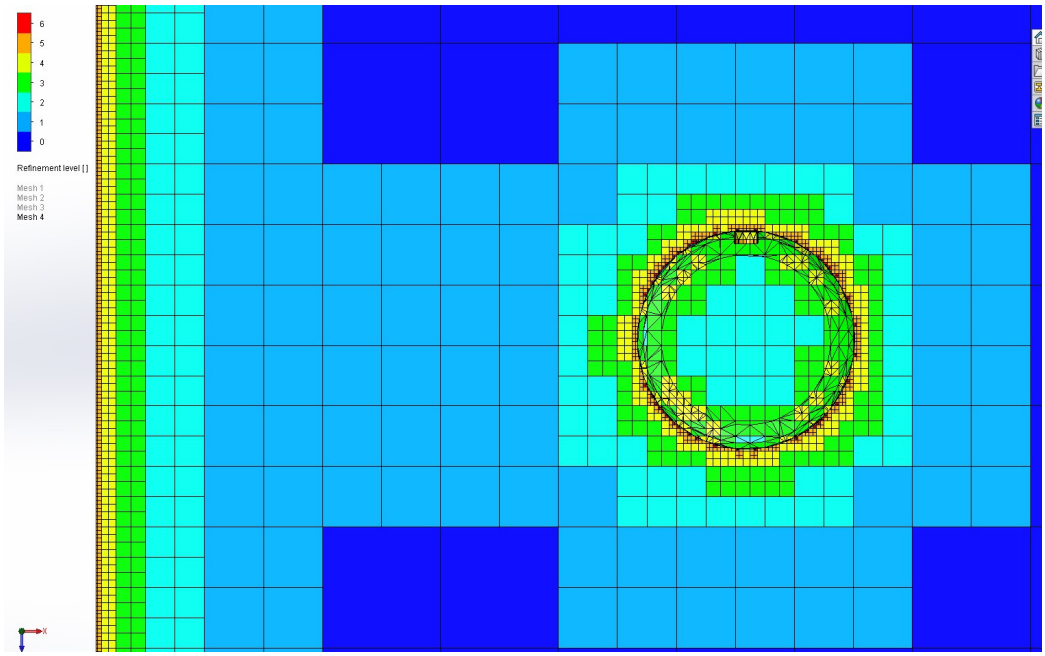

Figure 45 Meshing details at inlet pipe – all cases

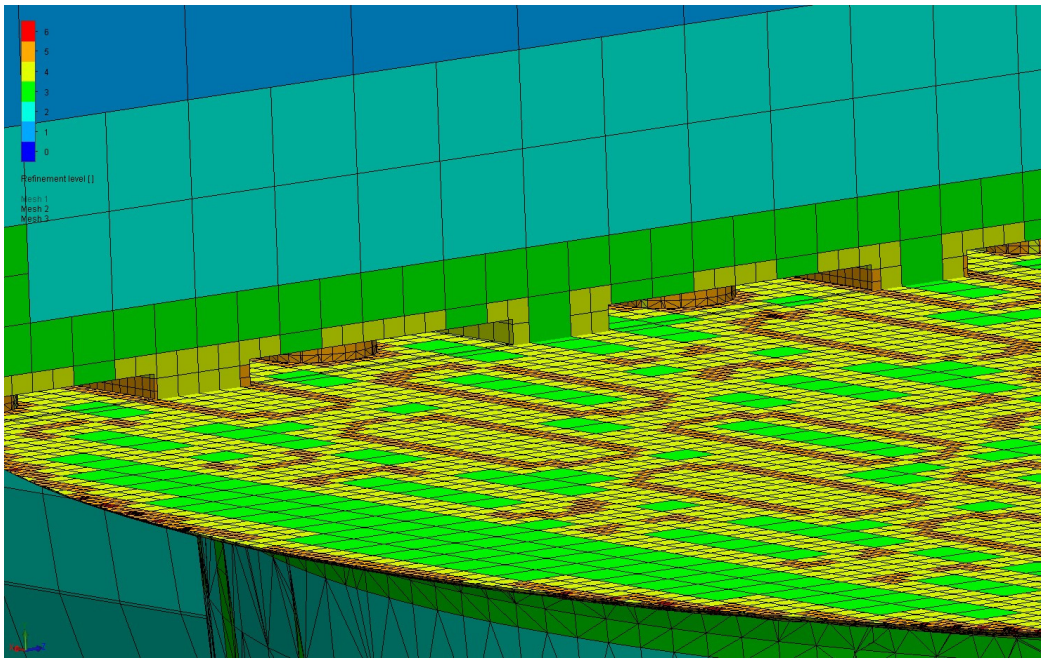

Figure 46 Meshing details at outlet grating – all cases

3.4.2.2.3 Turbulence parameters

For both of the simulation cases (with or without the velocity meter), the turbulence parameters used for the initial conditions were: turbulence intensity of 5% with a turbulence length of 0,0035m; while for the Inlet Volume Flow a turbulence intensity of 2% and turbulence length of 0,015125 m (software recommended) were used. Turbulent only flow was selected based on the experience from Case 25 on the overall effect on the results when using a combined laminar and turbulent flow. It is also understood that the flow that occurs in aquaculture tanks is of a turbulent nature, besides deep in the boundary layer (An et al., 2018; Gorle et al., 2019; Oca & Masalo, 2013).

3.4.2.2.4 Position and type of goals

Velocity Goals and Velocity Goals in the z-direction were created at 18 locations along the xy-plane, thus matching the sampling positions at the laboratory.

The location of these evaluation points along the x-axis was at a ratio x/R of +/-0,25, +/- 0,5 and +/- 0,89; R being the tank's width measured at the top of the tank. While R was measured pretty accurately to 1m, this way of representing the measurement positions as a ratio of x/R allows for better comparison among flow behavior of tanks of different size.

The vertical position of the samplings was defined as the water depth to the center of the velocity meter, these being 100 mm, 300 mm and 600 mm.

The nomenclature used for the sampling points is a modified version of the recommendations done by Lekang (2007) in his book. The number on the code name represents the ring level (when seen from the top) of the measuring position, being 1 the outer most ring and 3 the inner most ring. The first letter on the code name represents the sector or quadrant where the sample is taken, for this case left and right quadrants were utilized (in Norwegian V=Venstre=Left; H=Høyre=Right). The second letter of the code name represents the water depth of the measurement location, being T=Top, M=Middle and B=Bottom.

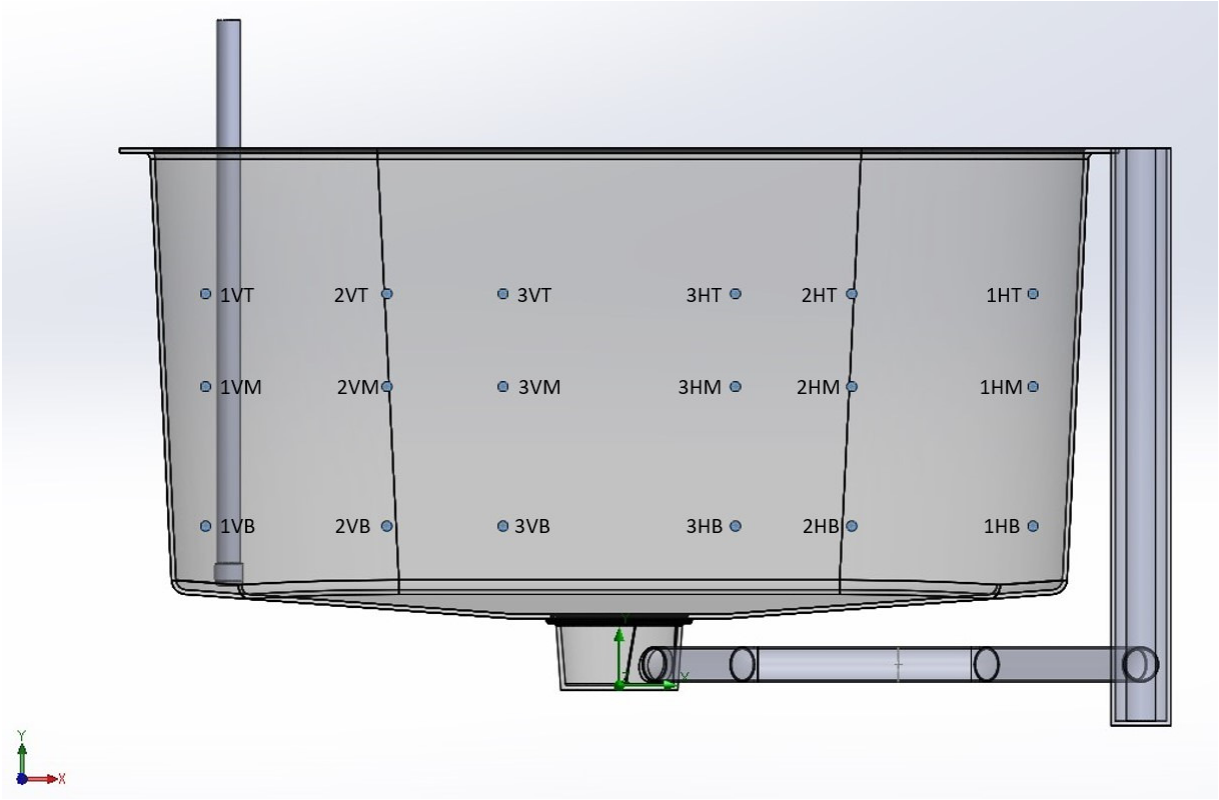

Figure 47 Sampling points at +/- 0,25; 0,5 and 0,89 x/R and water depth of 100, 300 and 600 mm

The goals selected for convergence where those corresponding to the sampled positions of each particular day, for example, for Case 30 six sampling positions where used for the solution convergence, while for combined Case 30-32 simulation all 18 sampling points helped for the convergence of the solution.

The water level measured was used to update the simulations accordingly. An extra configuration was added in the simulations to determine only the tank volume (without considering the volume inside the outlet pipe) and used for calculating the hydraulic retention time. The actual flow calculations considered the flow extending all the way to the outlet pipe as shown in the meshing section.

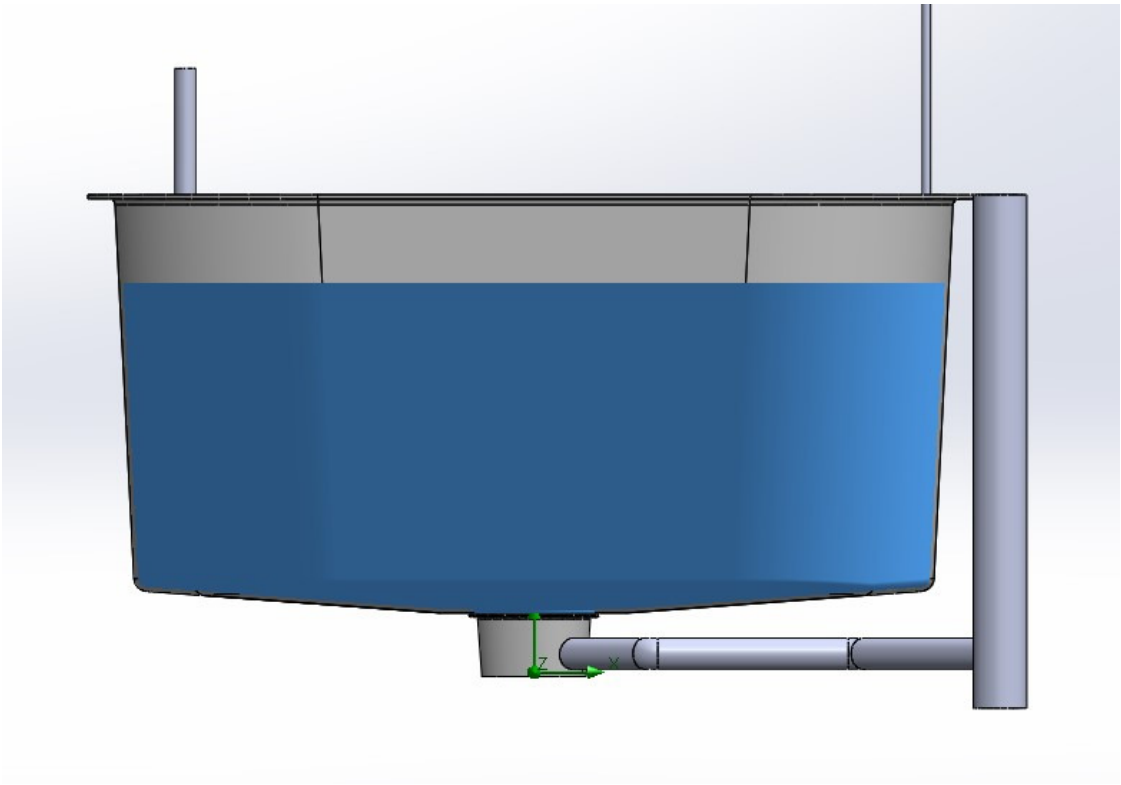

Figure 48 Fluid volume considered for calculating the hydraulic retention time

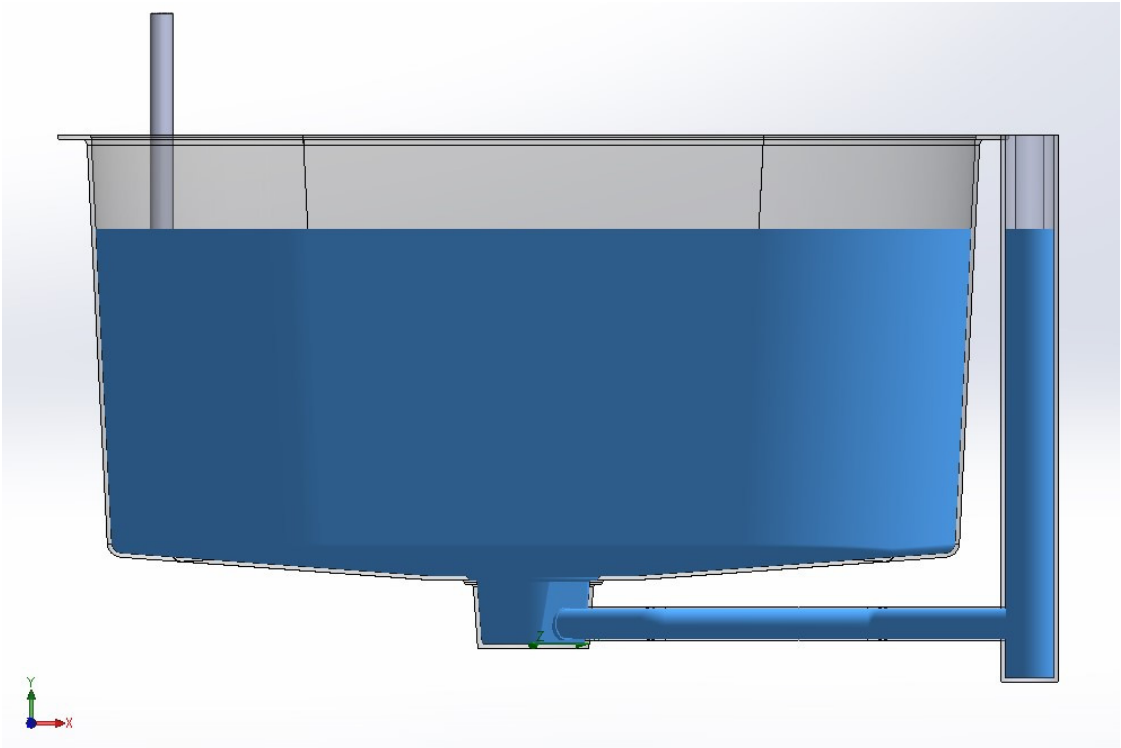

Figure 49 Fluid volume considered for the flow simulations

4 Results

4.1 Validation against An et al. (2018)

4.1.1 Main simulation

The computational time required to solve the simulation was of 3:54:24 [hr:min:s]. The flow trajectories captured from the CFD simulation for the selected tank to be replicated are presented in Figure 50. These were found to be very similar to those encountered by An et al. (2018), where the kinetic energy from the inlet flow is effectively utilized to create the rotating flow and dissipating gradually towards the center of the tank. From the visualization of water velocities and flow pattern, an increase in the rotational energy is seemingly experienced again near the center of the tank.

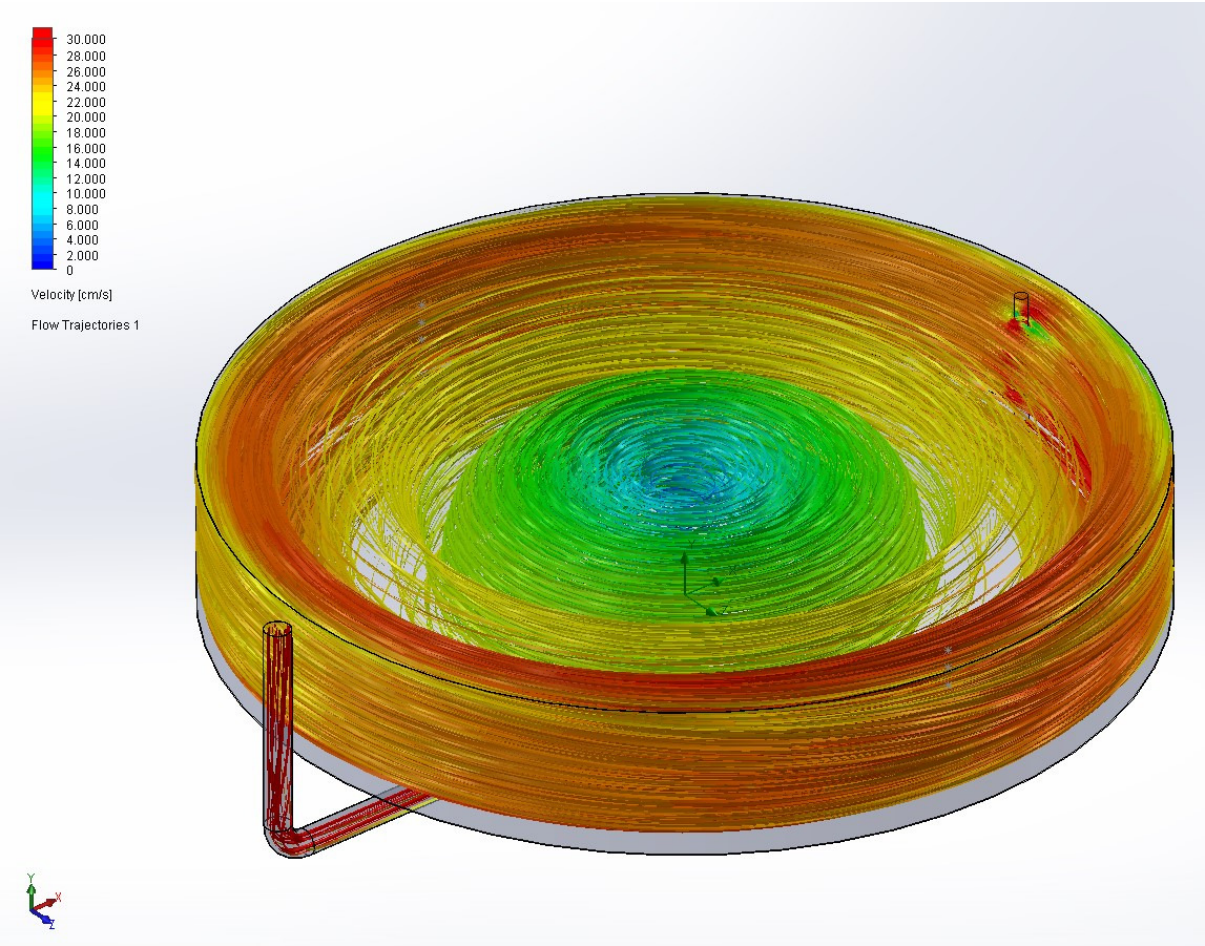

Figure 50 Flow trajectories - validation against An et al. (2018)

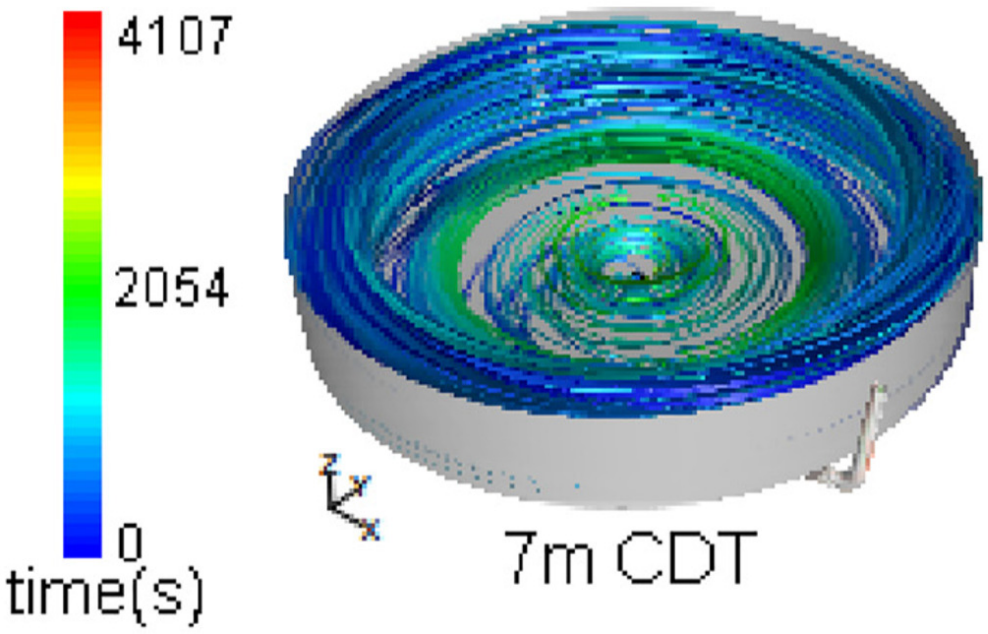

Figure 51 Flow trajectories from simulation by An et al. (2018) - Extracted from An et al. (2018)

Also visible in An et al.(2018) CFD simulations (reproduced on Figure 51), this could possibly be explained as the result of the free-vortex at the inner third section of the tank created by the outgoing flow (Oca & Masalo, 2013).

The CFD simulated total velocities and the calculated horizontal velocities as well as the laboratory measurements performed by An et al. are presented in Table 2. The horizontal velocities from the CFD velocities estimated from An et al. are also presented in the table for comparison purposes of the accuracy between simulation approaches.

Table 2 Horizontal velocities - Validation against An et al. (2018)

Sampling position name	Goal Name	Averaged Value	Horizontal Velocity CFD [cm/s]	Horizontal Velocity LAB [cm/s]	Std Dev. LAB (+/-) [cm/s]	Horizontal Velocity An et al. CFD [cm/s]	Relative error An et al. [%]	Relative error CFD vs LAB [%]	
A1	PG Velocity (X) 7	25,74579232	25,745833	29	26	31,7	9,310345	-11,221266	
	PG Velocity (Z) 7	0,045690337							
A2	PG Velocity (X) 8	25,68802749	25,688137	34	14	36,1	6,176471	-24,4466569	
	PG Velocity (Z) 8	-0,074890737							
A3	PG Velocity (X) 9	25,86250922	25,862649	36	3	37,7	4,722222	-28,1593084	
	PG Velocity (Z) 9	-0,085022664							
B1	PG Velocity (X) 10	-26,9401676	26,950485	28	22	30,4	8,571429	-3,74826826	
	PG Velocity (Z) 10	-0,745657752							
B2	PG Velocity (X) 11	-26,73537663	26,736604	30	12	32	6,666667	-10,8779866	
	PG Velocity (Z) 11	-0,256184931							
B3	PG Velocity (X) 12	-26,25856528	26,260175	32	2	33,6	5	-17,9369521	
	PG Velocity (Z) 12	0,290786532							
							6,741189	-16,0650731	Average

The estimated error was calculated in the same way as it was calculated by An et al. (2018). The equation describing this calculation is as follows:

$$\left(\frac{V_{CFD} - V_{LAB}}{V_{LAB}}\right) \times 100$$

Where the horizontal velocity measured at the laboratory was subtracted from the estimated CFD horizontal velocity and the result then divided on the laboratory horizontal velocity. This all was later multiplied by 100 to show the results as a percentage. The same approach was used for finding the relative error in the other simulation cases against literature and against own laboratory measurements.

It was noted that one of the calculated errors presented by An et al. (2018) was done not in accordance with the rest of the presented values, and therefore corrected on Table 2 (indicated with a red triangle at the corner). The wrongly presented value was of 4,76, corresponded to the difference between values divided by the CFD velocity instead of the LAB velocity.

It can be seen from the tables that the accuracy of the estimates from the own CFD simulation deviates further near the bottom of the tank, contrary to what was experienced by An et al. (2018) where their estimations deviated more closer to the water surface.

There was not sufficient samples from the literature to evaluate how the predictions of flow behave along the radius of the tank. It is nevertheless possible to see that the predictions of the own CFD simulation are better at the B side of the tank, being this the first measuring points downstream of the inlet pipe position.

4.1.2 Results from the variation on boundary layer conditions

The required to solve the simulation was of 2:22:21 [hr:min:s] (Note: the meshing process was run as a separate operation therefore the simulation solving time does not include the time previously spent on meshing). The effect on the overall accuracy of the CFD estimations when using Real Wall condition at the tank's wall and bottom is presented in Table 3.

Table 3 Horizontal velocities with use of Real Wall

Sampling position name	Goal Name	Averaged Value	Horizontal Velocity my CFD [cm/s]	Horizontal Velocity An et al. LAB [cm/s]	Std Dev. LAB (+/-) [cm/s]	Relative error CFD vs LAB [%]
A1	PG Velocity (X) 7	25,74043522				
	PG Velocity (Z) 7	0,055124158	25,7404942	29	26	-11,239675
A2	PG Velocity (X) 8	25,67479362				
	PG Velocity (Z) 8	-0,068938002	25,6748862	34	14	-24,48562891
A3	PG Velocity (X) 9	25,84922307				
	PG Velocity (Z) 9	-0,089146324	25,8493768	36	3	-28,19617557
B1	PG Velocity (X) 10	-26,95006241				
	PG Velocity (Z) 10	-0,750677718	26,9605152	28	22	-3,712445643
B2	PG Velocity (X) 11	-26,73059854				
	PG Velocity (Z) 11	-0,272933452	26,7319919	30	12	-10,89336032
B3	PG Velocity (X) 12	-26,23530653				
	PG Velocity (Z) 12	0,297351552	26,2369916	32	2	-18,00940133
						-16,0894478 Average

It can be seen that the use of Real Wall affected the accuracy of the results only in the range of decimals of percentage. As mentioned earlier, it was therefore decided not to use this approach on the other simulations and considered not as necessary in order to make use of the Two-Scale Wall functions (2SWF) in the software.

4.2 Validation against Gorle et al. (2019)

4.2.1 Main simulation

The computational time required to solve the main simulation (Case 28) was of 0:19:28 [hr:min:s]. The resultant CFD water velocity streamline profiles at the yz-plane are presented in Figure 52.

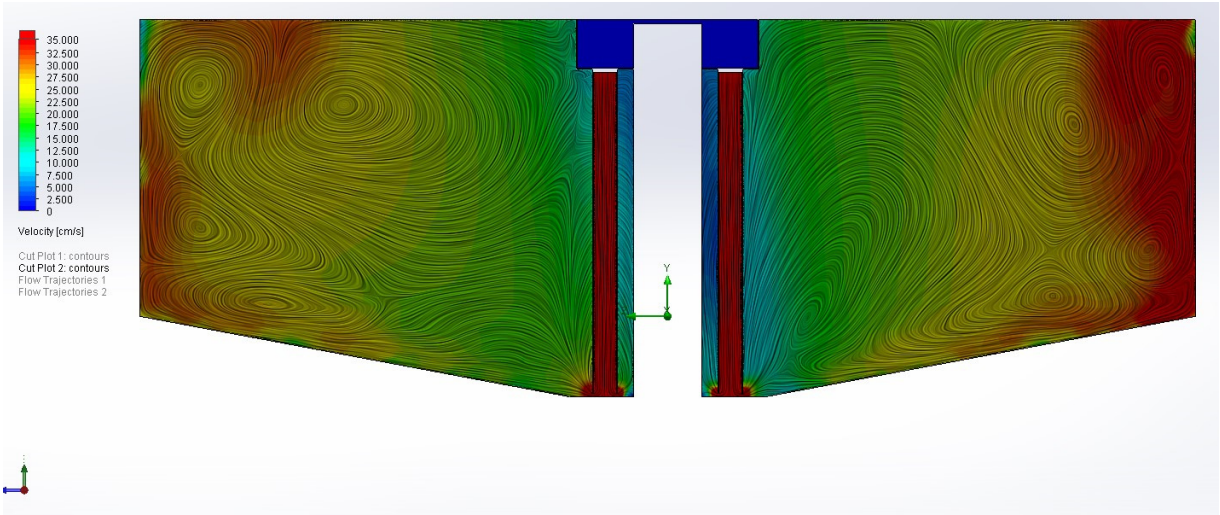

Figure 52 Water velocities - streamline profile at yz-plane

Figure 53 and Figure 54 show the streamline profiles at the xy-plane and sampling plane (z=1,5 m) respectively.

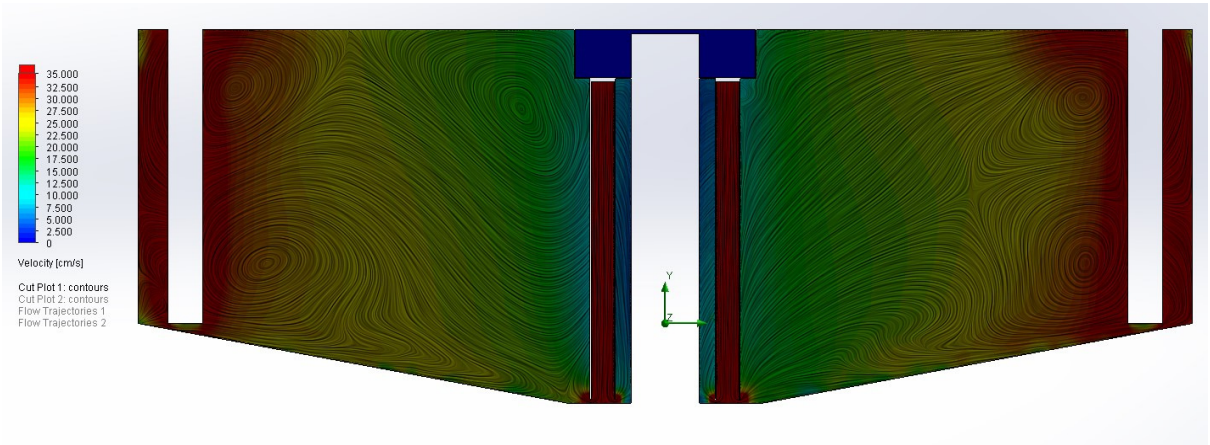

Figure 53 Water velocities - streamline profiles at xy-plane

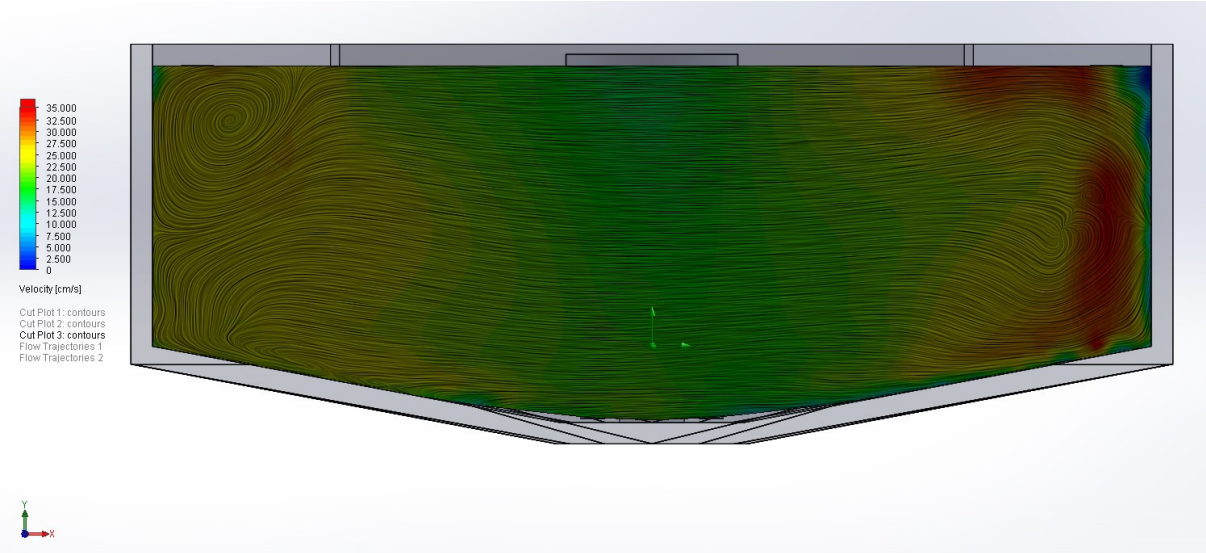

Figure 54 Water velocities - streamline profiles at the sampling plane (z=1,5m)

As can be seen in the streamline profiles at the sampling plane, the amount of secondary vortices in the flow are reduced at this position, as most of the flow in the projection corresponds to the main columnar vortex. This further depicted in Figure 55.

The position of the projection plane is therefore important for being able to make conclusions and eventual design decisions based on them; as the represented vortex could only be a very local feature in the overall flow pattern. This was tried to be visually explained in Figure 55 where the vortex at the top left of the picture corresponds to a relatively small local variation in the flow pattern when the water is approaching the inlet pipe.

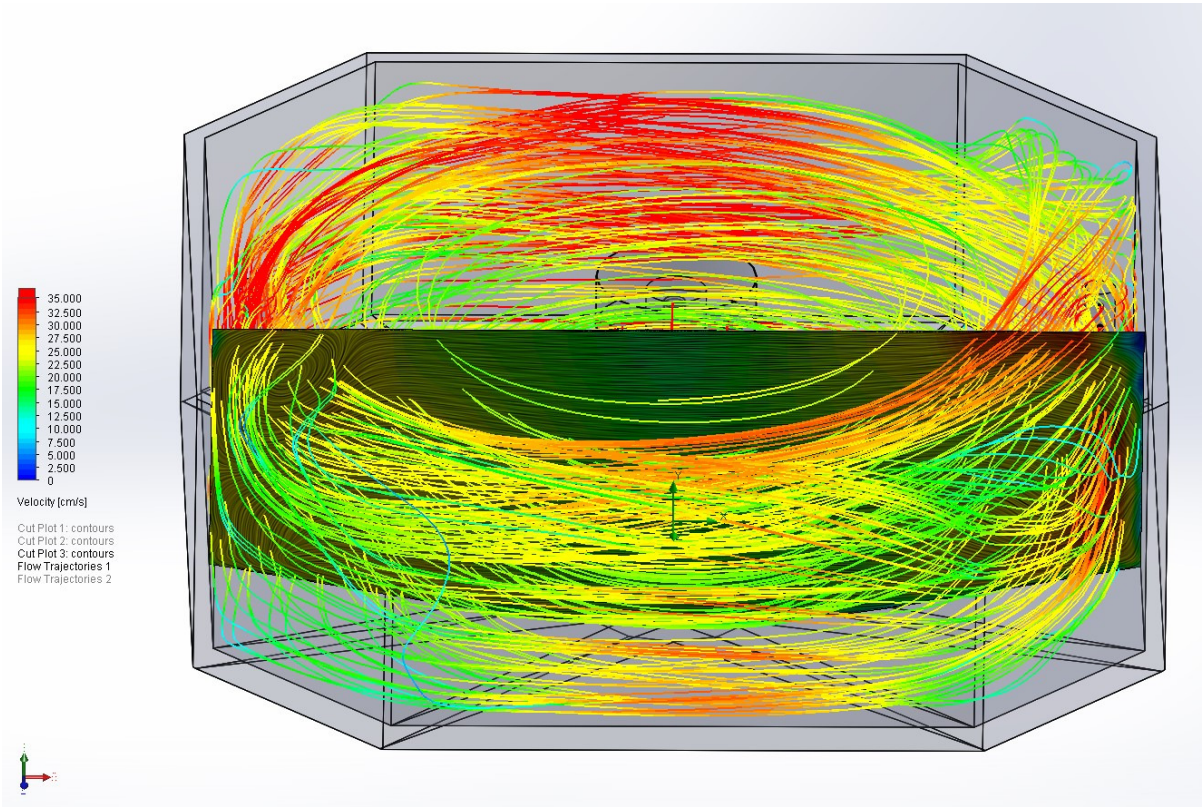

Figure 55 Water velocities - streamline profiles at sampling plane and flow trajectories, isometric view.

The features recognizable in a streamline profile will depend on the time in the analysis where these are taken for a time-dependent analysis (as the one performed by Gorle et al. (2019)). The streamline profiles created for this work correspond to the steady-state flow conditions.

In order to be able to compare numerically the results of the own CFD simulation against the experimental measurements performed by Gorle et al. (2019), it was necessary to extract the data from the graphs presented in their work. This was done by inserting pictures of the graphs in a 2D drawing and projecting lines from the points in the graphs towards the x-axis and y-axis. The measured dimensions in the drawing were used to calculate by triangulation the water velocities (y-axis) and the x/R position of the samplings (x-axis). These values were tabulated and new graphs generated.

Figure 56 exemplifies how the data for the y=0,17h samplings was extracted from the graphs. The solid lines and dimensions to the left correspond to the measured velocities. An automatic curve passing above all of the measured velocities was also drawn. The dotted lines to the right correspond to the +/- 0,25, +/- 0,5 and +/- 0,75 x/R values and its intersection point on the drawn curve (also the position of the evaluated goals on the CFD simulations). The drawing used for extraction of the data with the corresponding graphs for y=0,17h; y=0,43h and y=0,68h are presented in Appendix 7: Gorle et al. (2019) graphs for data extraction – Rev3.

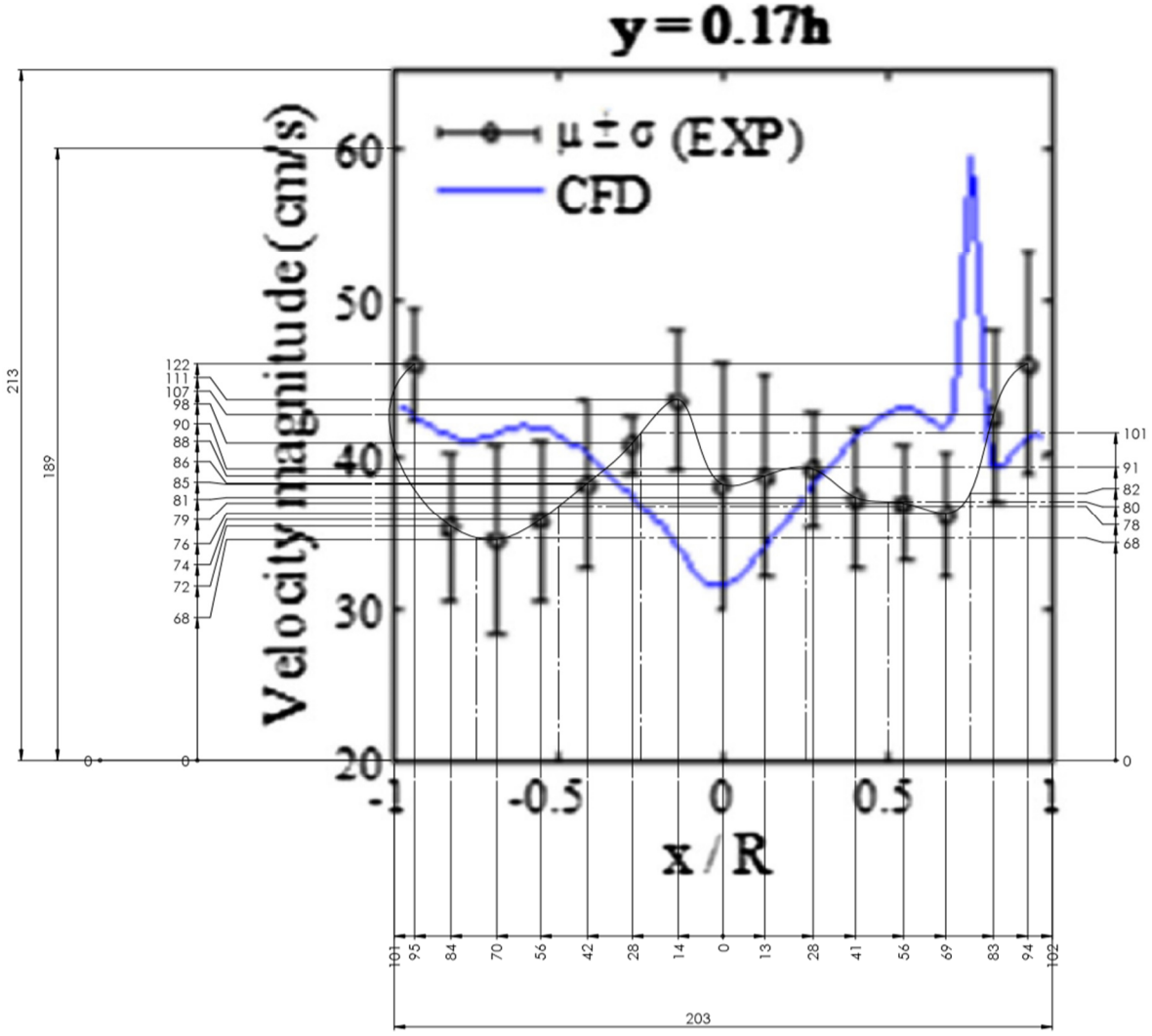

Figure 56 Method for determining numerically the laboratory measurements from graphs in Gorle et al. (2019).

The extracted numerical values, including the minimum and second maximum standard deviations found at each sampling level, the standard deviation at the center of the tank (found maximum for all cases) and the predicted values from the CFD simulations are presented in Table 4, Table 5 and Table 6.

It was not clearly specified if the velocities measured at the tank by Gorle et al. (2019) were done before or after the modifications on the outlet casing were performed. These modifications consisted on rectangular cut-outs which diverted the flow from fully passing through the four small pipes, to be split between the small pipes and the cut-outs at the top of the outlet column. The CFD evaluations performed in this work does not consider these cut-outs in the outlet casing.

Table 4 Numerical data extracted from graphs on Gorle et al. (2019) for y=0,17h

y=0,17h		Bottom				
	min	max				
y	0	189				
Corresponding Velocity	20	60	40	Difference		
x	-101	102	101,5	Absolute Average		
Corresponding x/R	-1	1				
x	x/R	y	Velocity	Case 28	Case 29	Case 33
-95	-0,93596	122	45,82011			
-84	-0,82759	72	35,2381			
	-0,75	68	34,39153	24,20588	22,60521	24,17714
-70	-0,68966	68	34,39153			
-56	-0,55172	74	35,66138			
	-0,5	78	36,50794	22,54709	21,79286	22,40586
-42	-0,41379	86	38,20106			
-28	-0,27586	98	40,74074			
	-0,25	101	41,37566	20,47783	20,7437	20,67522
-14	-0,13793	111	43,49206			
0	0	85	37,98942	17,92948	18,17401	18,24209
13	0,128079	88	38,62434			
	0,25	91	39,25926	18,78813	18,60676	18,98019
28	0,275862	90	39,04762			
41	0,403941	81	37,14286			
	0,5	80	36,93122	21,5592	22,2513	21,77193
56	0,551724	79	36,71958			
69	0,679803	76	36,08466			
	0,75	82	37,3545	27,10745	25,18624	27,95227
83	0,817734	107	42,6455			
94	0,926108	122	45,82011			
Min Std Dev. Range		18	1,904762	Std Dev (Range /2)		
Max Std Dev. Range		69	7,301587	Std Dev (Range /2)		
Center Std Dev. Range		76	8,042328	Std Dev (Range /2)		

Table 5 Numerical data extracted from graphs on Gorle et al. (2019) for y=0,43h

y=0,43h		Middle				
	min	max				
y	0	188				
Corresponding Velocity	20	60	40	Difference		
x	-101	102	101,5	Absolute Average		
Corresponding x/R	-1	1				
x	x/R	y	Velocity	Case 28	Case 29	Case 33
-95	-0,93596	107	42,76596			
-85	-0,83744	85	38,08511			
	-0,75	81	37,23404	25,55487	21,74726	25,70885
-69	-0,6798	80	37,02128			
-56	-0,55172	81	37,23404			
	-0,5	84	37,87234	23,54625	22,72047	23,42192
-41	-0,40394	94	40			
-28	-0,27586	106	42,55319			
	-0,25	106	42,55319	20,29899	21,00573	20,45292
-13	-0,12808	83	37,65957			
0	0	45	29,57447	17,17617	17,75004	17,45288
14	0,137931	85	38,08511			
	0,25	108	42,97872	19,11699	19,39532	19,32685
28	0,275862	108	42,97872			
42	0,413793	93	39,78723			
	0,5	85	38,08511	20,9224	22,29117	21,15084
56	0,551724	83	37,65957			
70	0,689655	90	39,14894			
	0,75	104	42,12766	23,75452	25,47271	23,99343
84	0,827586	119	45,31915			
96	0,945813	118	45,10638			
Min Std Dev. Range		19	2,021277	Std Dev (Range /2)		
Max Std Dev. Range		73	7,765957	Std Dev (Range /2)		
Center Std Dev. Range		84	8,93617	Std Dev (Range /2)		

Table 6 Numerical Data extracted from graphs on Gorle et al. (2019) for y=0,68h

y=0,68h		Top				
	min	max				
y	0	189				
Corresponding Velocity	20	60	40	Difference		
x	-101	101	101	Absolute Average		
Corresponding x/R	-1	1				
x	x/R	y	Velocity	Case 28	Case 29	Case 33
-95	-0,94059	116	44,55026			
-84	-0,83168	110	43,28042			
	-0,75	86	38,20106	27,10198	22,0397	26,62735
-70	-0,69307	78	36,50794			
-56	-0,55446	86	38,20106			
	-0,5	94	39,89418	22,6158	25,23254	22,6024
-42	-0,41584	109	43,06878			
-28	-0,27723	114	44,12698			
	-0,25	113	43,91534	19,42426	20,94841	19,50145
-14	-0,13861	99	40,95238			
0	0	68	34,39153	16,28206	16,67618	16,4378
14	0,138614	93	39,68254			
	0,25	104	42,01058	19,81311	20,67087	20,10898
28	0,277228	104	42,01058			
42	0,415842	96	40,31746			
	0,5	87	38,4127	22,00993	22,52285	22,17783
56	0,554455	84	37,77778			
70	0,693069	113	43,91534			
	0,75	118	44,97354	23,56787	26,46769	23,42687
84	0,831683	120	45,39683			
95	0,940594	121	45,60847			
Min Std Dev. Range		22	2,328042	Std Dev (Range /2)		
Max Std Dev. Range		66	6,984127	Std Dev (Range /2)		
Center Std Dev. Range		94	9,94709	Std Dev (Range /2)		

The plotted values of the water velocities measured by Gorle et al. (2019) at the three different water depths are compared against the estimated CFD water velocities from Case 28 in Figure 57.

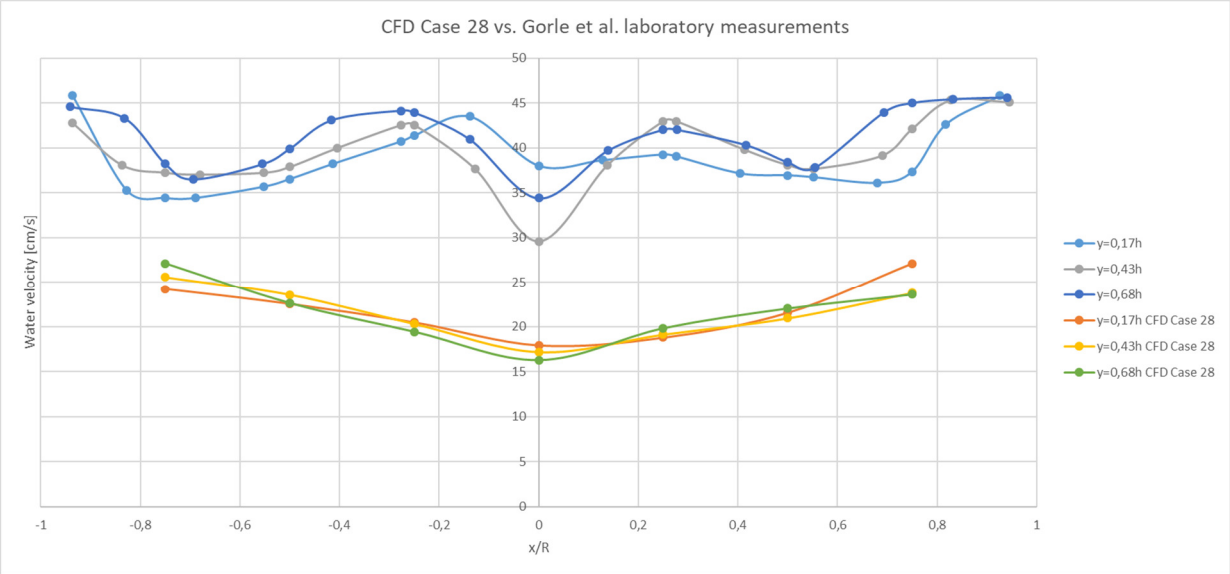

Figure 57 Gorle et. al. (2019) laboratory measurements vs. CFD water velocities

The CFD simulations estimated water velocities of lesser magnitude than those measured by Gorle et al. (2019). While an exhaustive comparison for each measured velocity was not performed due to the laborious and potentially inaccurate task of extracting from the presented graphs the measured standard deviations for each sample, it can be observed that the CFD velocities differed in around two times the maximum standard deviation of the measuring equipment utilized by Gorle et al. (2019). When looking at the CFD simulations from the paper, their estimated water velocity values fell within one standard deviation from the measured values and were considered by them as a "quality solution to analyze the flow and make decisions to improve the system" (Gorle et al., 2019).

4.2.2 Results from the variations on turbulence parameters

The computational times required to solve the simulations (Case 29 and Case 33) were of 0:17:46 and 0:22:45 [hr:min:s] respectively. The effect on the estimated velocities by the CFD simulations when varying the turbulence parameters at the inlet flows for Case 29 and Case 33 are presented in Figure 58, Figure 59 and Figure 60.

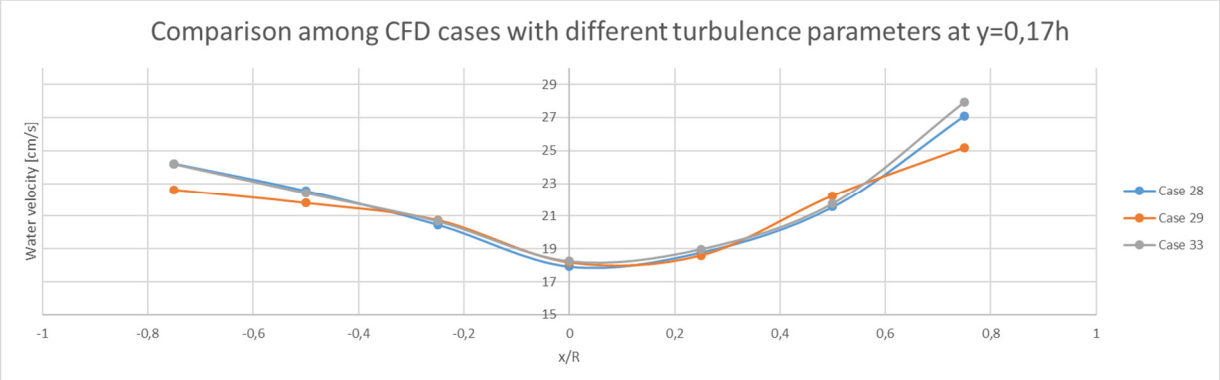

Figure 58 Effect of changes in turbulence parameters on the estimated water velocities for y=0,17h

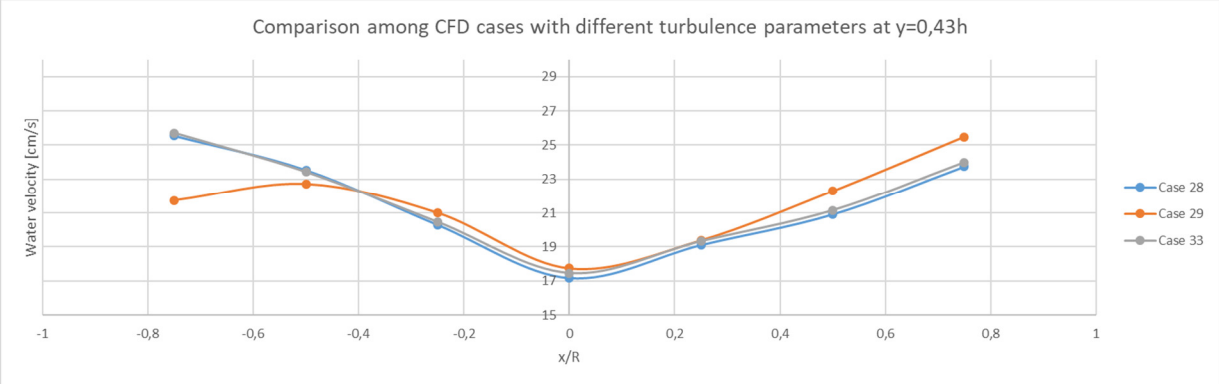

Figure 59 Effect of changes in turbulence parameters on the estimated water velocities for y=0,43h

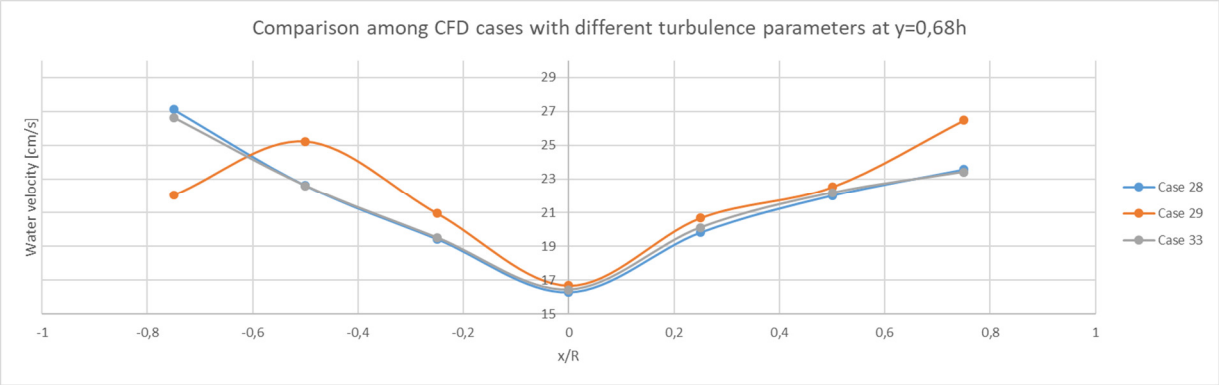

Figure 60 Effect of changes in turbulence parameters on the estimated water velocities for y=0,68h

Compared against the base case (Case 28), no large effect on the velocity profiles was observed when varying the turbulence length parameter at Case 33 for the inlet flow (from 0,0035m to 0,3m).

On the contrary, a noticeable change in the velocity profiles for the three water depths, particularly at larger x/R positions, was observed when drastically increasing the turbulence intensity from 5% to 15%.

While the scope of this work is not to investigate the water flow within the inlet pipe and resultant turbulence properties of the water jets exiting the nozzles, this points out an interesting area for further research and possible optimization of inlet pipe designs in order to provide favorable turbulence characteristics to control the overall water flow patterns and water velocities in the tank.

4.3 Validation against experimental data

4.3.1 Inlet pipe separated from the tank's wall

4.3.1.1 Case 30 (with and without velocity meter)

A simulation including the velocity meter at the 1HT position was performed for the first day of sampling, namely *Case 30*. The resultant flow pattern was found, as expected, to be affected by the presence of the velocity meter. As seen on Figure 61 and Figure 62, the flow was deviated from its natural trajectory towards the inside of the flow meter, thus changing the flow from a multidirectional flow to almost a purely flow in the z-direction.

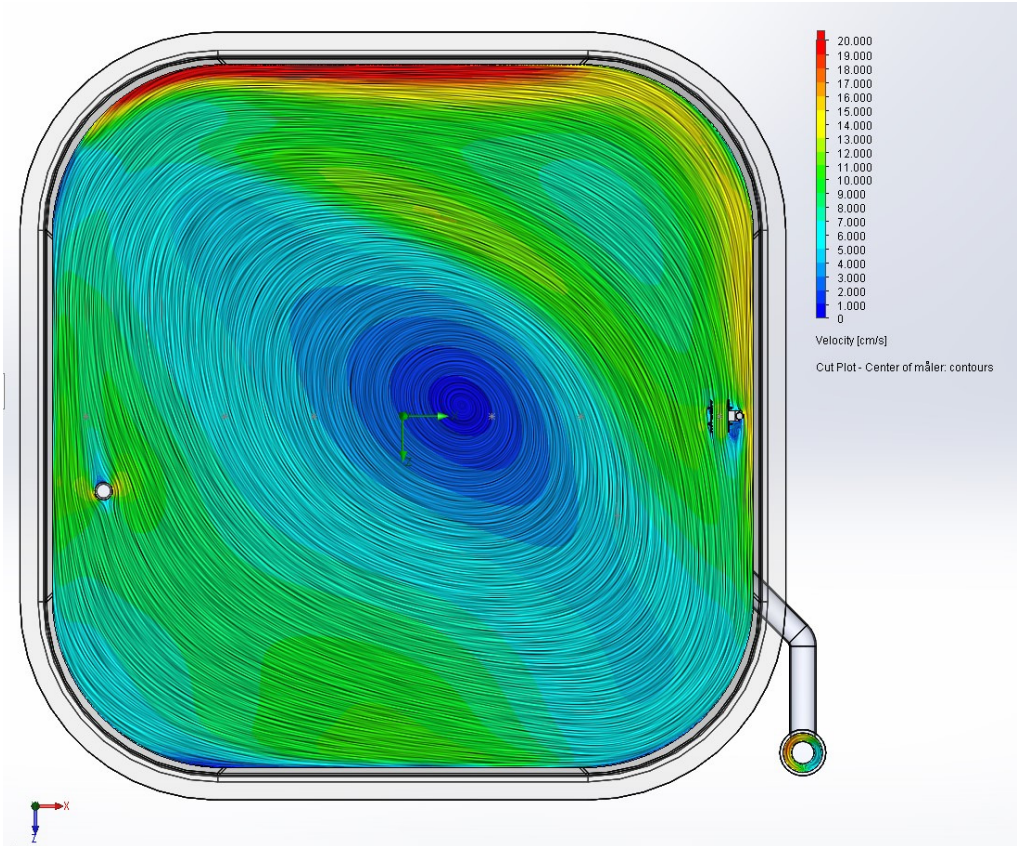

Figure 61 Water velocity Case 30, 1HT - streamline profile at middle plane of velocity meter

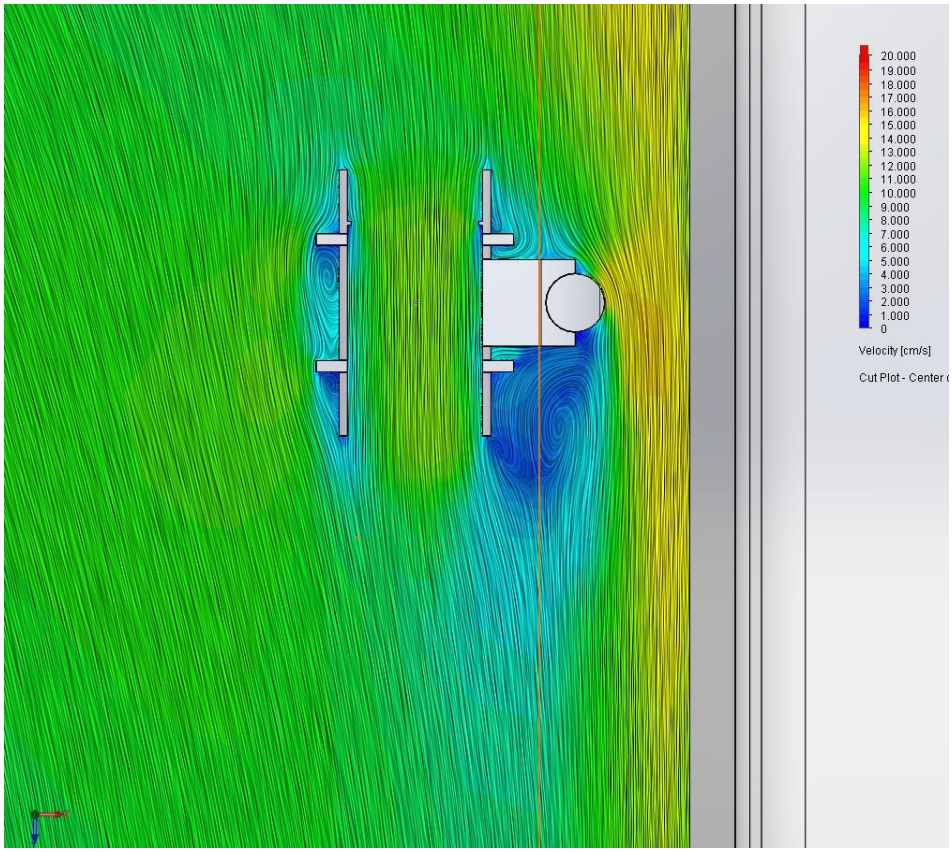

Figure 62 Water velocity Case 30, 1HT - streamline profile detail at middle plane of velocity meter

The degree of how much the flow is affected from its natural path will depend on the direction of the flow compared to the alignment of the velocity meter. Since the velocity meter was always aligned with the z-axis, this meant that the tested location for that particular water depth was one of the less affected by the presence of the meter, as can be deducted from the overall flow pattern in Figure 61.

Case 30 without velocity meter evaluated the velocities without the presence of the meter. Table 7 shows the estimated water velocities for both cases. It can be seen that the presence of the meter did not only affect the velocities at the position of the meter but also the overall distribution of the velocities tested (for that particular sampling day).

The CPU time required to solve the simulation with the velocity meter was of 6:39:21 (hr:min:s). The CPU time used to solve the simulation without the velocity meter was of 8:56:6.

Table 7 Comparison of CFD velocities for Case 30 with and without meter at 1HT

	Case 30 without velocity meter	Case 30 with velocity meter at 1HT
Goal Name	Averaged Value	Averaged Value
PG Velocity 1HT	10,91224687	11,82675108
PG Velocity (Z) 1HT	10,52109389	11,82431132
PG Velocity 1HB	10,64987651	10,0302032
PG Velocity (Z) 1HB	9,432259142	8,820550602
PG Velocity 2HT	5,814656468	5,306063222
PG Velocity (Z) 2HT	5,404392659	4,904806367
PG Velocity 2HB	7,21597511	6,987809573
PG Velocity (Z) 2HB	7,010934677	6,764671431
PG Velocity 3HT	1,14006339	0,837601629
PG Velocity (Z) 3HT	1,057949398	0,643516319
PG Velocity 3HB	4,28601971	4,42689095
PG Velocity (Z) 3HB	3,963550249	4,023400259

It can also be seen that the velocity in the z-direction for the location of the velocity meter (1HT) is almost identical to the total velocity simulated, while for the rest of the locations there is a larger difference between the total velocity and its z-component.

4.3.1.2 Case 30-32

For the simulations of the combined measurements from the three days of sampling, the velocity meter was not further included in the model.

The water level measured at the three days as well as the measured water flow (bucket and stop-clock method) were averaged to use in this combined simulation. The resultant effective D/H ratio with this water level was of 1,3575.

The computational time to solve the simulation was of 14:29:17 [hr:min:s]. The resultant flow trajectories are shown in Figure 63, Figure 64, Figure 65, Figure 66, Figure 67 and Figure 68.

While it was not possible to capture in a good way the water behavior at the laboratory in pictures, it should be mentioned that some of the flow features were recognizable also in real life; such as the abrupt change in direction near the water surface at the first corner downstream of the inlet flow and the low velocity zone behind the inlet pipe.

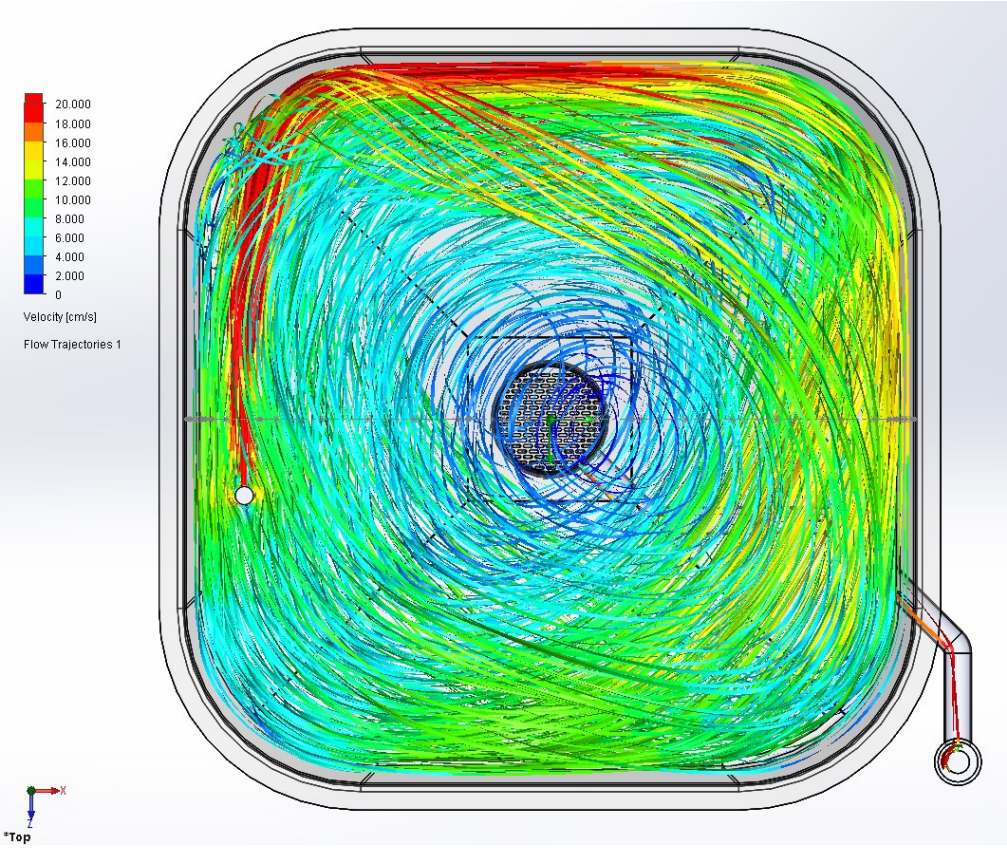

Figure 63 Flow trajectories combined Case 30-32 - top view

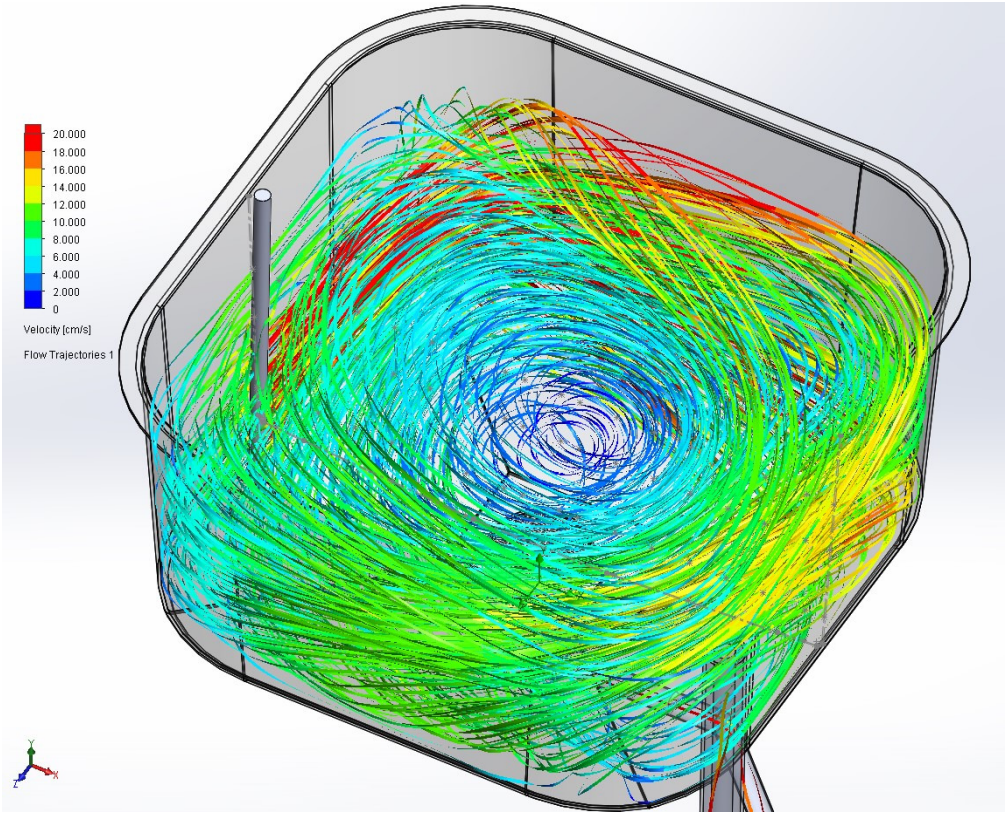

Figure 64 Flow trajectories combined Case 30-32 - Isometric front view

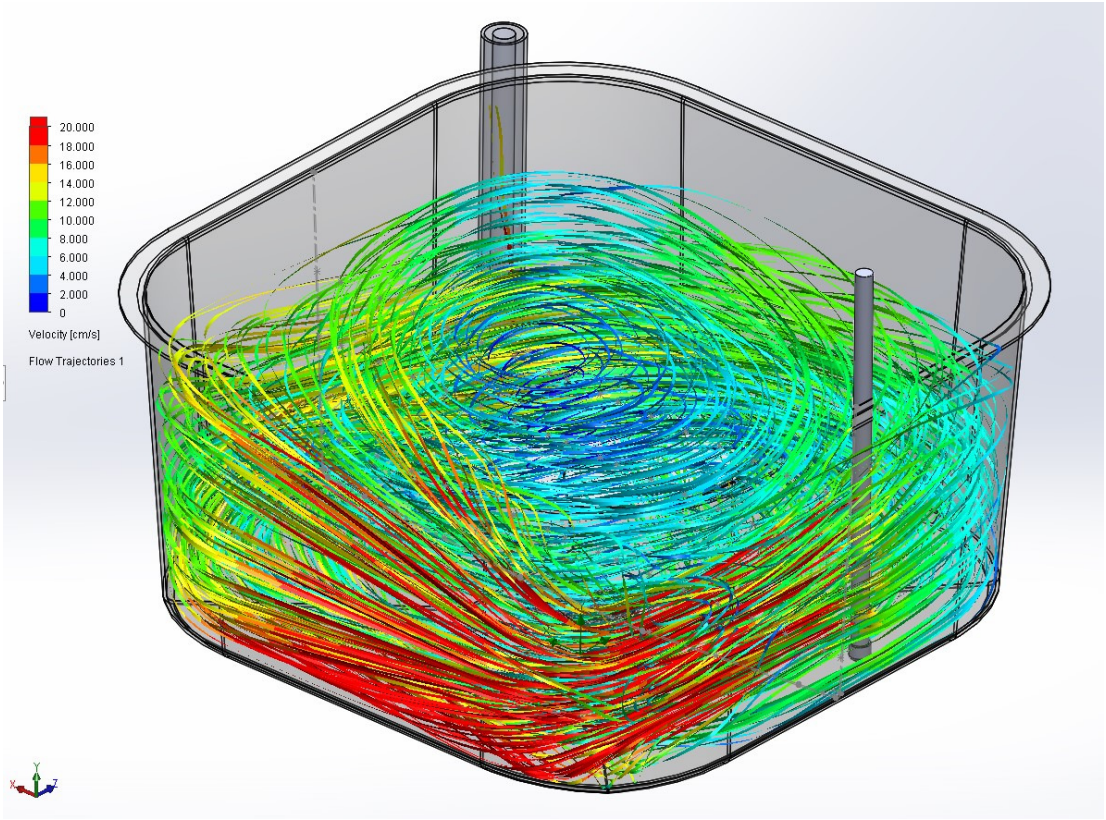

Figure 65 Flow trajectories combined Case 30-32 - isometric back view

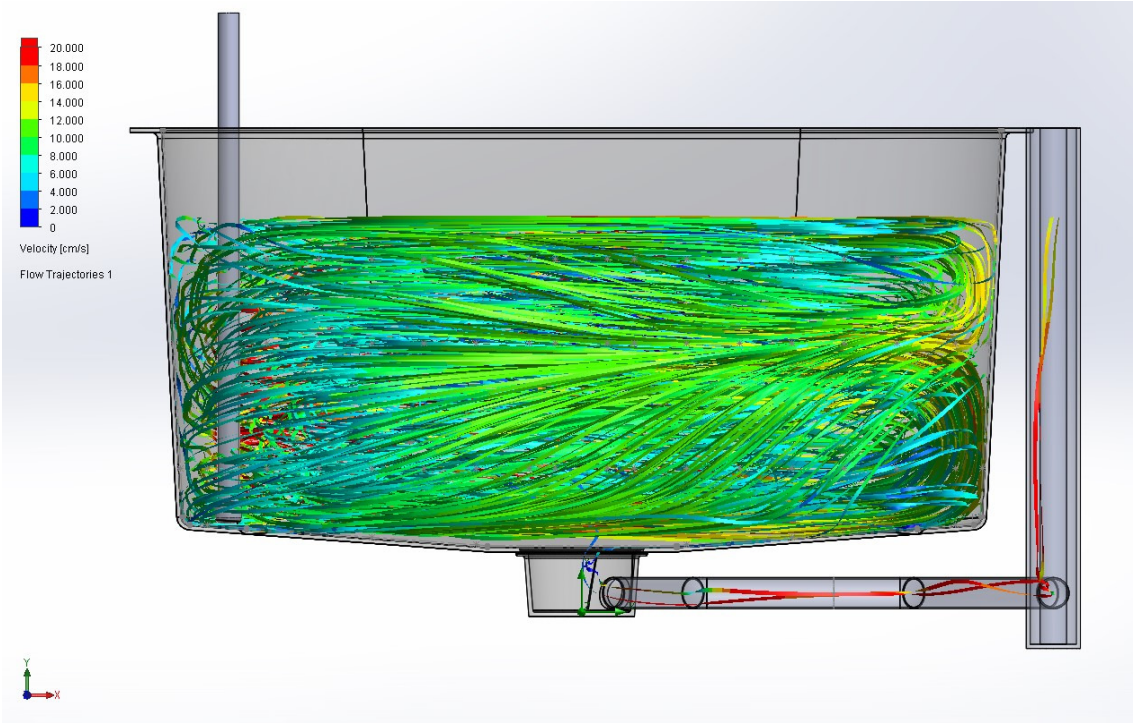

Figure 66 Flow trajectories combined Case 30-32 - front view

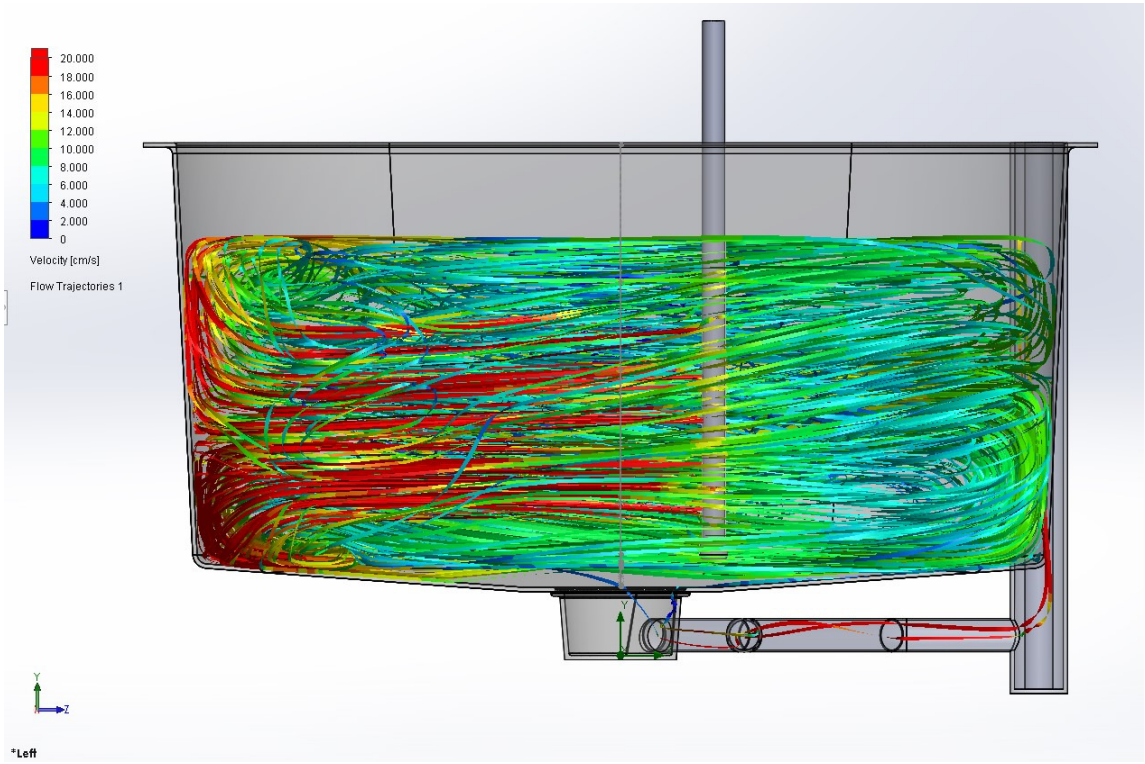

Figure 67 Flow trajectories combined Case 30-32 - left view

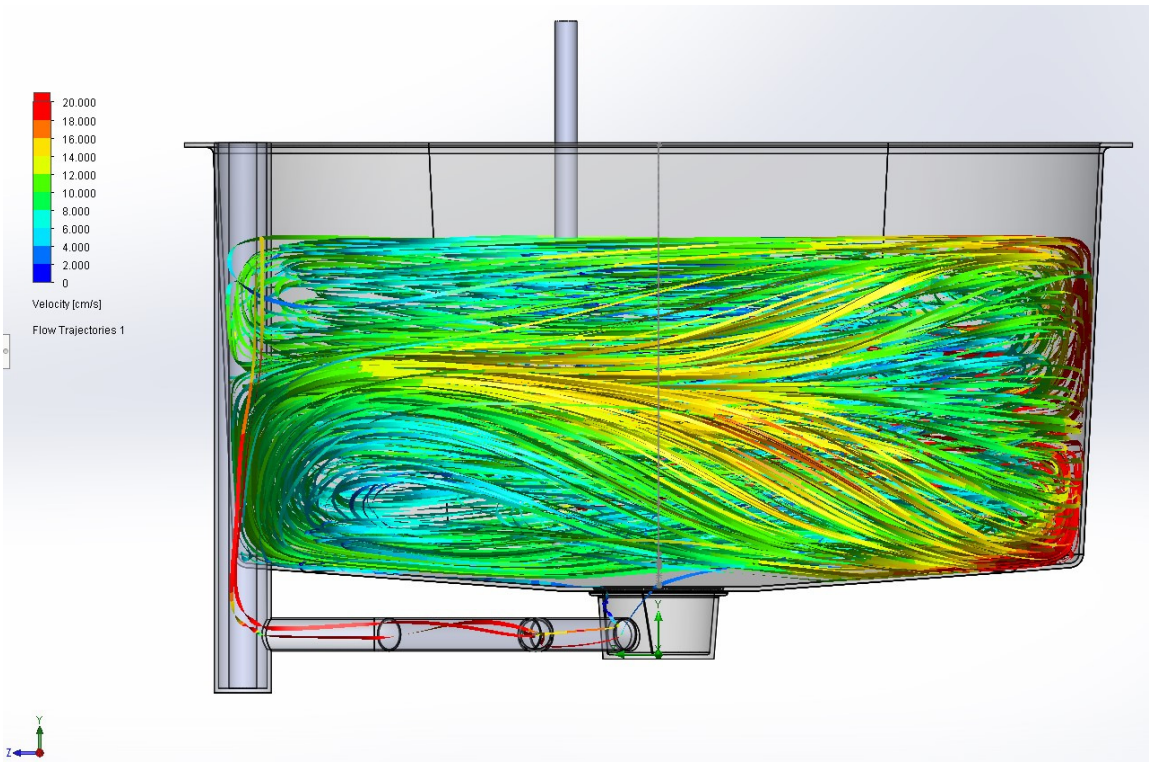

Figure 68 Flow trajectories combined Case 30-32 - right view

The average velocities measured at the laboratory for the three days of sampling are presented in Table 8. Additionally the standard deviation of the measured velocities and the CFD velocities (total and in z-direction) are presented in the same table for comparison purposes.

Table 8 Measured water velocities and CFD velocities for combined Case 30-32

		Combined 30-32			
Name	x [m]	Velocity [cm/s]	Std. Dev. [cm/s]	CFD velocity [cm/s]	CFD Velocity (Z) absolute [cm/s]
1VB	-0,89	0,233090283	0,197982806	13,05470925	12,99446207
1VM	-0,89	0,582725708	0,257446863	11,80344761	11,47350513
1VT	-0,89	0,336685965	0,176072187	8,706760803	8,420030424
2VB	-0,5	0,336685965	0,207646118	7,541123343	7,072002801
2VM	-0,5	0,155393522	0,186871972	6,192918287	6,053355066
2VT	-0,5	0,220140823	0,246124922	5,46000317	5,279444349
3VB	-0,25	0,077696761	0,13347998	3,686003654	2,443506782
3VM	-0,25	0,116545142	0,157935643	3,888784972	3,765433818
3VT	-0,25	0,142444062	0,173009828	3,733174678	3,710115895
3HB	0,25	0,097840366	0,223177392	4,59462332	4,167012151
3HM	0,25	0,336685965	0,221753598	2,704715398	2,671495365
3HT	0,25	0,073380274	0,220140823	0,721496482	0,460159917
2HB	0,5	0,097840366	0,223177392	7,36855562	7,047512212
2HM	0,5	0,466180566	0,310179444	8,234132878	7,940310337
2HT	0,5	0,51366192	0,38129509	5,575946483	5,31867453
1HB	0,89	0,244600914	0,232048802	10,4646044	9,118108202
1HM	0,89	1,307895478	0,164565172	14,96585071	14,41704483
1HT	0,89	0,220140823	0,190647545	11,0061934	10,75841041

When the information from Table 8 is presented in a graph, it is also obvious that the measured velocities are quite far below the estimations from the CFD simulations. The data from Table 8 is plotted in Figure 69 and Figure 70.

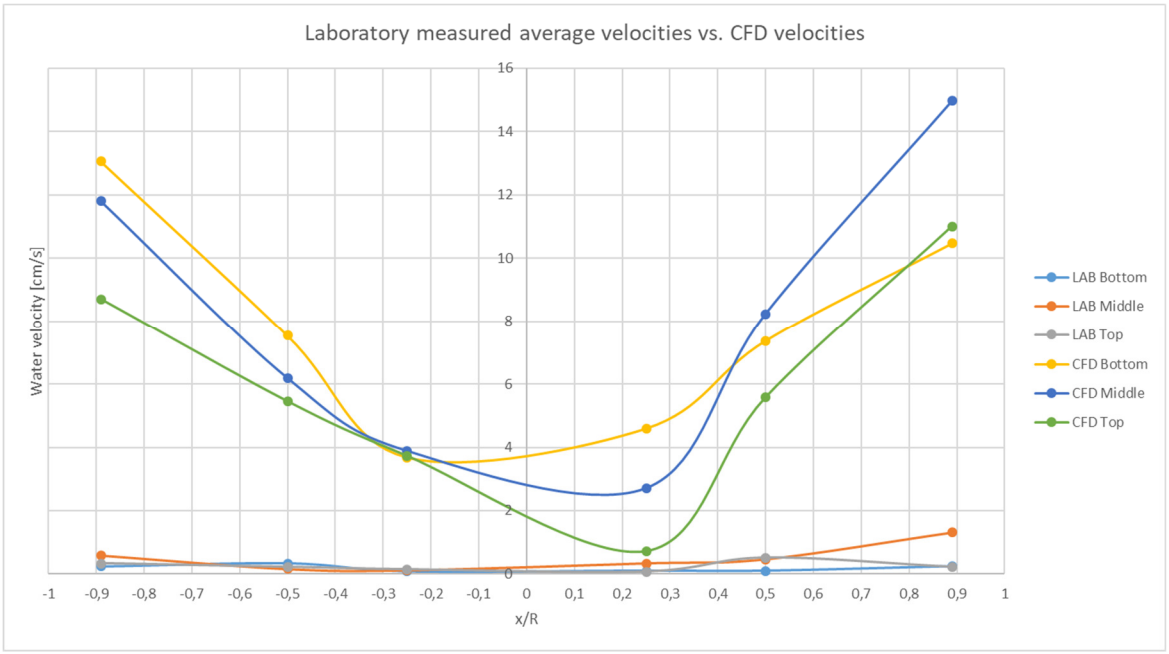

Figure 69 Laboratory measured water velocities vs CFD velocities

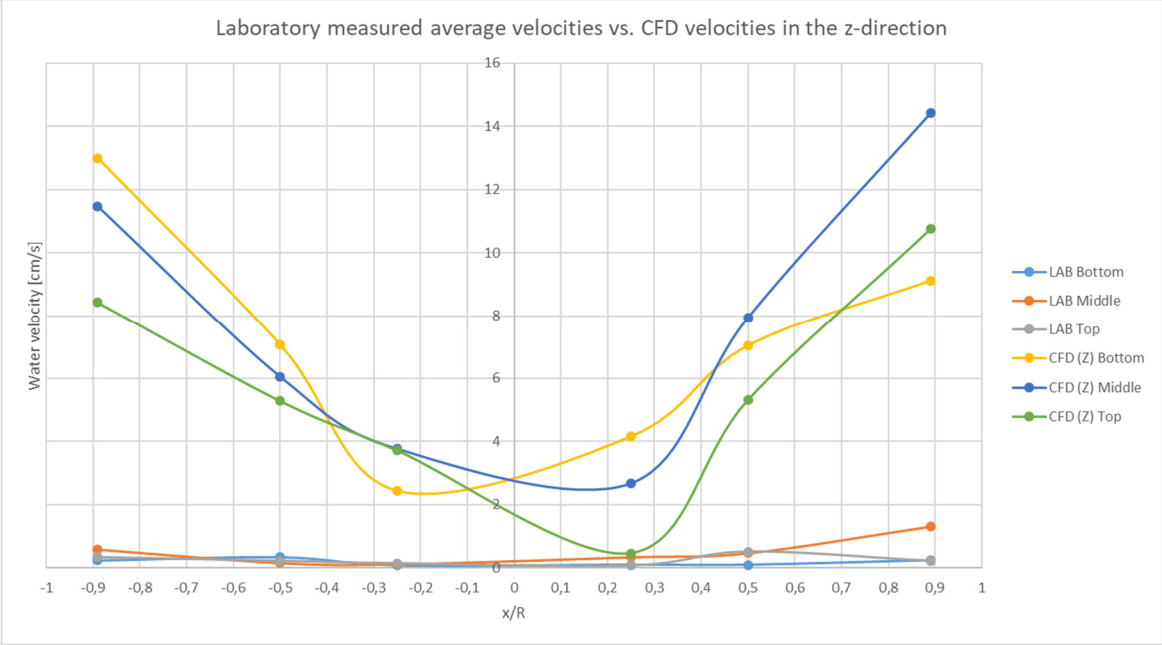

Figure 70 Laboratory measured water velocities vs. CFD velocities in the z-direction

It can be seen that neither the velocities nor the velocities in the z-direction simulated with help of CFD are close to the values measured at the laboratory. This difference in values goes also far beyond the standard deviation of the measurements (see Table 8).

It is believed, as previously pointed out, that the velocities registered by the velocity meter are not representative of the actual velocities in the tank. The extremely lower values registered are believed to be due to the fact that the equipment was operating far below its range of measurement. It is worth recalling that the equipment was believed to be composed of a flow meter which had a measuring range starting from a value 10 times larger the registered flow measurements at the lab. The operational range extended to approximately 200 times the water flow measurements at the lab.

Each of the flow measurements registered when sampling was later converted to velocity measurements by dividing the flow on the cross sectional area of the meter. Care was taken in the conversion and consistency of the units utilized, so the differences are not believed to be error related to this conversion of values.

The sampling registers for all sampling days are presented in Appendix 8: Water velocities sampled at the laboratory. Additionally all of the goal tables exported from the simulation software are included in Appendix 9: Goal tables from simulations

4.3.2 Inlet pipe adjacent to tank's wall

4.3.2.1 Case 34-37

In the same way as for in Case 30-32, in the simulations for Case 34-37 the average of the water level measured, as well as the average of the water flow on the sampling days was used. The effective D/H ratio for this water level was of 1,3580.

The computational time required to solve the simulations was of 9:39:13 [hr:min:s]. The resulting flow trajectories were are depicted in Figure 71, Figure 72, Figure 73, Figure 74, Figure 75 and Figure 76.

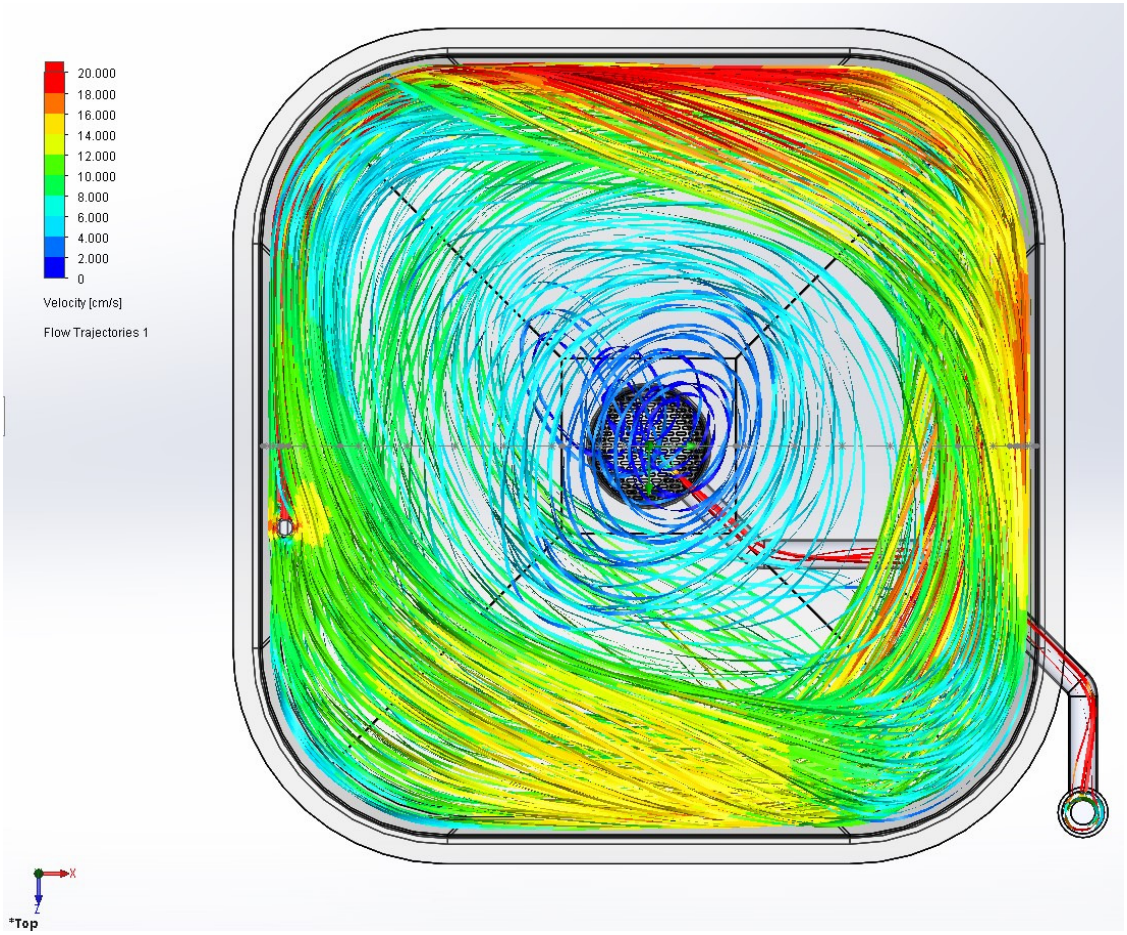

Figure 71 Flow trajectories combined Case 34-37 - top view

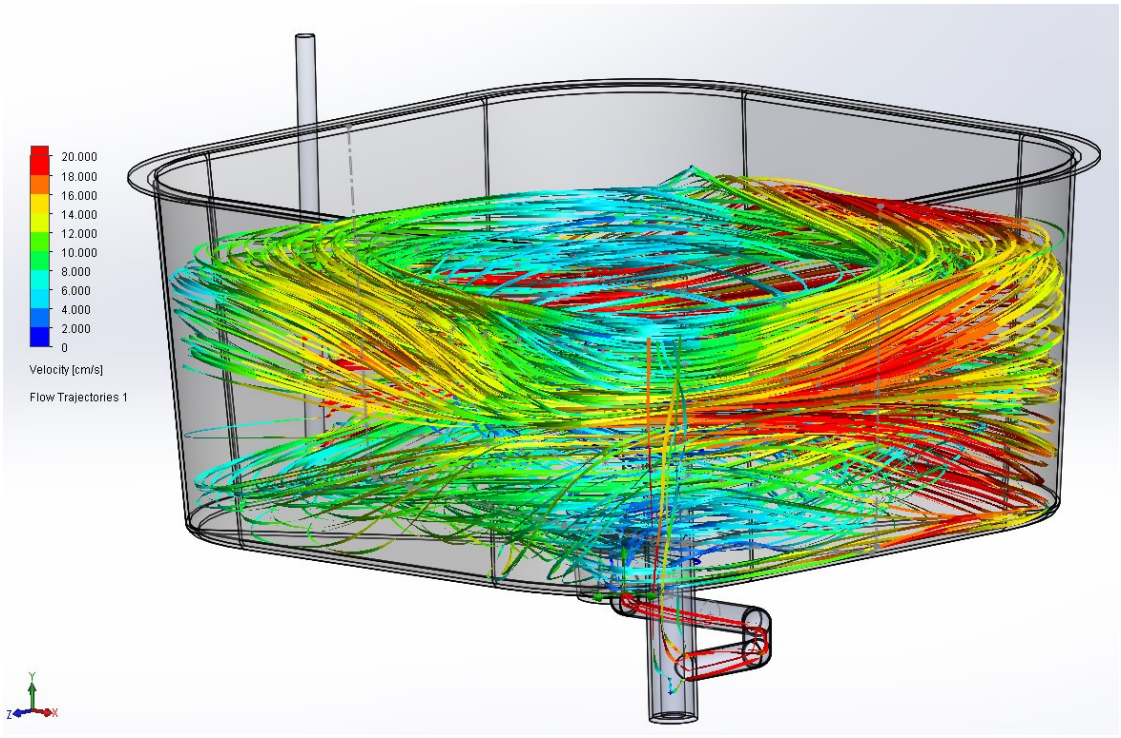

Figure 72 Flow trajectories combined Case 34-37 - isometric front view

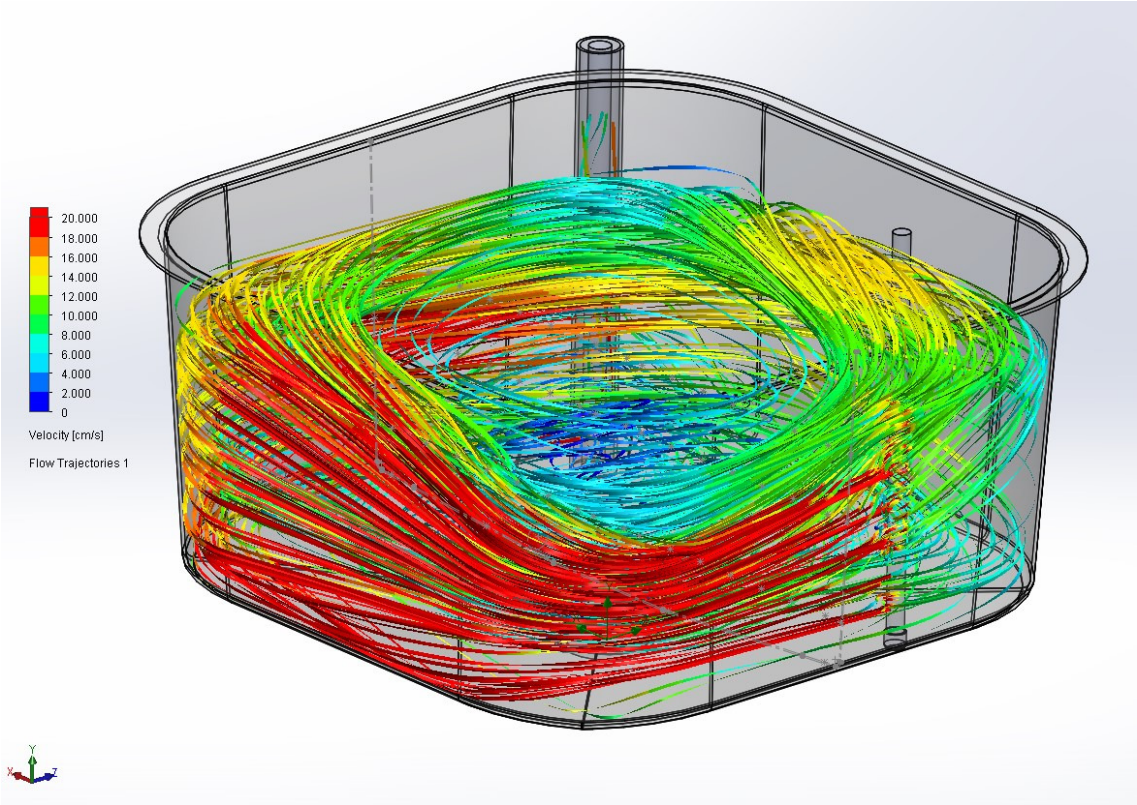

Figure 73 Flow trajectories combined Case 34-37 - isometric back view

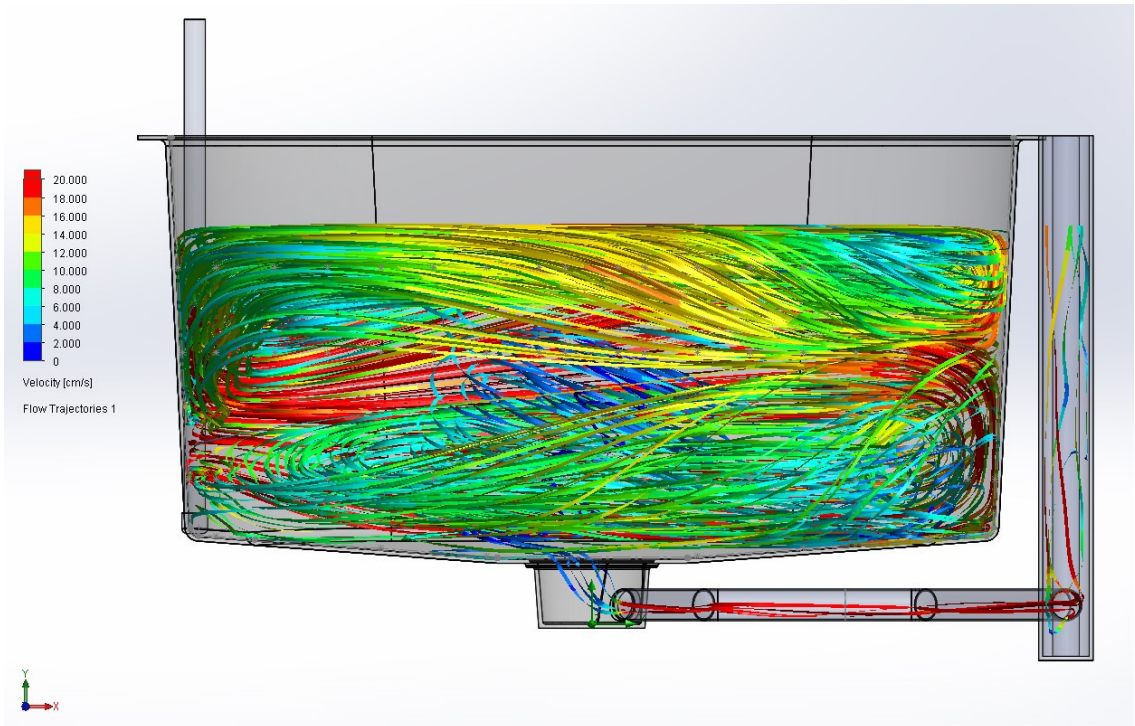

Figure 74 Flow trajectories combined Case 34-37 - front view

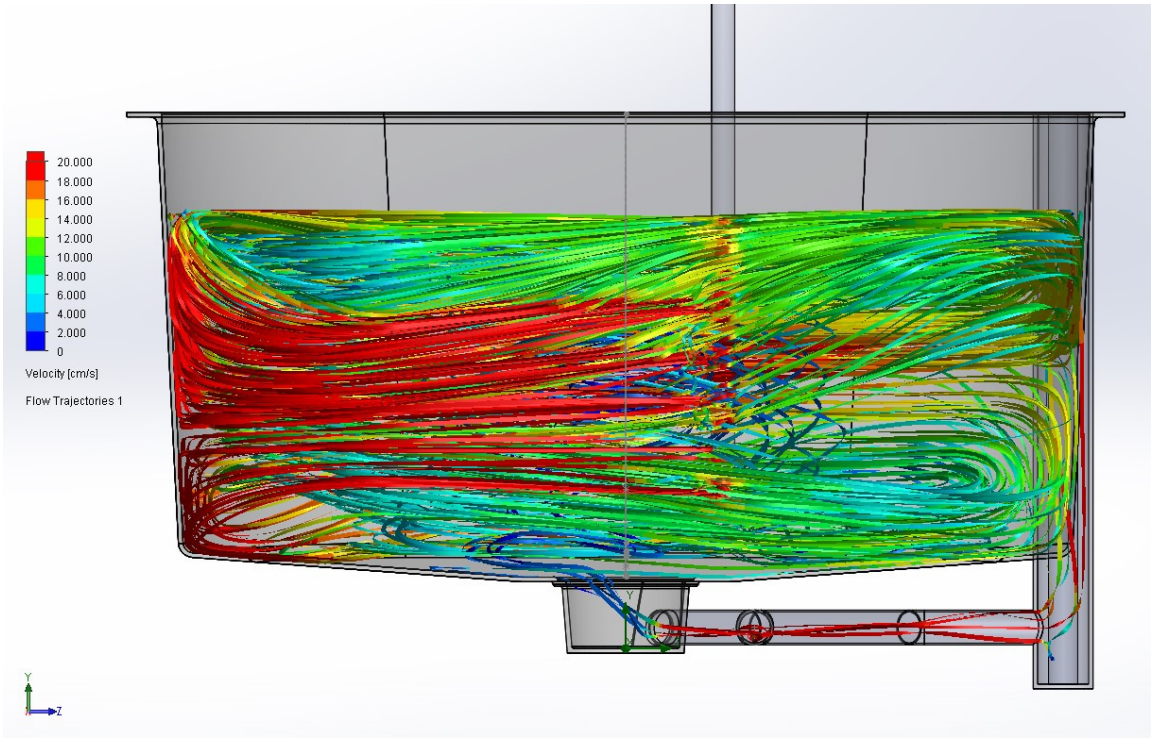

Figure 75 Flow trajectories combined Case 34-37 - left view

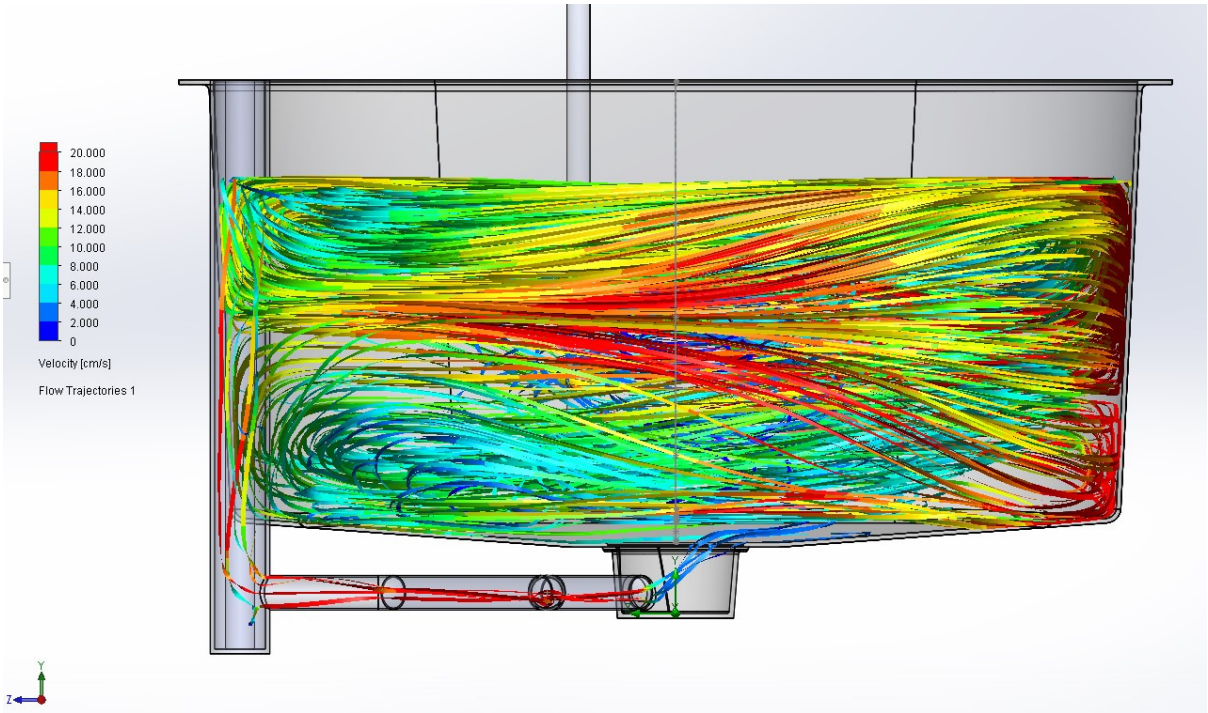

Figure 76 Flow trajectories combined Case 34-37 - right view

While the flow pattern looks similar to that of the combined Case 30-32, some discrepancies were encountered. The most notably is the seemingly stronger split of the flow into two layers, an upper and a lower layer.

Each of this layers has a characteristic rotation created by the flow trying to get spread from about its centerline towards the water surface and tank's bottom. Since the water surface and tank's bottom represent boundaries for the flow to further ascend or descend, respectively, a rotation of

each individual layer is achieved. This apparent rotation could contribute as a secondary flow for the transport of particles.

While the intensity of this rotation may not be adequately represented in a streamline profile representation, the division of the flow in layers and its rotating action is clearly visible in Figure 77.

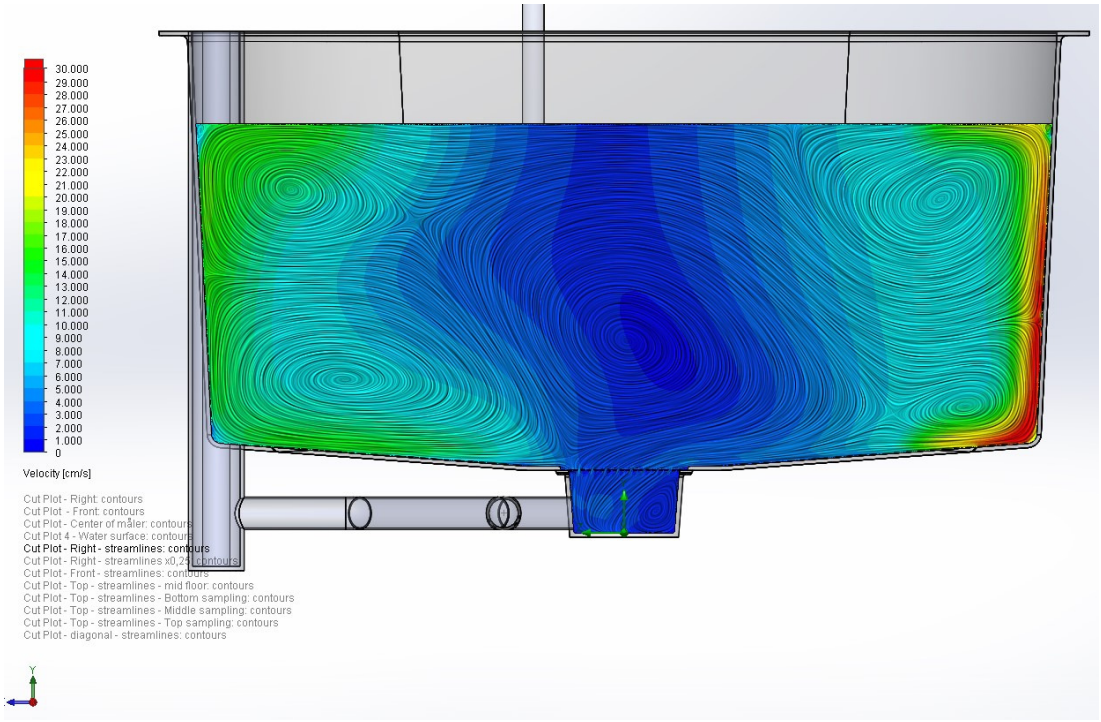

Figure 77 Water velocities combined Case 34-37 - streamline profiles at right plane

The presence of all of the secondary rotating vortices is not experienced at all locations of the tank, as can be seen when projecting the streamline profiles at the front plane in Figure 78.

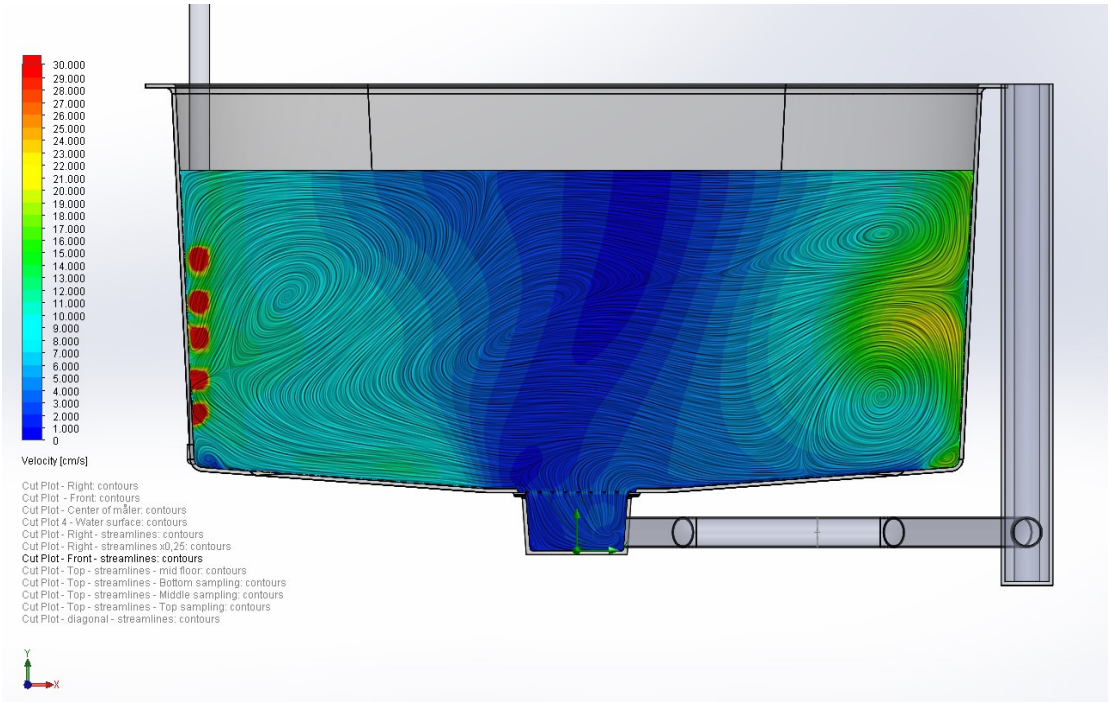

Figure 78 Water velocities combined Case 34-37 - streamline profiles at front plane

It is nevertheless possible to infer the possibility of particle transport when looking at a streamline profile velocity projection near the tank's bottom, particularly at the front sector of the tank, as depicted in Figure 79.

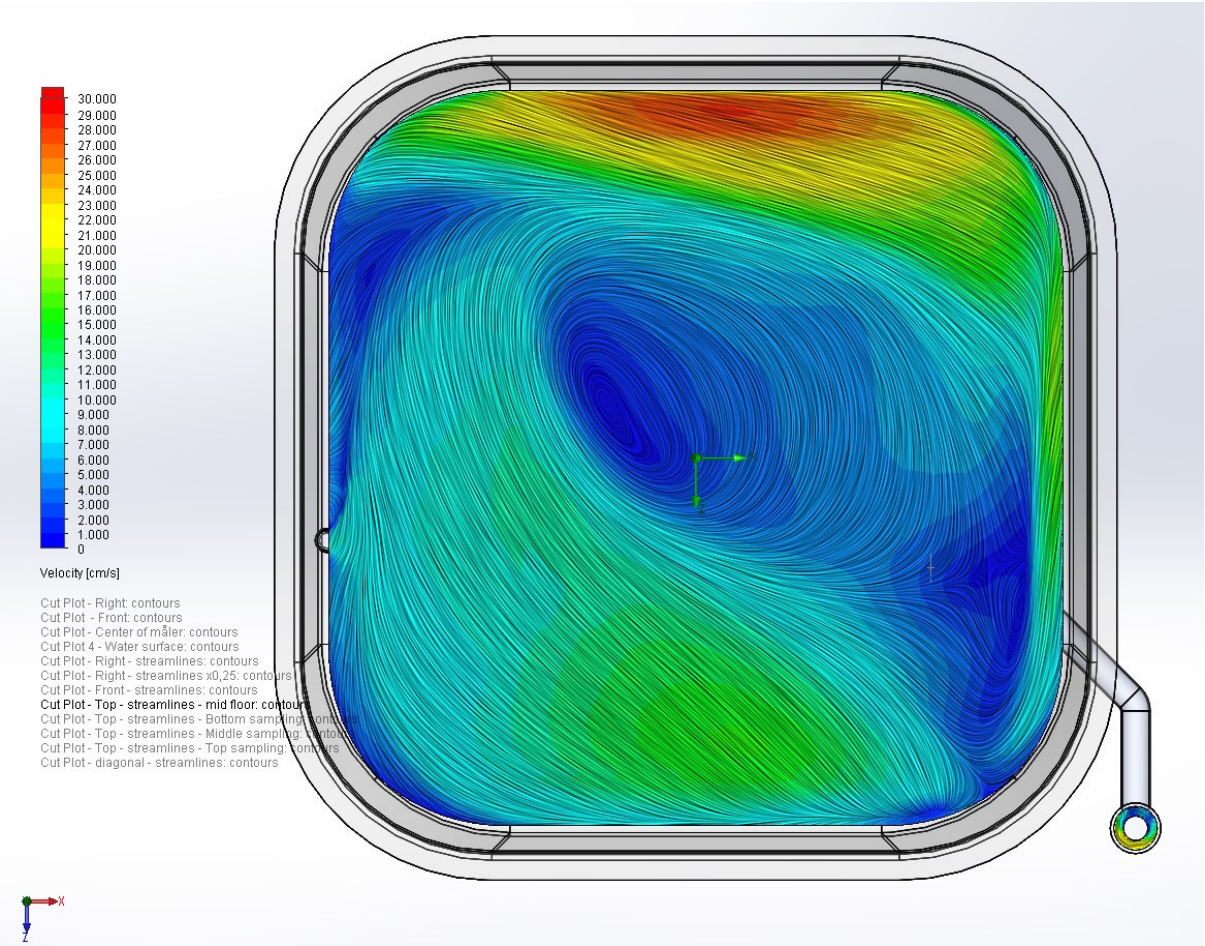

Figure 79 Water velocities combined Case 34-37 - streamline profiles near tank bottom

Another characteristic feature of the flow is a scarcely dense flow area behind the inlet pipe, see Figure 74. This feature is more pronounced for this inlet pipe position and may indicate poor water mixing at this area.

Another feature visible was that the abrupt change in direction downstream the inlet jets was partially reduced (Figure 71 vs. Figure 63). This may be explained by the water jets hitting the start of the corner radius of the tank instead than hitting at the middle or end section of the radius closer to the perpendicularly placed wall in front.

The measured water velocities at the laboratory and their standard deviation are presented in Table 9 . The estimated CFD velocities and the CFD velocities in the z-direction are also presented in the table.

Table 9 Measured water velocities and CFD velocities for combined Case 34-37

		Combined			
Name	x [m]	Velocity [cm/s]	Std. Dev. [cm/s]	CFD velocity [cm/s]	CFD velocity (Z) absolute [cm/s]
1VB	-0,89	1,333794398	0,094384599	10,67526359	10,30915933
1VM	-0,89	1,346743859	0,106783984	11,5228462	10,77180785
1VT	-0,89	1,281996558	0,160175976	11,05164608	10,52758979
2VB	-0,5	0,297837584	0,279989969	7,957000049	7,64358222
2VM	-0,5	0,854664372	0,153356822	7,191928776	6,994036453
2VT	-0,5	0,906462213	0,171976924	5,31117698	5,078276325
3VB	-0,25	0,077696761	0,13347998	3,505941821	3,129246622
3VM	-0,25	0,556826788	0,113261519	4,34606774	4,261134873
3VT	-0,25	0,556826788	0,137426051	3,389601531	3,368109964
3HB	0,25	0,517978407	0,108439649	3,931202217	3,664136314
3HM	0,25	0,530927867	0,191579813	2,285662453	2,272091059
3HT	0,25	0,530927867	0,258827285	1,37009922	1,288080877
2HB	0,5	0,492079487	0,183018528	6,633379453	6,505964565
2HM	0,5	0,906462213	0,073109996	6,888093557	6,840660407
2HT	0,5	0,958260053	0,205055837	5,190402332	5,120991054
1HB	0,89	1,307895478	0,144996373	10,61324549	9,872985982
1HM	0,89	1,696379283	0,129413642	18,24395152	17,82310921
1HT	0,89	1,385592239	0,129413642	13,12103219	12,95120175

As with the measured velocities for Case 30-32, there is a large difference between the readings from the velocity meter and what has been calculated in the CFD simulations for both the total velocities and their z-component.

Figure 80 and Figure 81 show the plotted velocity values from the laboratory measurements and the CFD simulations.

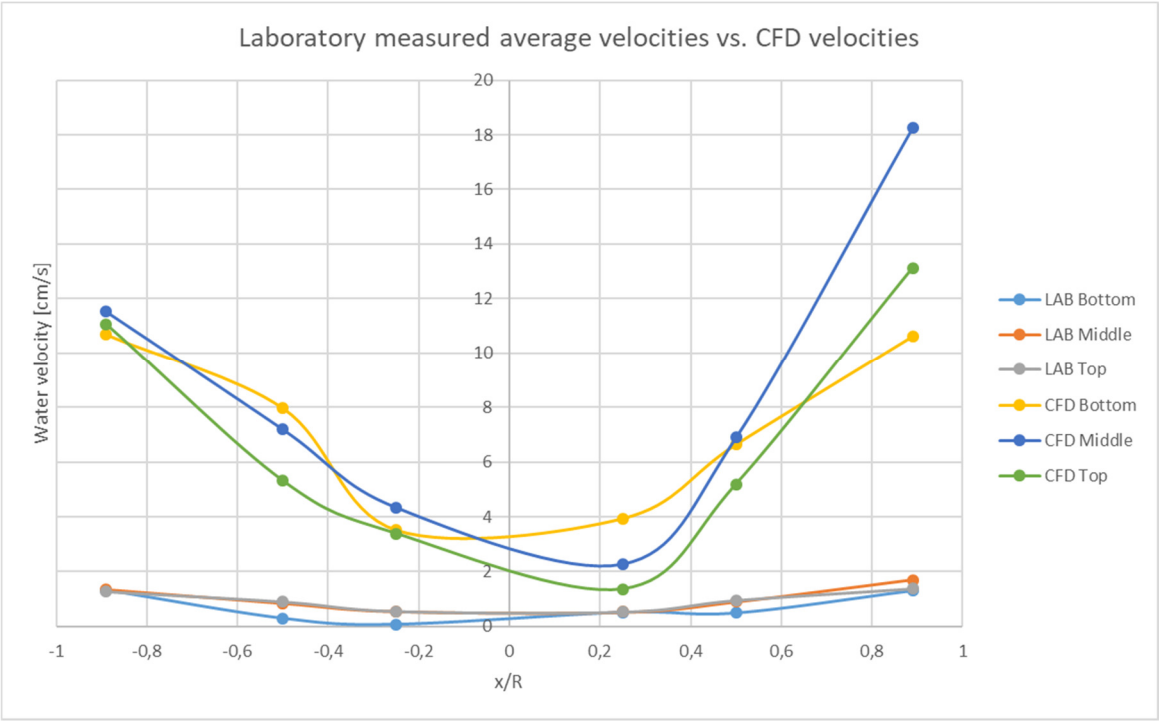

Figure 80 Laboratory measured water velocities vs. CFD velocities

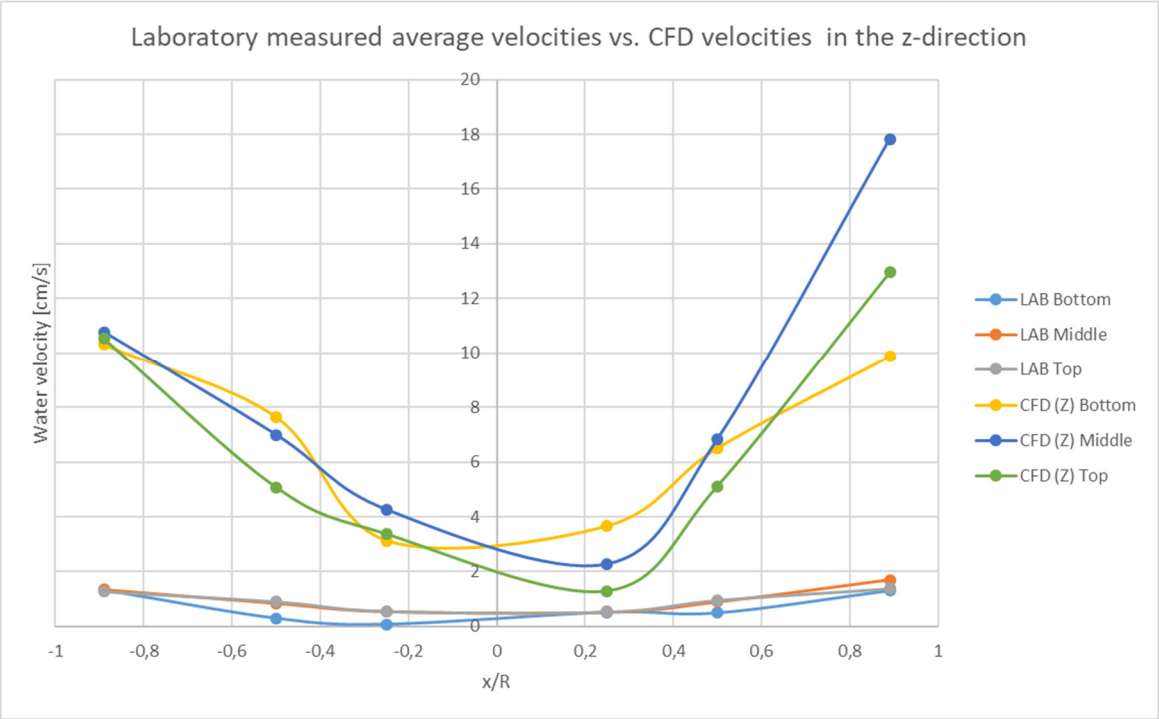

Figure 81 Laboratory measured water velocities vs. CFD velocities in the z-direction

For both the simulated and measured velocities, the maximum velocities are those of the middle plane of sampling, to a level close to the highest inlet nozzle. This is in line with what could be expected from theory; based on the fact that the inlet nozzles did not extend to the top level of the water column, the maximum velocities therefore would be expected at the locations of less energy losses and maximum torque. For an inlet with nozzles along the whole water column these maximum velocities would be expected near the water surface and away from the tank's center (Oca & Masalo, 2013).

While it can be said that the estimated velocities and the laboratory measurements follow a similar trend, with lower values near the center of the tank, the extremely low values registered by the meter and the poor resolution does not allow in a reliable manner for further trying to identify similitudes with the CFD simulations.

4.3.3 Turbulence parameters evaluation

The turbulence properties of the flow were evaluated at the locations of the sampling points for both of the inlet configurations. The software iterates from the initial values and adjust continuously along the solution process. While these goals were not used for convergence of the solution, it could be seen from the progress graphs in the solver monitor that both the turbulence intensity and turbulence length had already acquired a seemly stable state, see Figure 82 and Figure 83. It is nevertheless considered not suitable to include these as goals for convergence assistance due to the relative large variation in the values which may impede to reach a convergence given the convergence criteria given automatic by the software.

It is observed in the tabulated results of the turbulence length and turbulence intensity, shown in Table 10 and Table 11 , that a broad range of values are experienced, indicating thus the multi-scalar complexity of the small turbulent features in the tank.

Table 10 CFD turbulence length at sampling positions for both inlet configurations

Cases 30-32		
PG Turbulence Length - 1HB	[m]	0,02028
PG Turbulence Length - 1HM	[m]	0,012471
PG Turbulence Length - 1HT	[m]	0,036285
PG Turbulence Length - 2HB	[m]	0,051953
PG Turbulence Length - 2HM	[m]	0,052078
PG Turbulence Length - 2HT	[m]	0,049662
PG Turbulence Length - 3HB	[m]	0,066701
PG Turbulence Length - 3HM	[m]	0,088958
PG Turbulence Length - 3HT	[m]	0,094767
PG Turbulence Length - 1VB	[m]	0,004274
PG Turbulence Length - 1VM	[m]	0,005975
PG Turbulence Length - 1VT	[m]	0,010772
PG Turbulence Length - 2VB	[m]	0,04343
PG Turbulence Length - 2VM	[m]	0,080787
PG Turbulence Length - 2VT	[m]	0,087838
PG Turbulence Length - 3VB	[m]	0,032739
PG Turbulence Length - 3VM	[m]	0,083035
PG Turbulence Length - 3VT	[m]	0,092081

Cases 34-37		
PG Turbulence Length - 1HB	[m]	0,020499
PG Turbulence Length - 1HM	[m]	0,007491
PG Turbulence Length - 1HT	[m]	0,034155
PG Turbulence Length - 2HB	[m]	0,066404
PG Turbulence Length - 2HM	[m]	0,087244
PG Turbulence Length - 2HT	[m]	0,098091
PG Turbulence Length - 3HB	[m]	0,075407
PG Turbulence Length - 3HM	[m]	0,124396
PG Turbulence Length - 3HT	[m]	0,132787
PG Turbulence Length - 1VB	[m]	0,010632
PG Turbulence Length - 1VM	[m]	0,016077
PG Turbulence Length - 1VT	[m]	0,02905
PG Turbulence Length - 2VB	[m]	0,044845
PG Turbulence Length - 2VM	[m]	0,084323
PG Turbulence Length - 2VT	[m]	0,089716
PG Turbulence Length - 3VB	[m]	0,04249
PG Turbulence Length - 3VM	[m]	0,093171
PG Turbulence Length - 3VT	[m]	0,104304

Table 11 CFD Turbulence intensity at sampling positions for both inlet configurations

Cases 30-32		
PG Turbulence Intensity - 1HB	[%]	16,9043
PG Turbulence Intensity - 1HM	[%]	9,437329
PG Turbulence Intensity - 1HT	[%]	20,92962
PG Turbulence Intensity - 2HB	[%]	30,22159
PG Turbulence Intensity - 2HM	[%]	29,25869
PG Turbulence Intensity - 2HT	[%]	38,38063
PG Turbulence Intensity - 3HB	[%]	36,71351
PG Turbulence Intensity - 3HM	[%]	69,24062
PG Turbulence Intensity - 3HT	[%]	273,0532
PG Turbulence Intensity - 1VB	[%]	13,26887
PG Turbulence Intensity - 1VM	[%]	20,31915
PG Turbulence Intensity - 1VT	[%]	17,65979
PG Turbulence Intensity - 2VB	[%]	25,77633
PG Turbulence Intensity - 2VM	[%]	32,1815
PG Turbulence Intensity - 2VT	[%]	36,73827
PG Turbulence Intensity - 3VB	[%]	40,90583
PG Turbulence Intensity - 3VM	[%]	45,53364
PG Turbulence Intensity - 3VT	[%]	50,0969

Cases 34-37		
PG Turbulence Intensity - 1HB	[%]	16,8993
PG Turbulence Intensity - 1HM	[%]	5,279365
PG Turbulence Intensity - 1HT	[%]	17,25052
PG Turbulence Intensity - 2HB	[%]	30,26291
PG Turbulence Intensity - 2HM	[%]	33,12536
PG Turbulence Intensity - 2HT	[%]	38,08949
PG Turbulence Intensity - 3HB	[%]	37,90601
PG Turbulence Intensity - 3HM	[%]	79,90479
PG Turbulence Intensity - 3HT	[%]	131,9523
PG Turbulence Intensity - 1VB	[%]	18,61727
PG Turbulence Intensity - 1VM	[%]	21,13354
PG Turbulence Intensity - 1VT	[%]	21,77567
PG Turbulence Intensity - 2VB	[%]	27,16263
PG Turbulence Intensity - 2VM	[%]	32,89231
PG Turbulence Intensity - 2VT	[%]	43,97239
PG Turbulence Intensity - 3VB	[%]	41,12569
PG Turbulence Intensity - 3VM	[%]	44,98293
PG Turbulence Intensity - 3VT	[%]	59,05219

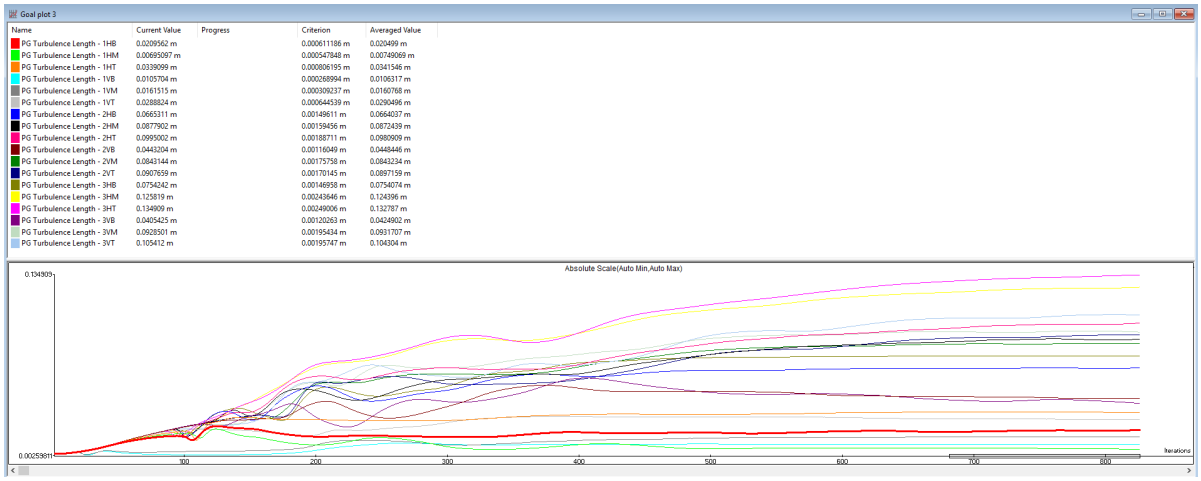

Figure 82 Convergence progress of turbulence length - Case 34-37

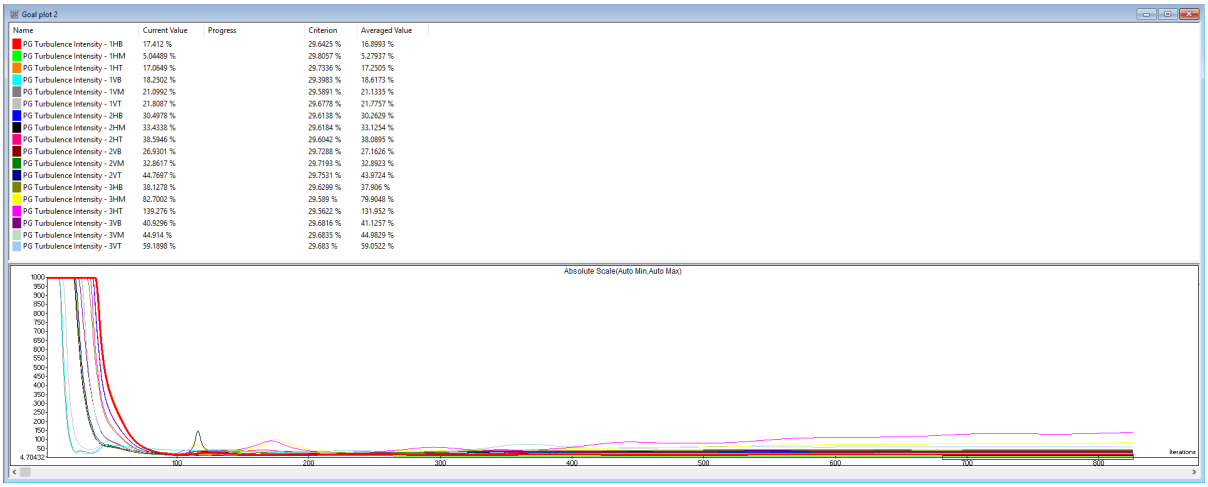

Figure 83 Convergence process of turbulence intensity - Case34-37

The information obtained by studying these parameters in the simulation is useful for determining the initial conditions for subsequent analysis, in such a way that the initial values are as close as possible to the final values and the computational efforts optimized (SOLIDWORKS-Corp., 2018a).

It can be said that the initial turbulence length values utilized in the simulations were satisfactorily well chosen and provided a good start point for further work. For the turbulence intensity values there is still room for further adjusting the initial conditions in order to potentially minimize the calculation time, as the calculated values are surprisingly greater than the chosen initial conditions.

These high turbulence intensity and small turbulence length properties of the flow confirm also the predominantly turbulent flow experienced in an aquaculture tank.

5 Discussion

Previous extensive experience on the use of SOLIDWORKS and other 3D modelling programs facilitated the task of creating appropriate models in an efficient way. Previous experience on the use of FEM structural analysis software additionally provided the basis to promptly decide the desirable characteristics of the 3D models for an effective use of the CFD simulation package.

No part of the course or the software tutorials (SOLIDWORKS-Corp., 2018c) explained how to simulate the conditions experienced in a water tank open to the atmosphere where the water level is regulated by the achieved static pressure at the bottom of the tank. It was here where the challenges of effectively simulating an aquaculture tank fell and what has been attempted through this work.

The cases for the determination of the main flow conditions, as mentioned earlier, were made to test hypotheses on how the software interpreted the conditions applied to the model.

For those cases where the Free Surface option was enabled, it was expected that the computational time would be drastically increased. Nevertheless it was decided to try this way of creating simulations in order to acquire a better sense of how much the computational time would be increased.

The simulations with the Free Surface option enabled are supposedly be able take in consideration the energy dissipation at the interface between water and air, however for the purposes of simplifying the simulation set-up and minimizing the computational efforts it was decided to continue only with steady-state, non-time dependent type of simulations. The following was considered for making this decision:

- Flow Simulation solves the time-dependent form of the Navier Stokes equations. For steady flow problems the solver iterates on the variables until there is no appreciable change. For unsteady (time-dependent) problems the solver “time-marches” in time-steps from the specified initial conditions until reaching the physical time that is specified. (SOLIDWORKS-Corp., 2018a)
- The transient state of the water flow, from when the inlet flow is started to when the flow has achieved a stable pattern was not of interest for this work. The thesis focuses on the water velocities when the tank is already in continuous operation.
- The expected time it would take for the water flow to stabilize after starting the inlet flow had to be set as the minimum Physical Time to be calculated in the simulation. The physical time would therefore be in the order of several minutes to perhaps hours.
- For all of the main flow condition settings evaluation cases, a very simple automated mesh without any refinement has been used, while for the actual investigations against literature and laboratory measurements it was expected to develop a more complex and refined mesh. Thus the expected time to solve the actual investigations was expected to be much larger.
- The computational resources available.
- It was of the interest of this work to simplify the simulation creation and solving process as much as possible while still achieving representative results.

A different type of condition at the tank water level surface was therefore needed in order to properly represent in a steady-state flow analysis the conditions inherent of an aquaculture tank.

Based on the work presented in the selected validation literature (An et al., 2018; Gorle et al., 2019) it was decided to find in the software a frictionless, symmetry or slip condition that could be used at the water surface.

It was therefore decided to seek advice with the Flow Simulation course responsible to find out if some sort of shear-free, frictionless surface condition was available in the software package. It was pointed out, and later confirmed in the software User's Guide and its Technical Reference, that the Ideal Wall condition provided the desired slip condition. (SOLIDWORKS-Corp., 2018a; SOLIDWORKS-Corp., 2018b).

This approach was also taken as an acceptable approximation of the behavior at the water-air interface even in environments more prone to wave formation such as sea cages (Gorle et al., 2018a; Klebert et al., 2018), thus neglecting in the calculations the energy dissipation effect of waves and air friction.

The criteria to stop the calculations in the simulations was chosen to be the convergence of all goals. This was decided because it was observed incomplete convergence of goals when utilizing other means to stop the simulation; such as maximum number of travels, or when trying to simultaneously satisfy multiple criterions including maximum number of travels and goal convergence. Additionally it was found that the full convergence of the goals was achievable in a reasonable amount of computational time as well as travels and iterations, meaning the flow of the aquaculture tanks studied is inherently a steady one.

Regarding the turbulence model used, other simulation software, such as ANSYS Fluent or OpenFOAM, seem to have diverse turbulence models available to solve the Reynolds Averaged Navier-Stokes (RANS) equations and apply these at the whole computational domain or even choosing different turbulent models at the boundary layer and open-water areas (An et al., 2018; Gorle et al., 2018a; Gorle et al., 2018c; Gorle et al., 2019; Klebert et al., 2018; Liu et al., 2016).

The software used in this work does not provide such flexibility. The user can nevertheless select the way the initial turbulence parameters are specified, either in terms of the turbulence length and turbulence intensity (in %) or by setting directly turbulent energy and dissipation (k-ε) values. While the main scope of this thesis work was not to evaluate the much discussed accuracy of the different turbulence models, it is important to recognize the limitations of the software in terms of the in-built single turbulence model and settings alternatives.

The 3D modelling task for the validation cases against literature could have represented a source of inaccuracy for the simulations, as not all the details of the geometry were described. For the validation against An et al. (2018) it was possible to build a very similar model by assuming some of the few missing information.

In the validation case against Gorle et al. (2019) more information about the geometry of the system was missing or unclear. It is also suspected that the authors themselves did not manage to replicate the geometry of the studied tank from reality into the simulation. These based on the apparent differences in the tank's bottom geometry used in the simulation (Fig. 4 in the paper) and the 3D model illustration presented (Fig. 1 in the paper), which could possibly be obtained from the fabrication drawings and not self-made. This could also explain the differences in the calculated volume from this work and the one presented in the paper.

The meshing was done by using a structured mesh of hexahedral cells on all cases. High degree of refinement near the solid surfaces or boundary layer was used in order to increase the solution

accuracy. Other types of mesh structure such as tetrahedral volume cells were not found available in Flow Simulation and therefore not investigated.

The total amount of fluid cells used in the validation of the simulations against literature was generally smaller than the ones used by the respective authors. For the validation against An et al. (2018), the ratio between the total amount of fluid cells in the literature against the total amount of cells used in the simulations of this work was of 4,67. The overall accuracy of the simulation was anyway considered satisfactory for this much less refined mesh. Nevertheless, the few amount of experimental sampling points presented in this paper does not allow for a comprehensive evaluation of the accuracy of the method at different sections of the tank.

In the validation against Gorle et. (2019) al, due to the different type of fluid cells used in the literature (a combination of tetrahedral, hexahedral and triangular) and that the total amount of fluid cells was not presented in the paper, it is not possible to directly calculate a ratio for the amount of total cells used in literature vs. the ones used in the simulations of this work.

Nevertheless, the total amount of cells on the validation simulations against An et al. (2018) was approximately the double than in the validation simulations against Gorle et al. (2019). By considering the volumes of the tanks, the higher refinement of the cells in the validation against An et al.(2018) becomes evident. It is therefore believed that this difference in meshing intensity is reflected in the inaccuracy of the CFD simulations vs. the laboratory measurements for the validation case against Gorle et al. (2019).

As mentioned in 3.2.6, two approaches can be taken by the software to couple the boundary layer to the main flow depending on number of cells across the boundary layer. The thickness of the boundary layer is inversely proportional to the angular velocity of the flow (Oca & Masalo, 2013). This points out further areas of investigation where the accuracy of the two approaches taken by the simulation software can be evaluated by controlling the meshing density at the boundary layer once its thickness is determined for the given flow conditions.

Another possible source of inaccuracy in the validation against Gorle et al. (2019) could be the laboratory water velocities presented in the paper and used for comparison against the CFD simulations. It was unclear if the velocities were measured before or after some modifications were performed on the outlet system. Unfortunately there was no opportunity to simulate the scenario with the modifications included and check if the simulations would match better the laboratory measurements.

For the validation against experimental data, a lot of work was put into measuring and describing the geometry accurately. It is difficult to generalize what geometry details should be included in a 3D model for CFD simulations. Nevertheless for such a small tank, the relatively large size of the included geometry features, compared to the overall water volume, are believed to have an impact in the flow patterns.

The same applies for the objects or structures within the tank, and how these affect the overall flow patterns. For instance, the velocity meter caused noticeable changes in the water velocity distribution in the entirety of the tank, but it was deemed unpractical to create individual simulations for every position where the velocity meter would be placed during sampling. The inlet pipe also created significant flow deflections, but since this is part of the normal operation conditions of the tank, its representation in the simulations should be considered.

The amount of sampling locations at the laboratory was chosen to balance what was achievable within the time frame of this work and the information needed for proper validation of the simulations. A higher number of water velocity samples would definitely provide tools for more detail analysis of the accuracy of the simulations. As a good example can be sited the work done by Oca & Masalo (Oca & Masalo, 2013) where a high number of measurements (thirteen) along the radius of the tank was adequate to characterize in detail the free-vortex and the forced-vortex zones.

In the laboratory measurements performed, the +/-0,25 and +/-0,5 locations were selected in order to try to cover the entirety of the tank's width with a manageable number of laboratory samples. Additionally the +/-0,25 location was selected in order to also evaluate the velocities inside the R/3 free-vortex zone (Oca & Masalo, 2013).

The +/-0,89 locations were selected on the basis that previous flow simulation works reported peak velocities at this particular x/R location (Gorle et al., 2019) and other authors selected exactly this or very similar locations (x/R=0,89 and 0,86) as seemly the only locations of interest and considered enough for experimental validation (An et al., 2018).

The tank's geometry and size of the velocity meter barely allowed to achieve measurements this close to the tank's wall, therefore the velocity profile at any closer to the boundary layer near the wall was not possible to be investigated.

The vertical location of the sampling points was selected trying to cover the entirety of the water depth with a reasonable amount of measurements. The top measurement was selected as a reasonable depth where the velocity meter could be completely covered by the water while allowing enough water thickness above it in such a way that the water deformation at the surface due to the presence of the meter was not too big that would create waves or air pockets that may interfere with the readings.

The vertical positions were defined as water depth instead of a fixed distance from the bottom in order to facilitate the positioning of the instrument with help of the included markings when handled from above water. This approach also accounted for possible variations in water level / water flow being able to later evaluate the velocity distributions from the water surface level. The size of the velocity meter did not allow to investigate velocities too close to the bottom of the tank, therefore the validation near this other boundary layer was also not possible.

Different authors have used different velocity meters; An et al. (2018) used the well-known propeller type commonly used in open water aplications, such as in rivers and channels. Gorle et al. (2019) and Oca&Masalo (2013) relied on an Acoustic Doppler Velocimeter (ADV). The ADV is a sophisticated equipment which has many settings and could probably be configured to suit the measuring needs in aquaculture tanks. It is nevertheless believed that the equipment is in excess sensitive in its measurements, suitable for measuring the characteristics of small turbulent eddies (Nortek Group, 2019) and therefore acquiring highly variable measurements with significant noise that has to be post-processed away (Gorle et al., 2019; Klebert et al., 2018; Oca & Masalo, 2013).

The available water velocity equipment available for the measurements at the laboratory was found not suitable for measure the range of velocities experienced (see sections 3.4.1.2, 3.4.1.3.1 and 3.4.1.4.3). This meant that the inclusion of more sampling points would have represented excessive work when compared to the quality of the information obtained from the measurements.

Based on the degree of accuracy of the predictions in the validation against literature, the discrepancies between the CFD estimated velocities and the laboratory measurements are believed to be caused by the inappropriate range of measurements of the velocity meter and not from the inability of the simulation to predict the flow.

It is considered that the amount of measurements that comprised an individual sampling for a particular position of the velocity meter (n=17), was a good balance between achieving statistical significance and what was practically possible. Nevertheless due to the large variation in values experienced also by other authors when taking velocity samples, it may result convenient to take advantage of technological solutions such as logging of the velocity readings for post-processing of the information at a later stage and not rely so much in manual sampling methods.

On the other side, the flow meter installed in-line at the outlet system also experienced large fluctuation in the values measured, but this was believed to be characteristic of air being transported in the outlet pipe, modifying drastically the instantaneous resistance experienced by the propeller, translating into instable flow readings. These values when compared to the bucket and stop-clock measurements did not differ much, therefore suggesting that the flow meter is able to measure accurately the flow values but only when these are within its range of operation.

The inclusion of the laminar component of the flow in the simulation set-up, as investigated in Case 25, was found to have a minor effect in the estimated velocities in CFD. This is in line with what could be expected from a fully turbulent flow expected in aquaculture tanks. It was nevertheless not possible of determine if the small variation in the estimated velocities was a negative or a positive effect since the measured velocities with the available velocity meter cannot fully be considered a reliable source of validation.

The use of surface roughness in the tank walls and bottom (Case 26) practically did not affect the estimated velocities by CFD. The typically smooth surfaces used in aquaculture tanks and the relatively unrestricted flow in the main portion in the tank could explain the small effect roughness has under these conditions; when compared, for example, to high flow rates going through pipes.

The turbulence parameters indicated at the initial conditions can help the solution to achieve convergence at a faster time. Nevertheless, these values would be constantly computed during the iteration process and are not expected to have an impact on the final values achieved. This could be observed in the convergence graphs for turbulence at selected locations, as presented in section 4.3.3.

On the other hand, changes in the turbulence parameters at the inlet water flow, as presented in section 4.2.2, did exhibit an effect on the overall water velocities estimated by CFD. The further investigation in the field of water turbulence at the inlet pipe is definitely an interesting opportunity area for the design optimization of aquaculture tanks systems.

In the validation of the simulations against An et al. (2018), it was possible to see a matching flow pattern very similar between the different simulation approaches. An overall accuracy of around 16%, against 7% of the more complex simulation approach taken in the literature, can also be considered a very good numerical estimation of the water velocities.

The few laboratory measurements however, did not allowed for drawing too many conclusions about the accuracy of the simulations for particular zones within the tank. This emphasizes the importance of having sufficient measuring to evaluate better the performance of the different methodologies.

Regarding the validation of the simulations against Gorle et al. (2019), the lack of information presented in the paper made difficult the replication of their work and the ability to fully verify their results. It was, anyway, possible to compare the accuracy between simulation approaches in a generalized way and draw conclusions about the accuracy expected when using this simplified simulation set-up approach combined with a much simpler meshing strategy. As expected, the numerical estimation of the results was not as precise as with the more advanced and resource-demanding methodologies, but probably still within the acceptance criteria for many actors in the aquaculture industry which currently rely only on experience for the design of tanks, and this technological advances may seem unreachable for them. It is worth recalling that the estimations from the simulations from the paper itself were not particularly accurate, and considered appropriate and of high quality for velocity estimations which fell within the standard deviation of the laboratory sampling. For the simplified approach taken on this work (and latent possibility to further refine the results by an improved meshing and geometry), the velocity estimations at approximately two standard deviations from the laboratory measurements are considered still acceptable for general studies of flow patterns and rough guidelines for the optimization of velocity profiling within an aquaculture tank.

Other authors have pointed out that a 30% difference between the CFD estimations and laboratory measurements represents the quality acceptance threshold (Liu et al., 2016).

When extrapolating these acceptance criteria among authors, it can be said that the water velocity estimations on the validation case against An et al. (2018) were exceptionally good, as these were well within the one standard deviation criteria proposed by Gorle et al. (2019) and around half of the 30% difference threshold proposed by Liu et al. (2016).

It was unfortunate that the velocity meter used for the laboratory measurements could not provide adequate velocity profiling for the validation against experimental data. All the detailed preparation and care taken into preparing the experimental set-up and sampling methodologies would have ensured that the sources of inaccuracy and uncertainty of the measurements were minimized, potentially offering a more reliable validation than one against literature.

The computational times required for solving the steady-state simulations varied from minutes to several hours. The meshing intensity, initial turbulence parameters, geometry complexity and volume of the tank are considered the main factors that affected the computational time needed. Nevertheless these calculation times are definitely considered more practical than the expected solution times from time-dependent simulations, given the experience obtained in the few simulations performed of transient behavior at the beginning of this work.

By using the findings on this thesis as a starting point, further work should focus on acquiring numerous water velocity measurements performed with a reliable and precise equipment. This would allow for a more detailed profiling of the velocities along the width and depth of the tank and provide additional means for evaluating the accuracy of the simulations at different sectors of the tank.

The resultant turbulence properties of the flow from different inlet pipe/ nozzle designs could also be investigated separately. The results from that research could later be implemented across tank investigations where typically, in the aim to minimize the computational efforts, the flow inside the inlet pipe is not evaluated.

6 Conclusions

The simplified approach taken on the simulations for this thesis work provides valuable and efficient means for the prediction and verification of the resultant flow patterns in aquaculture tanks. Additionally it offers a level of accuracy for numerically estimating the water velocities within the tanks which is considered from “acceptable” to “high-quality” by specialist in the field.

The application of this methodology is limited to the study of stable flow conditions. Diverse water quality indicators of a transient (time-dependent) nature, while not possible to be directly calculated with this methodology, are possible to be indirectly assessed when combined with theoretical knowledge and practical experience. For example, the instantaneous local concentration of new (oxygen rich) vs. old water cannot be numerically calculated, but poor water mixing zones can be identified from the flow behavior and water velocity profiles.

The accuracy of the simulations was influenced by diverse factors, such as the ability to replicate the geometries of the tanks studied, the turbulence model used to solve the conservation equations, the type of volume cells and mesh refinement intensity, as well as some of the investigated simulation parameters, particularly the turbulence properties at the inlet flow.

For the validations against An et al. (2018), an overall difference in water velocities of around 16% was found between the CFD prognosis and the presented laboratory measurements. The overall relative error of the estimations reported in the paper was of about 7%.

For the validation against Gorle et al. (2019), the CFD-estimated water velocities were approximately at two standard deviations of the measured velocities in experiments. The predicted water velocities reported in the paper were close to one standard deviation of the measurements.

The equipment available for performing water velocity measurements at the university’s laboratory was not suitable for the range of velocities experienced in the tank. The larger relative error in the CFD estimations was therefore considered not representative of the actual accuracy of the simulations.

The amount and quality of experimental data for validating the simulations (either obtained from literature or from own experiments) played a very important role in determining the accuracy of the software predictions. While the amount of data used to validate the simulations of this work was considered sufficient to draw general conclusions about the effectivity of the simplified methodology, more and better data would have been beneficial in validating a more detailed water velocity profile within the tanks.

It is hoped that the insights from this work, presented primarily in the discussions but also along the main text, are useful and inspiring for continuing the work of fine tuning the simulation set-up and, nonetheless, to plan accordingly for obtaining the most and best experimental data possible to aid the validation process.

7 References

An, C.-H., Sin, M.-G., Kim, M.-J., Jong, I.-B., Song, G.-J. & Choe, C. (2018). Effect of bottom drain positions on circular tank hydraulics: CFD simulations. *Aquacultural Engineering*, 83: 138-150. doi: 10.1016/j.aquaeng.2018.10.005.

Castro, V., Grisdale-Helland, B., Helland, S. J., Kristensen, T., Jorgensen, S. M., Helgerud, J., Claireaux, G., Farrell, A. P., Krasnov, A. & Takle, H. (2011). Aerobic training stimulates growth and promotes disease resistance in Atlantic salmon (Salmo salar). *Comp Biochem Physiol A Mol Integr Physiol*, 160 (2): 278-90. doi: 10.1016/j.cbpa.2011.06.013.

Duarte, S., Reig, L., Masalo, I., Blanco, M. & Oca, J. (2011). Influence of tank geometry and flow pattern in fish distribution. *Aquacultural Engineering*, 44 (2): 48-54. doi: 10.1016/j.aquaeng.2010.12.002.

FAO, F. a. A. O. o. t. U. N.-F. a. A. D. (2019). *Global Aquaculture Production 1950-2017*. Available at: www.fao.org/fishery/statistics/global-aquaculture-production/query/en (accessed: 02.04.19).

Gorle, J. M. R., Terjesen, B. F., Holan, A. B., Berge, A. & Summerfelt, S. T. (2018a). Qualifying the design of a floating closed-containment fish farm using computational fluid dynamics. *Biosystems Engineering*, 175: 63-81. doi: 10.1016/j.biosystemseng.2018.08.012.

Gorle, J. M. R., Terjesen, B. F., Mota, V. C. & Summerfelt, S. (2018b). Water velocity in commercial RAS culture tanks for Atlantic salmon smolt production. *Aquacultural Engineering*, 81: 89-100. doi: 10.1016/j.aquaeng.2018.03.001.

Gorle, J. M. R., Terjesen, B. F. & Summerfelt, S. T. (2018c). Hydrodynamics of octagonal culture tanks with Cornell-type dual-drain system. *Computers and Electronics in Agriculture*, 151: 354-364. doi: 10.1016/j.compag.2018.06.012.

Gorle, J. M. R., Terjesen, B. F. & Summerfelt, S. T. (2019). Hydrodynamics of Atlantic salmon culture tank: Effect of inlet nozzle angle on the velocity field. *Computers and Electronics in Agriculture*, 158: 79-91. doi: 10.1016/j.compag.2019.01.046.

GPA Flowsystem, A. S. (2018a). *Rør produktark*. PVC-rør PN10 Ski.

GPA Flowsystem, A. S. (2018b). *Rørdeler produktark*. PVC-albue 90 PN16. Ski.

GPA Flowsystem, A. S. (2018c). *Rørdeler produktark*. PVC-endekappe PN16. Ski.

GPA Flowsystem, A. S. (2018d). *Rørdeler produktark*. PVC-muffe PN16. Ski.

GPA Flowsystem, A. S. (2018e). *Rørdeler produktark*. PVC-T-rør 90 med redusert uttak PN16. Ski.

Holtschmit M, K.-H. (2000). *Acuacultura General*. Guaymas: Instituto Tecnológico y de Estudios Superiores de Monterrey.

HOW TO: Free Surface Flow with SOLIDWORKS Flow Simulation 2018. Instructional video. (2018). Uploaded by: Quest Integration. Available at: https://www.youtube.com/watch?v=p7jtf0xHYN4 (accessed: 10.02.2019).

Klebert, P., Volent, Z. & Rosten, T. (2018). Measurement and simulation of the three-dimensional flow pattern and particle removal efficiencies in a large floating closed sea cage with multiple inlets and drains. *Aquacultural Engineering*, 80: 11-21. doi: 10.1016/j.aquaeng.2017.11.001.

Lekang, O.-I. (2007). *Aquaculture Engineering*. 1st ed. Oxford: Blackwell Publishing Ltd.

Liu, Y., Liu, B., Lei, J., Guan, C. & Huang, B. (2016). Numerical simulation of the hydrodynamics within octagonal tanks in recirculating aquaculture systems. *Chinese Journal of Oceanology and Limnology*, 35 (4): 912-920. doi: 10.1007/s00343-017-6051-3.

Nortek Group, A. S. (2019). *Velocimeter - Vector - 300m*. Available at: https://www.nortekgroup.com/products/vector-300-m (accessed: 03.2019).

Oca, J. & Masalo, I. (2013). Flow pattern in aquaculture circular tanks: Influence of flow rate, water depth, and water inlet & outlet features. *Aquacultural Engineering*, 52: 65-72. doi: 10.1016/j.aquaeng.2012.09.002.

Rasmussen, M. R. & McLean, E. (2004). Comparison of two different methods for evaluating the hydrodynamic performance of an industrial-scale fish-rearing unit. *Aquaculture* 242 (1-4): 397-416. doi: 10.1016/jaquaculture.2004.08.045.

SOLIDWORKS-Corp. (2018a). *SOLIDWORKS Flow Simulation 2018 Online User's Guide* (accessed: February-May 2019).

SOLIDWORKS-Corp. (2018b). *SOLIDWORKS Flow Simulation 2018 Technical Reference* (accessed: February-May 2019).

SOLIDWORKS-Corp. (2018c). *SOLIDWORKS Flow Simulation Online Tutorial* (accessed: February-May 2019).

SOLIDWORKS Flow 2018 - Free Surface Simulation. Instructional video. (2017). Uploaded by: GoEngineer. Available at: https://www.youtube.com/watch?v=6w-coEgQpaQ (accessed: 10.02.2019).

Summerfelt, S. T., Mathisen, F., Holan, A. B. & Terjesen, B. F. (2016). Survey of large circular and octagonal tanks operated at Norwegian commercial smolt and post-smolt sites. *Aquacultural Engineering*, 74: 105-110. doi: 10.1016/j.aquaeng.2016.07.004.

Turbulence Intensity. (2018). CFD Online. Available at: https://www.cfd-online.com/Wiki/Turbulence_intensity (accessed: 08.03.19).

Turbulence lenght scale. (2012). CFD Online. Available at: https://www.cfd-online.com/Wiki/Turbulence_length_scale (accessed: 08.03.19).

Appendix 1: Survey process of studied tank system

System description

The main survey of the system was performed in a lapse of 10 days, starting on the 18. February 2019. It was later required to verify some of the tank measurements which seemed to be not accurate enough, but this later proved to be manufacturing imperfections on the tank.

The system was comprised of the tank with a vertical inlet pipe adjacent to one of the walls. The tank had an outlet pot located at the center and bottom of the tank. An outlet pipe exited the outlet pot from the side. The outlet pipe ran under the tank towards one of its corners where it intersected a vertical pipe. The vertical pipe extended to approximately the upper edge of the tank.

The tank had originally a cover placed above it to avoid fish escapees. This cover was removed to facilitate access for the measurements and experiments.

The water exited from one side of the vertically placed pipe by a smaller pipe at some distance below the tank's edge, thus controlling the water level in the tank to approximately this position. The water level in the tank could vary somehow depending on the magnitude of the water flow in the tank and the resultant thickness of the water layer.

The tank used for the experimental validation was a square tank with rounded corners which has been supplied from A-Plast AS. The tank it's believed to be fabricated on fiberglass reinforced polyester resin, but the full material specifications nor detailed drawings of the tank were available from the supplier's website or from the building documentation at the laboratory. Only a general schematic was available in the documentation, but since it only provided overall width and height of the tank, this was considered not sufficiently detailed for the construction of the 3D models to be used in CFD simulations.

Measuring equipment

The survey was carried out with basic measuring equipment and measuring aids available at the laboratory (Figure 84):

- Flexible measuring tape [m/cm/mm]
- Rigid measuring tape [m/cm/mm]
- 2 of two-ways water level of different lengths.
- Mechanical Vernier [mm/µm]
- 90 degrees angle tool with integrated ruler [cm/mm]
- Aluminum straight beam (approx. length: 2 m)
- Self-made device to check for verticality (balance weight and surgical filament)
- Small segments of PVC pipe of different diameters.
- Wood plank of approx. length of 240 cm (not shown in picture)
- Surgical filament
- Electrical tape

Figure 84 Measuring tools

Previous experience with similar and more advanced measuring tools and measurement techniques (from fabrication environments) proved to be helpful in capturing the geometry in an accurate manner. While the measuring devices and methodology used have their inherent inaccuracy, the geometries themselves also proved to be difficult objects of study. Details of this challenges are presented in the sub-sections ahead.

Tank survey

General

Numerous radiuses, draft angles (for ejection from the mold), inclined planes (such as at the tank bottom) and the general lack of suitable reference locations to start and finish the measurements was a constant difficulty through the measuring work. While this was something which was partially expected given the nature of the manufacturing process of fiberglass components, longer time than anticipated was used in achieving satisfactory measurements. It was nevertheless an enriching experience and valuable insight into how an “idealized” tank geometry (designed with CFD) may result in real-life and how this imperfections may affect its hydrodynamic performance.

The tank fiberglass construction was characterized by having 4 walls that were inclined towards the center of the tank, resulting in a smaller width at the base than at the top of the tank. The tank had a horizontal flange extending along the whole upper edge. The tank bottom consisted of 4 inclined trapezoidal surfaces with a negative slope towards the center. These 4 surfaces merged into a horizontal square surface. At the center of this square surface a circular recess allocated the outlet grating. Below the recess extended the cylindrical outlet pot further down, see Figure 85.

Figure 85 Rearing tank used for experimental validation

Tank corners

The large corner radius between tank walls were estimated by sliding the long flat edge of the angle tool along the walls, moving towards the corners until separation between the tool and the tank wall indicated the start of the radius. This was done minimum three times while observing the appearance of a gap between the tool against the flat wall. It was also possible to feel increasing sliding resistance when reaching the start of the radius. These start points of the radiuses were then marked on the tank bottom and used to draw lines perpendicular to the wall from those points. The intersection point of the two lines extending from two adjacent walls was later used to measure the radius towards the corner at three locations: start, center and end of the radius. The three measurements were then averaged to R480 mm.

At the top part of the walls, the radiuses start points were also identified and marked in the same way (sliding the angle tool). The distances from these points and the centerline of the tank were then measured to confirm the values. While the values coincided for this measurements, it was decided to generally rely on direct measurements only and avoid as much as possible indirect measurements, as in this case the use of a calculated centerline, in order to minimize the accumulated error.

Geometrical radiuses

Between the tank walls and tank bottom the radius was approximated to be of R22,5 mm. This was done by using the two segments of PVC pipe and placing them above the radiuses. The Ø50 mm diameter pipe segment sat outside the tank radius supported along two contact lines; indicating a smaller radius of the tank at this location. The Ø40 mm pipe, on the contrary, sat inside the tank radius contacting at only one line; indicating a larger radius. It was therefore decided to use an intermediate value of Ø45 mm (diameter), resulting in a corner radius of R22,5 mm.

The radius between the four inclined surfaces that comprise the tank's bottom was assumed to be also R22,5 mm. All other radiuses were considered not geometrical, but only needed to assist the fiberglass manufacturing process and roughly measured to be R5 mm.

Walls angle

The angle of the walls was estimated by positioning the long water level vertically at the starting point of the radius between the tank's wall and bottom (adjacent to the wall). From the water level edge it was measured (with the flexible tape) the horizontal distance towards the outer edge of the tank's flange.

Since there where discrepancies in the angle measurements between the different walls, the measurements were repeated. This time it was measured from the same absolute vertical (water level edge) to the start of the radius between the wall and the top flange (adjacent to the wall). It was then confirmed that, in fact, the angle of the walls were not the same for all of them and therefore an average value of the four measurements was used in the 3D modelling.

Tank's (wall) height

A variation of the method described to measure the wall angles was also used to measure the overall height of the tank. The long water level was used to ensure verticality of the measurements. Then it was measured, along the water level tool, the distance from the bottom radius to the wooden plank placed across the top of the tank.

Tank's width

The overall width of the tank was measured at its top part by supporting the rigid tape below the wooden plank and measuring between the start of the radiuses between the walls and the top flanges (adjacent to the wall).

Tank bottom

The inclination of the tank's bottom was measured placing the aluminum straight beam transversely across the highest part of the tank's bottom, and vertically measuring downwards towards the square flat surface, resulting in a 40 mm height difference.

It was noted that the surfaces that made up the tank bottom were convex when looking at them from the inside of the empty tank, and concave when looking from the outside. On another tank of the same type which was full of water, it was observed (from the outside) that these surfaces were straightened out by the effect of the water weight. The tank's bottom surfaces were then considered straight in the 3D model as they were in the full tank.

It was also observed that in the full tanks the whole tank's bottom was pressed downwards due to the water weight until the outlet pot became in contact with the building floor. This deformation was estimated by measuring the gap between the outlet pot and the floor on the studied empty tank and indicated a 13 mm vertical deformation. The overall height of the sloped tank's bottom was then adjusted to 53 mm in the 3D model.

Outlet pot

The outlet pot grating recess diameter was measured with the flexible tape at different locations, showing consistent measurements of Ø300 mm (inner side of radius). The depth of the grating

recess was measured only with the rigid tape; it was considered that in such short distance the variation of the measurement due to out of verticality would not be significant.

The depth of the outlet pot was measured with the rigid tape from the bottom of it to the small water level's edge, which was placed transversely on the horizontal square part of the tank bottom.

A flat protuberance inside the outlet pot provided the base surface for an outlet hole and a short pipe to exit the side of the outlet pot at approximately 45 degrees. This angular dimension was only verified visually due to the poor access and lack of reference points for an actual measurement.

The inner diameter at the bottom of the outlet pot was calculated by measuring the horizontal distance between a vertical line extending from the pot bottom's edge to the upper edge of the grating recess. Also the shape and inclination of the flat surface where the outlet pipe was placed was measured against the grating's same edge.

The measurements inside the outlet pot were difficult to take accurately due to poor access, as the grating was attached in place with silicon and therefore not removed. These were also not considered to be so relevant for the overall behavior of the flow in the main portion of the tank.

Tank's centerlines

The center lines of the tank were approximated by positioning the wooden plank near the middle line (visually) and then taking measurements with the flexible tape towards opposite sides of the tank (flange edge) and adjusting the position of the plank in order to have equal measurements on both sides. These measurements were taken at two (as far as possible) locations along the tank's edge in order to have the two point locations which are needed to geometrically determine a line.

The method to find the straight angle measurement (perpendicular to the centerline) was to continuously read the tape while slightly and slowly moving the end of the tape from side to side and then registering the minimum value observed.

This centerline was marked on the tank to later replace the plank with surgical filament attached in place with electrical tape above the markings. This procedure was then repeated at 90 degrees in order to find the second centerline of the tank. The intersection of the two centerlines was used to determine the center of the tank.

Since it was discovered that the top flanges didn't have a constant width, the position of the filaments (and thus the centerlines) was later rectified by taking instead measurements from the top part of the walls (below the radius) towards the centerlines. Here the plank itself placed parallel along the filament and the angle tool were used to determine the perpendicular lines along which the measurements had to be taken. The rigid tape was used at this rectification measurements.

Outlet pot relative position

The center of the tank was marked at the wooden plank and used to fix the weight-and-cord device and verify the central position of the outlet pot. It was then visually evident that the weight did not hang right on the center of the outlet pot.

Measurements from the grating recess towards the four wall were taken and it was then confirmed that the outlet pot was shifted approximately 5mm towards one of the walls. This measurements towards the wall were done using the rigid tape in combination with the long water level and measuring from the grating recess towards the start of the radius between the wall and the bottom of the tank (adjacent to the bottom). Considering the relatively small shift from the center of the

outlet pot and the possible accumulated error in this particularly challenging measurement location, the shift of the outlet center was therefore not considered in the 3D model.

Outlet pipe survey

The outlet pipe extended out from the side of the outlet pot, then turning three times with the use of 45 degrees elbows before intersecting the outlet column at a T-pipe connection. The T-pipe at the bottom of the outlet column was permanently attached to the main header of the drain system which was fixed to the ground with pipe-clamps. While on the empty condition of the tank the outlet pipe had a slight negative slope towards the T-pipe intersection, it was noted that on the full condition the pipe acquired a positive slope due to the deformations at the tank bottom, this going against recommendations of outlet design as those presented by Lekang (2007).

This angle of the outlet pipe was not considered in the 3D modelling and a full horizontal pipe was instead used.

The outlet column had internally a reducing slip-on at the bottom where a smaller pipe was placed. This arrangement guided the flow upwards before exiting sideways at a second T-pipe connection. At this upper T-pipe was where the totality of the flow exited during normal operational and sent back into the RAS system. The internal pipe in the outlet column, if removed, provided means of fully emptying the tank into the drain. It also could handle the overflow in any blockage situations by allowing the water to enter at the top of it and let it flow through the bottom T-pipe into the drain.

The measurements were taken using the flexible tape. The molding marks on the elbows where used for measurement references. The details of the pipe connections (T-pipe and elbows) were taken from the supplier's catalog and used in aiding to model as accurate as possible the details of the outlet system, such as bending radius, etc.

A simplified version of the outlet system was used at the 3D model where neither the lateral exiting pipe at the top T-pipe or the inner pipe inside the outlet column where necessary to fully represent the hydraulic conditions of the system. Details of the resultant model and measured dimensions are shown in Appendix 4: Outlet Pipe - As measured - Rev1.

Outlet grating dimensions

The outlet grating consisted of a circular stainless steel plate measured to be of 1,5 mm thickness and Ø288 mm in diameter. The plate had a perforation pattern of the oblong type. The oblong dimensions were measured to 25mm x 8 mm to the edges. The perforation pattern was measured to be 32mm x 15 mm, longitudinally and among rows respectively. The perforations were symmetrically staggered between rows.

The diameter of the grating was measured using a regular measuring tape while the perforated pattern and thickness were measured using the Vernier.

The thickness of the silicon and therefore the final vertical position of the grating was measured with the Vernier at several locations from the outlet pot grating recess bottom face to the top of the grating. The values were later averaged to 0,8mm.

While the outlet grating seemed to be cut from near the edge of the main plate (where no perforations were made), the perforations coincided entirely above the outlet pot opening. The relative position of the perforations against the outlet pot/grating recess was approximated and replicated visually from pictures into the 3D model.

Figure 86 Outlet grating

Appendix 2: Method for positioning of the water velocity meter

Support and measuring arrangement

Rigid beams and sampling markings

The wooden plank previously used for determining the centerline of the tank was used to build a beam arrangement which would provide support and leveling capabilities for the water velocity meter.

A second wooden beam was attached to the first beam at three locations spaced by smaller wooden blocks. Long screws were used to secure all the pieces together. Holes smaller than the screw diameter were pre-drilled at the components in order to avoid the wood from cracking when attaching the screws and to facilitate the assembly.

The beam arrangement was then position above the tank, supported at the tank top flange. It was secured in place by means of clamps intended for use in construction of wooden structures. The centerline, indicated by the previously located surgical filament, was used to mark the origin (x=0) on the lower wood plank.

Markings were made also at the sampling locations (short marking) and at the corresponding positions for mounting the velocity meter; this in order to account for the eccentricity of the flow meter relative to the center of the aluminum pole (65mm). The mounting markings were marked as a perpendicular line across the whole width of the wooden plank in order to facilitate visual identification and differentiate them from the sampling position marking. The perpendicularity of these marking was assured by using the 90 degrees angle tool against the edge of the wooden plank.

The beam arrangement was placed 60 mm behind the second centerline (Z=0) in order to allow for enough space for the mounting clamp arrangement in such a way that the center of the aluminum pole could be positioned exactly at the center of the tank (see Figure 87 and Figure 88).

Cord-line measuring references

The cord-line (surgical filament) indicating the z=0 centerline was repositioned at z=10mm, so that when positioning the velocity meter pole (of Ø20 mm in diameter) barely touching the cord-line, the center of the pole would be right at the z=0 axis, Figure 88.

Figure 87 Sampling markings on support beam

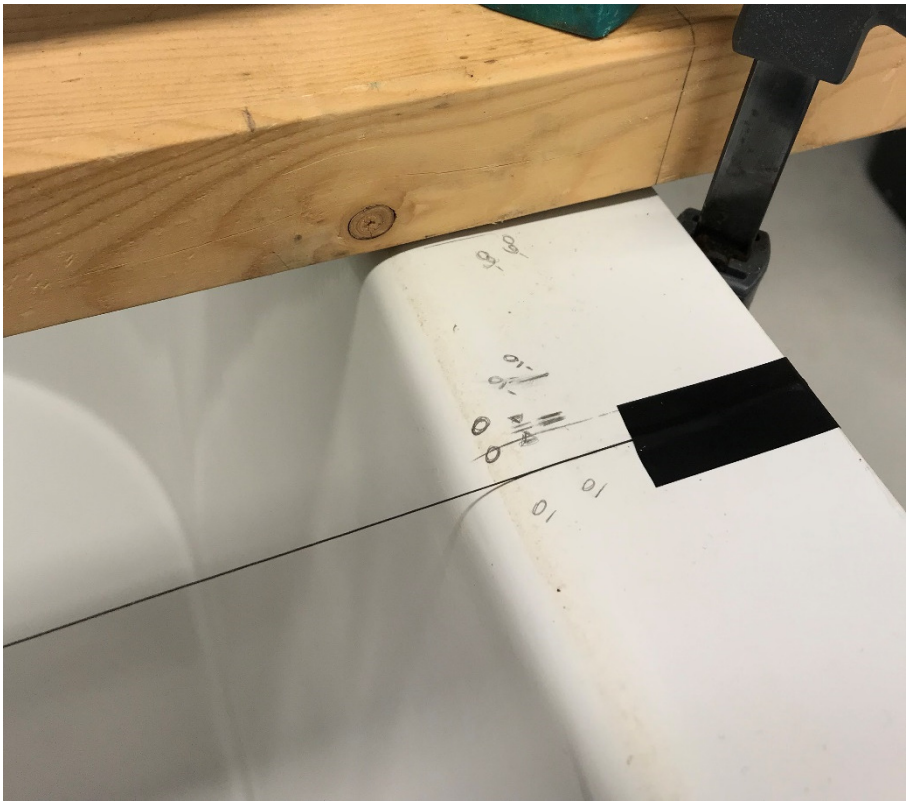

Figure 88 Centerline (z=0 mm), beam positioning (z=60 mm) and cord-line markings (z=10 mm)

Position assurance of the velocity meter

XZ plane

The lower mounting clamp on the velocity meter was positioned at the lower support beam were the mounting markings were drawn. The mounting clamps were made of cast-iron and had a split-line at the center of the clamp characteristic of the casting process. This split line was visually aligned to the mounting markings on the wooden plank so that they became collinear.

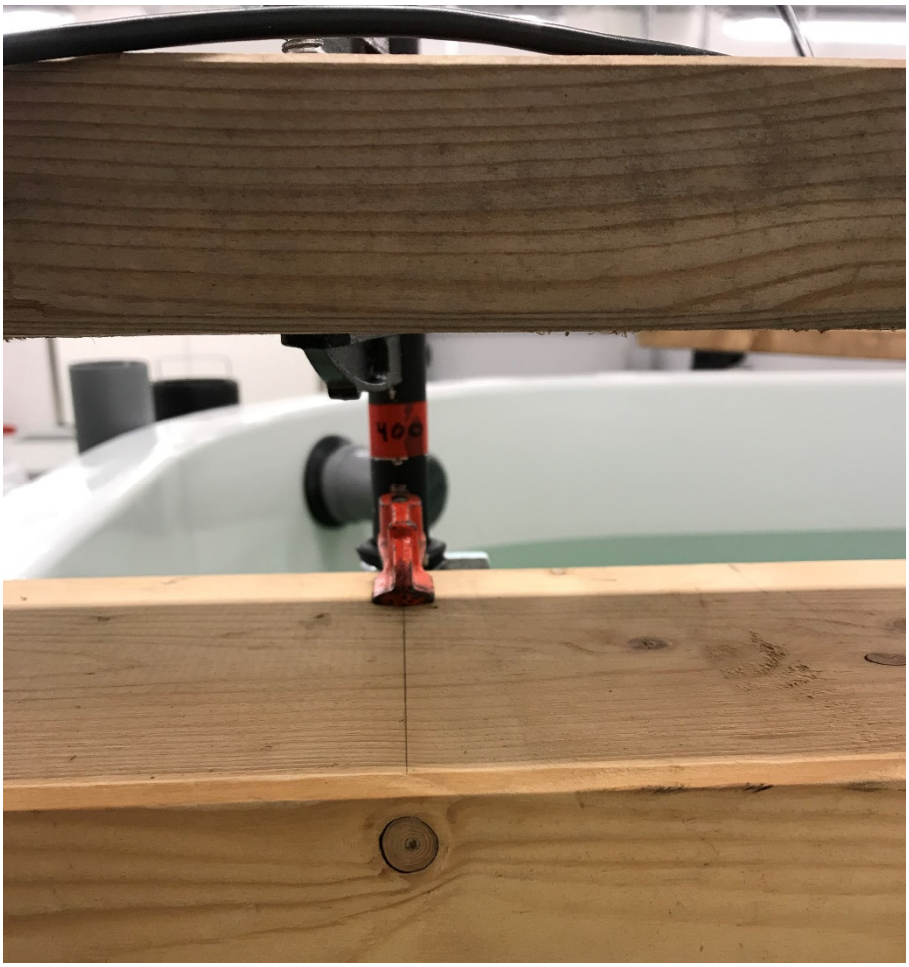

Figure 89 Position assurance xz-plane

This positioning was simultaneously coordinated with achieving a slight contact between the aluminum pole and the cord-line at z=10, to later tighten firmly the mounting clamp.

Y axis

The position of the velocity meter in the y-axis was determined by the use of the water depth markings placed on the velocity meter. The markings were placed in a way that the fully submerged marking would indicate the corresponding water depth of the center of the meter.

Figure 90 Position assurance y-axis / water depth

Verticality assurance

While the lower mounting clamp on the pole had a tight fit towards the pole, it still provided enough flexibility in order to use the upper mounting clamp for correction of the verticality. The small water level was used to check the verticality on the aluminum pole on two directions (along xy plane and yz plane). This verticality had to be checked multiple times on each direction and readjust the position of the upper mounting clamp on the upper support beam until the readings at the two directions showed a fully vertical pole.

Care was taken when placing the water level against the pole so no bending moments were introduced on the pole during reading, Figure 91.

Figure 91 Demonstration of verticality assurance method

This represents an opportunity area for the design of the velocity meter prototype where a set of water level bubbles could be integrated already on the pole to facilitate verticality assurance.

Angle assurance

The velocity meter was orientated parallel to the z axis in order to capture the water velocities in the z-direction. This was achieved by visually checking from above how the velocity meter aligned with the cord-line at z=10. Adjustment were then made and the orientation checked again until this condition was also satisfied, Figure 92.

Figure 92 Angle assurance

Final position inspection

All of the position and orientation check points were inspected multiple times after fully completing the positioning routine, ensuring all of them were simultaneously satisfied and no further adjustments were needed. This guaranteed that manipulation of the meter to comply with a condition would not have affected any of the previously checked position assurance checks.

Appendix 3: Fish Lab tank – As measured – Rev1

NOTES:
1. Dimensions in parentesis (xx,xx) are resultant from model / extrapolated.
2. Regular dimensions as measured on tank.
3. Approx. 13 mm deformation due to water weight is considered at tank bottom shown dimensions.
4. No other deformations considered.
5. All radius 5 mm unless otherwise specified.

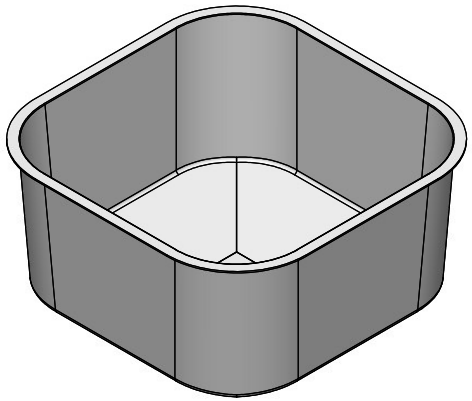

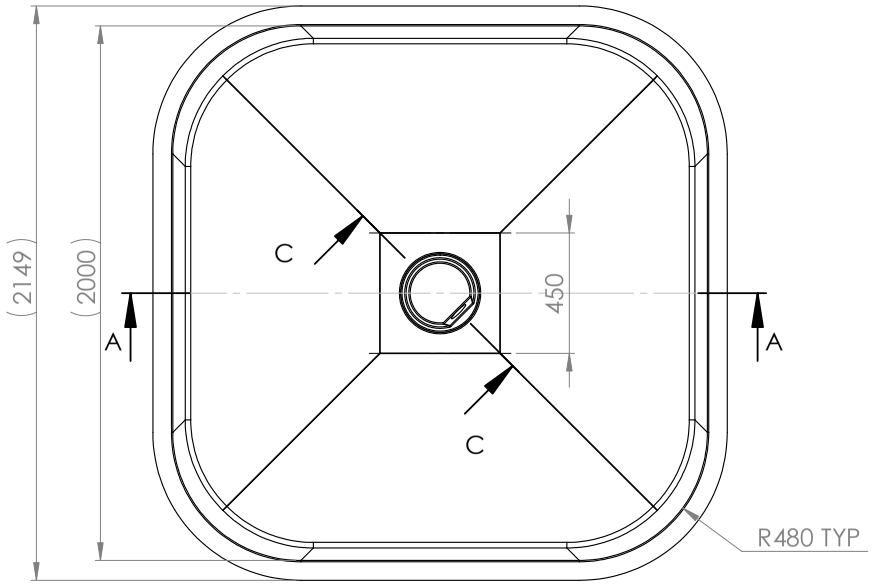

SECTION A-A
SCALE 1 : 20

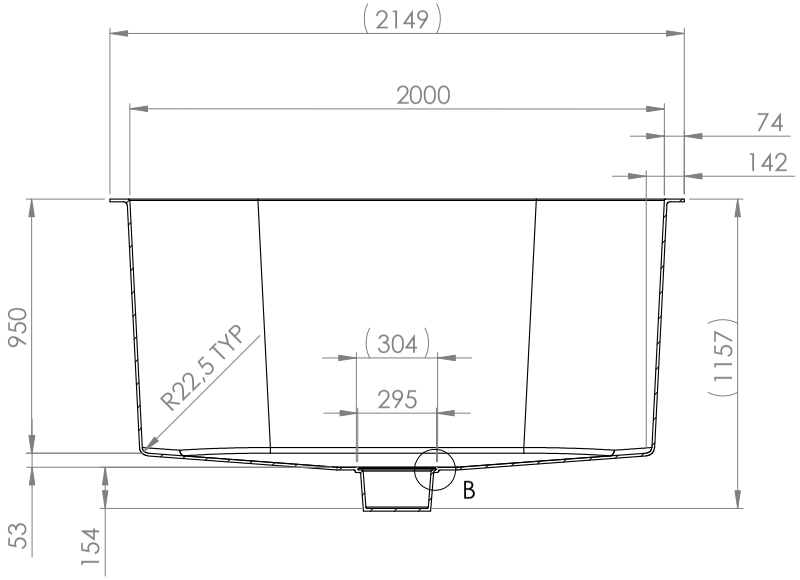

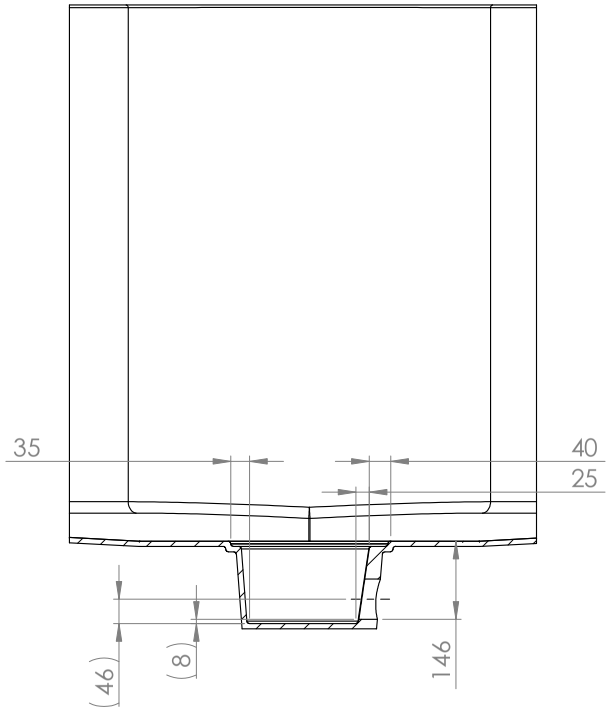

SECTION C-C
SCALE 1 : 10

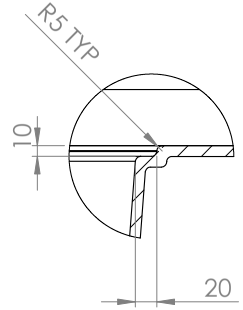

DETAIL B
SCALE 1 : 5

UNLESS OTHERWISE SPECIFIED: DIMENSIONS ARE IN MILLIMETERS SURFACE FINISH: TOLERANCES: LINEAR: ANGULAR:		FINISH:		DEBURR AND BREAK SHARP EDGES	DO NOT SCALE DRAWING	REVISION 1
	NAME	SIGNATURE	DATE	MEASURE DATE	TITLE: Fish Lab Tank As measured	
DRAWN	ACH		03.03.19	18-28.02.19		
CHK'D						
APPV'D						
MFG						
Q.A				MATERIAL: Glass fiber reinforced polyester resin	DWG NO. Tank_fishlab	A3
				WEIGHT:	SCALE:1:20	SHEET 1 OF 1

Appendix 4: Outlet pipe – As measured – Rev1

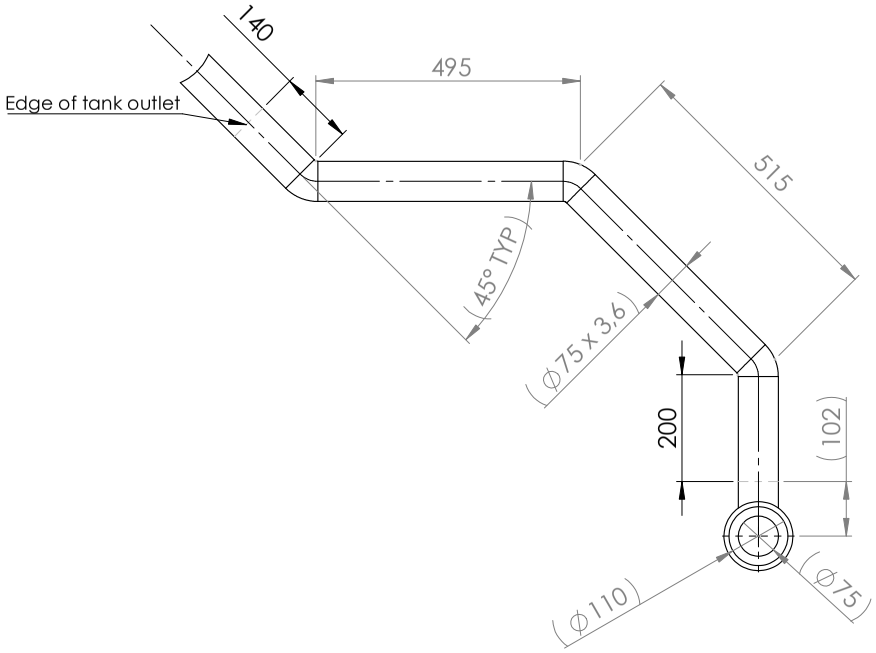

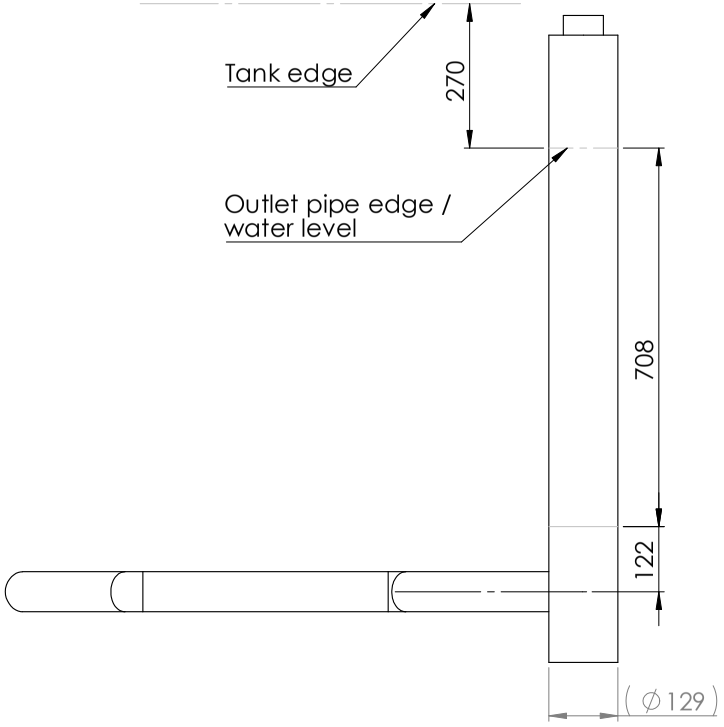

NOTES:
1. Dimensions in parentesis (xx,xx) are resultant from model / extrapolated / from catalog.
2. Regular dimensions as measured.

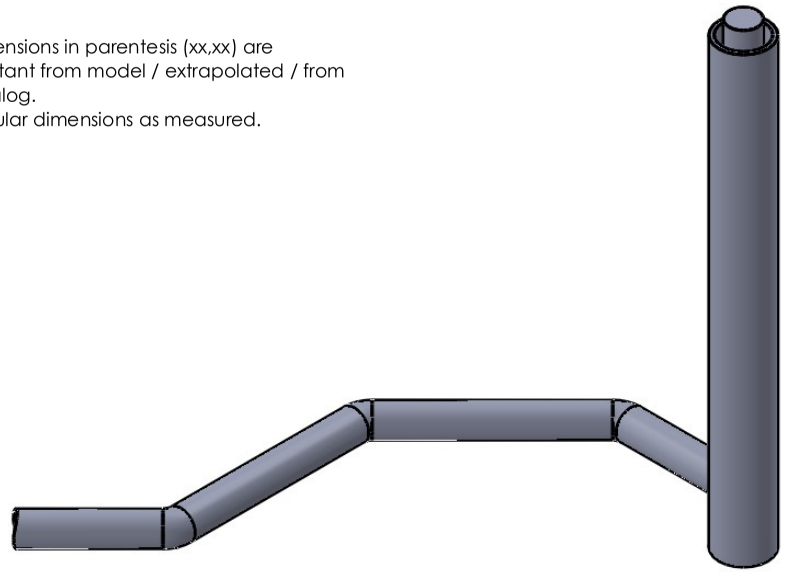

UNLESS OTHERWISE SPECIFIED: DIMENSIONS ARE IN MILLIMETERS SURFACE FINISH: TOLERANCES: LINEAR: ANGULAR:		FINISH:			DEBURR AND BREAK SHARP EDGES	DO NOT SCALE DRAWING / REVISION 1
	NAME	SIGNATURE	DATE		Measure date	TITLE: Outlet Pipe As measured
DRAWN	ACH		03.03.2019		20.02.2019	
CHK'D						
APPV'D						
MFG						
Q.A				MATERIAL:		DWG NO. Avløpsrør_fiskelab / A3
				WEIGHT:		SCALE:1:10 / SHEET 1 OF 1

Appendix 5: Tested positions of inlet pipe – Rev1

NOTES:
1. All regular dimensions as measured
2. Dimensions in parentesis from pipe supplier catalog

Case 30-32

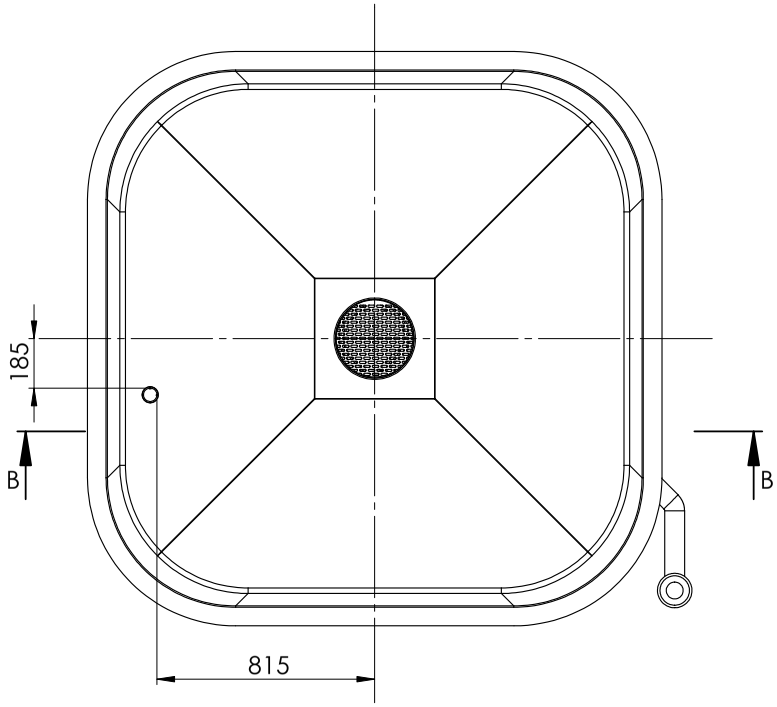

Case 34-37

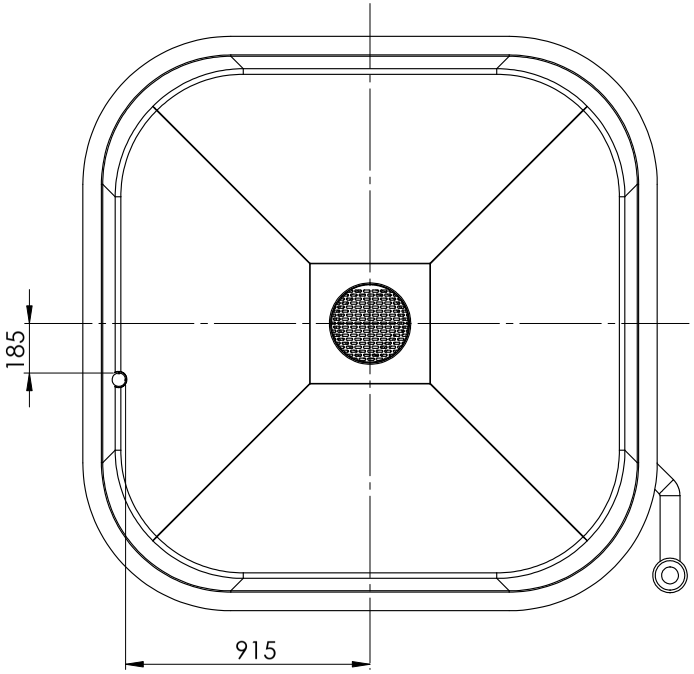

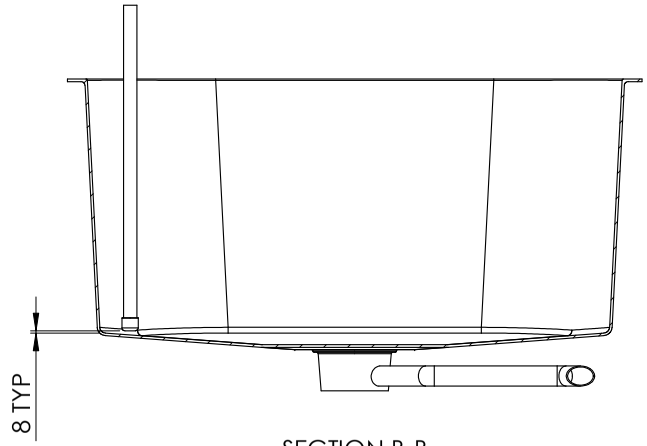

SECTION B-B

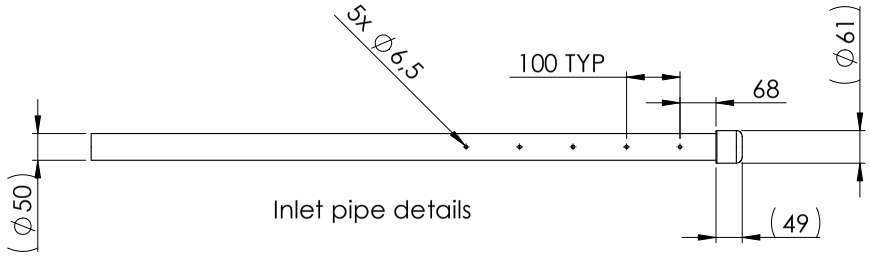

Inlet pipe details

UNLESS OTHERWISE SPECIFIED: DIMENSIONS ARE IN MILLIMETERS SURFACE FINISH: TOLERANCES: LINEAR: ANGULAR:		FINISH:		DEBURR AND BREAK SHARP EDGES		DO NOT SCALE DRAWING	REVISION
	NAME	SIGNATURE	DATE			TITLE: Tested positions of inlet pipe	
DRAWN	ACH		04.05.19				
CHK'D							
APP'V'D							
MFG							
Q.A				MATERIAL: N/A		DWG NO. Tank_fishlab_assy_Cases_Comb34-37-Correct_Inlet	A3
				WEIGHT:		SCALE:1:20	SHEET 1 OF 1

Appendix 6: Sampling Sheet – Rev 2

Andres Castro Herrera

Date: _____

					l/hr	13,32	26,64	39,96	53,28	66,6	79,92	93,24	106,56			
Measuring point					Flow - flowmeter [l/min]. Sampling every 15 s for **4** min. Total nr. of samples: **17**									Time of measurement		
Nr.	Name	x [m]	y [m]	z [m]	Error	0	0,222	0,444	0,656	0,888	1,11	1,332	1,554	1,776	(Re) Positioning	Time of the day from	to
4	1VB	-0,89	0	0													
5	1VM	-0,89	0	0													
6	1VT	-0,89	0	0													
10	1HB	0,89	0	0													
11	1HM	0,89	0	0													
12	1HT	0,89	0	0													
16	2VB	-0,5	0	0													
17	2VM	-0,5	0	0													
18	2VT	-0,5	0	0													
22	2HB	0,5	0	0													
23	2HM	0,5	0	0													
24	2HT	0,5	0	0													
28	3VB	-0,25	0	0													
29	3VM	-0,25	0	0													
30	3VT	-0,25	0	0													
34	3HB	0,25	0	0													
35	3HM	0,25	0	0													
36	3HT	0,25	0	0													

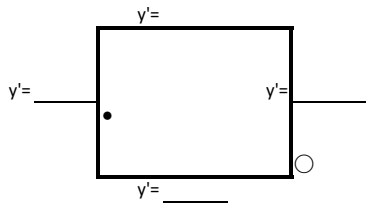

Vann stand

Ave. (y')= [mm]
H= [mm]
h= [mm]
yB= [mm]
yM= [mm]
yT= [mm]

Valve opening _____ [turns]

Water flow

Bucket & Stopclock (20 l)

Nr.	T (+10s)	T
1		[s]
2		[s]
3		[s]
4		[s]
5		[s]

Ave. Time 0 [s]
Flow #DIV/0! [l/min]

Outlet meter [l/min]

Min _____ [l/min]
Max _____ [l/min]

Median 0 [l/min]

Notes:

Appendix 7: Gorle et al. (2019) graphs for data extraction – Rev3

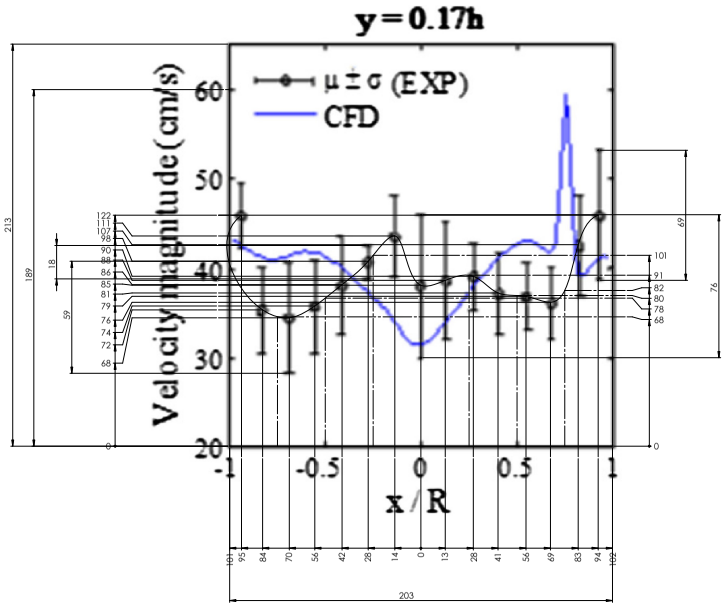

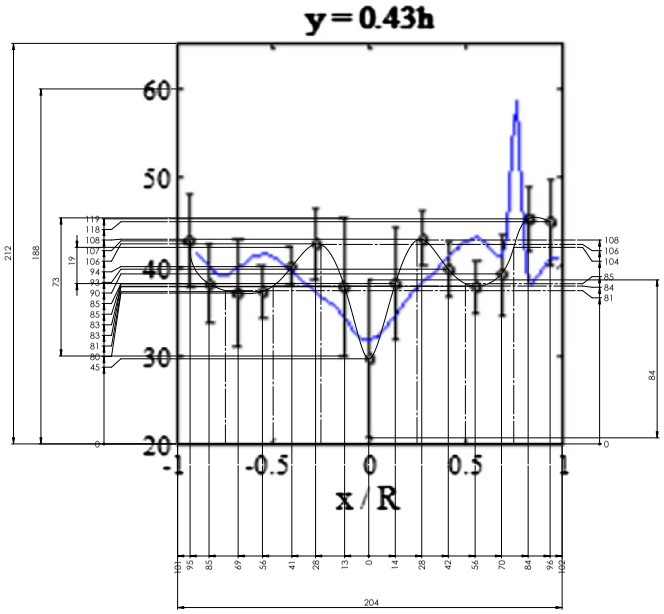

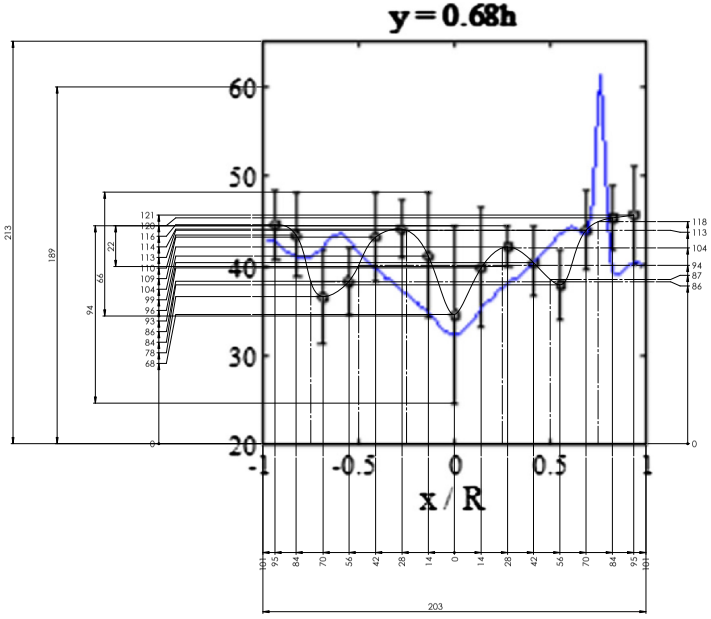

Graphs for data extraction - Gorlie et al. (2019)

Gorlie graphs for data extraction

A0

Appendix 8: Water velocities sampled at the laboratory

Andres Castro Herrera

Date: 07.03.2019

l/hr 13,32 26,64 39,96 53,28 66,6

Measuring point					Flow - flowmeter [l/min]. Sampling every 15 s for 2 min. Total nr. of samples: 9										Time of measurement		
Nr.	Name	x [m]	y [m]	z [m]	Error	0	0,22	0,44	0,67	0,89	1,11				(Re) Positioning	Time of the day from	to
1	1FB	0	127,5	0,89													
2	1FM	0	427,5	0,89													
3	1FT	0	627,5	0,89													
4	1VB	-0,89	127,5	0													
5	1VM	-0,89	427,5	0													
6	1VT	-0,89	627,5	0													
7	1BB	0	127,5	-0,89													
8	1BM	0	427,5	-0,89													
9	1BT	0	627,5	-0,89													
10	1HB	0,89	127,5	0													
11	1HM	0,89	427,5	0													
12	1HT	0,89	627,5	0	1			2	4	2						15:39	15:41
13	2FB	0	127,5	0,5													
14	2FM	0	427,5	0,5													
15	2FT	0	627,5	0,5													
16	2VB	-0,5	127,5	0													
17	2VM	-0,5	427,5	0													
18	2VT	-0,5	627,5	0													
19	2BB	0	127,5	-0,5													
20	2BM	0	427,5	-0,5													
21	2BT	0	627,5	-0,5													
22	2HB	0,5	127,5	0													
23	2HM	0,5	427,5	0													
24	2HT	0,5	627,5	0													
25	3FB	0	127,5	0,25													
26	3FM	0	427,5	0,25													
27	3FT	0	627,5	0,25													
28	3VB	-0,25	127,5	0													
29	3VM	-0,25	427,5	0													
30	3VT	-0,25	627,5	0													
31	3BB	0	127,5	-0,25													
32	3BM	0	427,5	-0,25													
33	3BT	0	627,5	-0,25													
34	3HB	0,25	127,5	0													
35	3HM	0,25	427,5	0													
36	3HT	0,25	627,5	0													

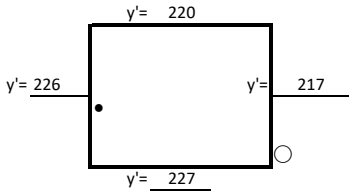

Vann stand

Ave. (y')=	222,5	[mm]
H=	950	[mm]
h=	727,5	[mm]
yB=	127,5	[mm]
yM=	427,5	[mm]
yT=	627,5	[mm]

Valve opening 2 [turns]

Water flow

Bucket & Stopclock (20 l)

Nr.	T (+10s)	T	
1	47,12	37,12	[s]
2	44,46	34,46	[s]
3	45,02	35,02	[s]
4	44,49	34,49	[s]
5	46,69	36,69	[s]

Ave. Time 35,556 [s]

Flow 33,74958 [l/min]

Outlet meter [l/min]

Min 30 [l/min]

Max 39 [l/min]

Median 34,5 [l/min]

Andres Castro Herrera

Date: 15.03.2019

Velocity cm/s

Flow l/hr 0 13,32 26,64 39,96 53,28 66,6

Measuring point					Flow - flowmeter [l/min]. Sampling every 15 s for 2 min. Total nr. of samples: 9										Time of measurement		
Nr.	Name	x [m]	y [m]	z [m]	Error	0	0,22	0,44	0,67	0,89	1,11				(Re) Positioning	Time of the day from	to
4	1VB	-0,89	137,25	0													
5	1VM	-0,89	437,25	0													
6	1VT	-0,89	637,25	0													
10	1HB	0,89	137,25	0		3	3	2	1						16:57	18:01	18:03
11	1HM	0,89	437,25	0													
12	1HT	0,89	637,25	0		3	3	3							21:58	22:29	22:31
16	2VB	-0,5	137,25	0													
17	2VM	-0,5	437,25	0													
18	2VT	-0,5	637,25	0													
22	2HB	0,5	137,25	0		7	1		1						18:40	19:12	19:14
23	2HM	0,5	437,25	0													
24	2HT	0,5	637,25	0		2	1	1	3	1	1				21:00	21:31	21:33
28	3VB	-0,25	137,25	0													
29	3VM	-0,25	437,25	0													
30	3VT	-0,25	637,25	0													
34	3HB	0,25	137,25	0		7	1		1						19:25	19:56	19:58
35	3HM	0,25	437,25	0													
36	3HT	0,25	637,25	0		8			1						20:14	20:46	20:48

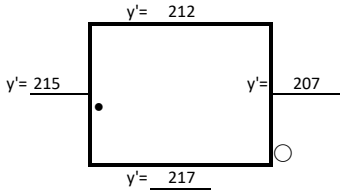

Vann stand

Ave. (y')=	212,75	[mm]
H=	950	[mm]
h=	737,25	[mm]
yB=	137,25	[mm]
yM=	437,25	[mm]
yT=	637,25	[mm]

Valve opening full [turns]

Water flow

Bucket & Stopclock (20 l)

Nr.	T (+10s)	T	
1	39,84	29,84	[s]
2	38,08	28,08	[s]
3	37,43	27,43	[s]
4	37,33	27,33	[s]
5	37,56	27,56	[s]

Ave. Time	28,048	[s]
Flow	42,784	[l/min]

Outlet meter [l/min]

Min	38	[l/min]
Max	55	[l/min]
Median	46,5	[l/min]

Notes:

*Samples in l/hr, using l/min to work with the spreadsheet

Andres Castro Herrera

Date: 16.03.2019

					l/hr	13,32	26,64	39,96	53,28	66,6	79,92	93,24	106,56			
Measuring point					Flow - flowmeter [l/min]. Sampling every 15 s for **4** min. Total nr. of samples: **17**									Time of measurement		
Nr.	Name	x [m]	y [m]	z [m]	Error	0	0,222	0,444	0,666	0,888	1,11	1,332	1,554	1,776	(Re) Positioning	Time of the day from	to
4	1VB	-0,89	137,13	0													
5	1VM	-0,89	437,13	0			4	3	5	5					22:10	22:42	22:46
6	1VT	-0,89	637,13	0													
10	1HB	0,89	137,13	0													
11	1HM	0,89	437,13	0							4	11	1	1	17:28	17:59	18:03
12	1HT	0,89	637,13	0													
16	2VB	-0,5	137,13	0													
17	2VM	-0,5	437,13	0		9	4	4							21:14	21:45	21:49
18	2VT	-0,5	637,13	0													
22	2HB	0,5	137,13	0													
23	2HM	0,5	437,13	0		3	2	5	5	1	1				18:20	18:51	18:55
24	2HT	0,5	637,13	0													
28	3VB	-0,25	137,13	0													
29	3VM	-0,25	437,13	0		10	5	2							20:28	20:59	21:03
30	3VT	-0,25	637,13	0													
34	3HB	0,25	137,13	0													
35	3HM	0,25	437,13	0		2	7	6	1	1					19:03	19:36	19:40
36	3HT	0,25	637,13	0													

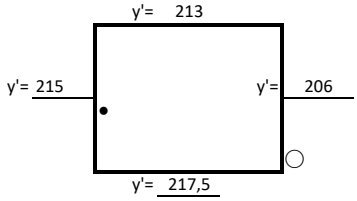

Vann stand

Ave. (y')=	212,875	[mm]
H=	950	[mm]
h=	737,125	[mm]
yB=	137,125	[mm]
yM=	437,125	[mm]
yT=	637,125	[mm]

Valve opening full [turns]

Water flow

Bucket & Stopclock (20 l)

Nr.	T (+10s)	T	
1	40,31	30,31	[s]
2	38,37	28,37	[s]
3	39,19	29,19	[s]
4	38,09	28,09	[s]
5	36,9	26,9	[s]

Ave. Time	28,572	[s]
Flow	41,999	[l/min]

Outlet meter [l/min]

Min	35	[l/min]
Max	56	[l/min]
Median	45,5	[l/min]

Notes:

*Samples in l/hr, using l/min to work with the spreadsheet

Andres Castro Herrera

Date: 18.03.2019

	l/hr	13,32	26,64	39,96	53,28	66,6	79,92	93,24	106,56			
Measuring point					Flow - flowmeter [l/min]. Sampling every 15 s for **4** min. Total nr. of samples: **17**									Time of measurement		
Nr.	Name	x [m]	y [mm]	z [m]	Error	0	0,222	0,444	0,666	0,888	1,11	1,332	1,554	1,776	(Re) Positioning	Time of the day from	to
4	1VB	-0,89	135,5	0		5	7	4	1						19:00	19:31	19:35
5	1VM	-0,89	435,5	0													
6	1VT	-0,89	635,5	0		2	5	9	1						14:11	15:17	15:21
10	1HB	0,89	135,5	0													
11	1HM	0,89	435,5	0													
12	1HT	0,89	635,5	0													
16	2VB	-0,5	135,5	0		2	7	5	3						18:02	18:35	18:39
17	2VM	-0,5	435,5	0													
18	2VT	-0,5	635,5	0		7	5	4		1					15:34	16:05	16:09
22	2HB	0,5	135,5	0													
23	2HM	0,5	435,5	0													
24	2HT	0,5	635,5	0													
28	3VB	-0,25	135,5	0		12	4	1							17:09	17:40	17:44
29	3VM	-0,25	435,5	0													
30	3VT	-0,25	635,5	0		9	5	3							16:16	16:50	16:54
34	3HB	0,25	135,5	0													
35	3HM	0,25	435,5	0													
36	3HT	0,25	635,5	0													

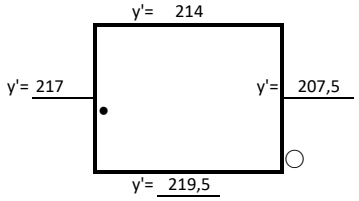

Vann stand

Ave. (y')=	214,5	[mm]
H=	950	[mm]
h=	735,5	[mm]
yB=	135,5	[mm]
yM=	435,5	[mm]
yT=	635,5	[mm]

Valve opening full [turns]

Water flow

Bucket & Stopclock (20 l)

Nr.	T (+10s)	T	
1	38,96	28,96	[s]
2	39,36	29,36	[s]
3	39,29	29,29	[s]
4	38,23	28,23	[s]
5	37,3	27,3	[s]

Ave. Time	28,628	[s]
Flow	41,917	[l/min]

Outlet meter [l/min]

Min	40	[l/min]
Max	53	[l/min]
Median	46,5	[l/min]

Notes:

*Samples in l/hr, using l/min to work with the spreadsheet

Andres Castro Herrera

Arrival at lab: 11:20

Date: 05.04.2019

					l/hr	13,32	26,64	39,96	53,28	66,6	79,92	93,24	106,56			
Measuring point					Flow - flowmeter [l/min]. Sampling every 15 s for **4** min. Total nr. of samples: **17**									Time of measurement		
Nr.	Name	x [m]	y [m]	z [m]	Error	0	0,222	0,444	0,666	0,888	1,11	1,332	1,554	1,776	(Re) Positioning	Time of the day from	to
4	1VB	-0,89	139,5	0													
5	1VM	-0,89	439,5	0													
6	1VT	-0,89	639,5	0													
10	1HB	0,89	139,5	0							4	10	3		17:14	18:19	18:23
11	1HM	0,89	439,5	0													
12	1HT	0,89	639,5	0													
16	2VB	-0,5	139,5	0													
17	2VM	-0,5	439,5	0													
18	2VT	-0,5	639,5	0													
22	2HB	0,5	139,5	0		1	1	8	7						18:53	19:26	19:30
23	2HM	0,5	439,5	0													
24	2HT	0,5	639,5	0													
28	3VB	-0,25	139,5	0													
29	3VM	-0,25	439,5	0													
30	3VT	-0,25	639,5	0													
34	3HB	0,25	139,5	0				11	6						19:45	20:22	20:26
35	3HM	0,25	439,5	0			3	5	8	1					20:41	21:12	21:16
36	3HT	0,25	639,5	0													

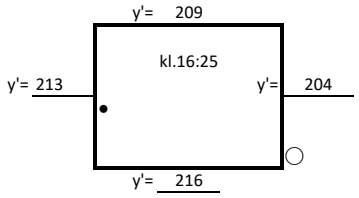

Vann stand

Ave. (y')=	210,5	[mm]
H=	950	[mm]
h=	739,5	[mm]
yB=	139,5	[mm]
yM=	439,5	[mm]
yT=	639,5	[mm]

Valve opening full [turns]

Water flow kl.17:07

Bucket & Stopclock (20 l)

Nr.	T (+10s)	T	
1	39,57	29,57	[s]
2	38,33	28,33	[s]
3	37,56	27,56	[s]
4	37,93	27,93	[s]
5	37,46	27,46	[s]

Ave. Time 28,17 [s]

Flow 42,59850905 [l/min]

Outlet meter [l/min] kl.16:31

Min 38 [l/min]

Max 53 [l/min]

Median 45,5 [l/min]

Notes:

*Samples in l/hr, using l/min to work with the spreadsheet

*Opened valve 14:52 after installing new straight inlet

*15:52 started positioning meter, in-line meter, osv

*Water/tank looks greener, little algae growth after being resting some days

*Decided to make 1 simulation with average of flows.

Arrival at lab: ~12:40

Andres Castro Herrera

Date: 06.04.2019

					l/hr	13,32	26,64	39,96	53,28	66,6	79,92	93,24	106,56	119,88			
Measuring point					Flow - flowmeter [l/min]. Sampling every 15 s for **4** min. Total nr. of samples: **17**											Time of measurement	
Nr.	Name	x [m]	y [m]	z [m]	Error	0	0,222	0,444	0,666	0,888	1,11	1,332	1,554	1,776	1,998	(Re) Positioning	Time of the day from	to
4	1VB	-0,89	137,75	0														
5	1VM	-0,89	437,75	0														
6	1VT	-0,89	637,75	0														
10	1HB	0,89	137,75	0														
11	1HM	0,89	437,75	0									6	10	1	14:43	15:15	15:19
12	1HT	0,89	637,75	0							1	10	6			15:35	16:06	16:10
16	2VB	-0,5	137,75	0														
17	2VM	-0,5	437,75	0														
18	2VT	-0,5	637,75	0					2	13		2				19:13	19:49	19:53
22	2HB	0,5	137,75	0														
23	2HM	0,5	437,75	0						15	2					13:39	14:25	14:29
24	2HT	0,5	637,75	0					3	7	5	2				16:26	16:57	17:01
28	3VB	-0,25	137,75	0														
29	3VM	-0,25	437,75	0														
30	3VT	-0,25	637,75	0				9	7	1						18:12	18:48	18:52
34	3HB	0,25	137,75	0														
35	3HM	0,25	437,75	0														
36	3HT	0,25	637,75	0		2		7	5	3						17:11	17:42	17:46

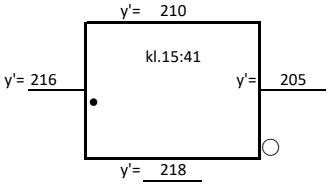

Vann stand

Ave. (y')=	212,25	[mm]
H=	950	[mm]
h=	737,75	[mm]
yB=	137,75	[mm]
yM=	437,75	[mm]
yT=	637,75	[mm]

Valve opening full [turns]

Water flow finished kl.13:23

Bucket & Stopclock (20 l)

Nr.	T (+10s)	T	
1	38,49	28,49	[s]
2	36,9	26,9	[s]
3	37,23	27,23	[s]
4	38,53	28,53	[s]
5	37,46	27,46	[s]

Ave. Time 27,722 [s]

Flow 43,287 [l/min]

Outlet meter [l/min] kl. 12:52-12:53

Min 51 [l/min]

Max 57 [l/min]

Median 54 [l/min]

Notes:

*Samples in l/hr, using l/min to work with the spreadsheet

*Tiny spider in tank's wall :)

Arrival at lab: ~12:30

Andres Castro Herrera

Date: 07.04.2019

	l/hr	13,32	26,64	39,96	53,28	66,6	79,92	93,24	106,56			
Measuring point					Flow - flowmeter [l/min]. Sampling every 15 s for **4** min. Total nr. of samples: **17**								Time of measurement		
Nr.	Name	x [m]	y [m]	z [m]	Error	0	0,222	0,444	0,666	0,888	1,11	1,332	1,554	1,776	(Re) Positioning	Time of the day from	to
4	1VB	-0,89	135,25	0													
5	1VM	-0,89	435,25	0							1	13	3		16:28	16:59	17:03
6	1VT	-0,89	635,25	0							6	8	3		14:29	16:16	16:20
10	1HB	0,89	135,25	0													
11	1HM	0,89	435,25	0													
12	1HT	0,89	635,25	0													
16	2VB	-0,5	135,25	0													
17	2VM	-0,5	435,25	0					5	9	3				17:17	17:48	17:52
18	2VT	-0,5	635,25	0													
22	2HB	0,5	135,25	0													
23	2HM	0,5	435,25	0													
24	2HT	0,5	635,25	0													
28	3VB	-0,25	135,25	0													
29	3VM	-0,25	435,25	0				8	9						18:06	18:37	18:41
30	3VT	-0,25	635,25	0													
34	3HB	0,25	135,25	0													
35	3HM	0,25	435,25	0													
36	3HT	0,25	635,25	0													

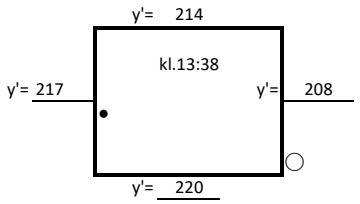

Vann stand

Ave. (y')=	214,75	[mm]
H=	950	[mm]
h=	735,25	[mm]
yB=	135,25	[mm]
yM=	435,25	[mm]
yT=	635,25	[mm]

Valve opening full [turns]

Water flow

Bucket & Stopclock (20 l) finished kl. 14:08

Nr.	T (+10s)	T	
1	39,28	29,28	[s]
2	37,47	27,47	[s]
3	36,26	26,26	[s]
4	38,36	28,36	[s]
5	36,93	26,93	[s]

Ave. Time 27,66 [s]

Flow 43,384 [l/min]

Outlet meter [l/min] kl.13:40-13:41

Min 51 [l/min]

Max 59 [l/min]

Median 55 [l/min]

Notes:

*Samples in l/hr, using l/min to work with the spreadsheet

Arrival at lab: ~15:00

Andres Castro Herrera

Date: 08.04.2019

	l/hr	13,32	26,64	39,96	53,28	66,6	79,92	93,24	106,56			
Measuring point					Flow - flowmeter [l/min]. Sampling every 15 s for **4** min. Total nr. of samples: **17**							Time of measurement		
Nr.	Name	x [m]	y [m]	z [m]	Error	0	0,222	0,444	0,666	0,888	1,11	1,332	1,554	1,776	(Re) Positioning	Time of the day from	to
4	1VB	-0,89	133	0							1	14	2		18:43	19:14	19:18
5	1VM	-0,89	433	0													
6	1VT	-0,89	633	0													
10	1HB	0,89	133	0													
11	1HM	0,89	433	0													
12	1HT	0,89	633	0													
16	2VB	-0,5	133	0		6	3	5	2	1					17:36	18:09	18:13
17	2VM	-0,5	433	0													
18	2VT	-0,5	633	0													
22	2HB	0,5	133	0													
23	2HM	0,5	433	0													
24	2HT	0,5	633	0													
28	3VB	-0,25	133	0		12	4	1							16:38	17:09	17:13
29	3VM	-0,25	433	0													
30	3VT	-0,25	633	0													
34	3HB	0,25	133	0													
35	3HM	0,25	433	0													
36	3HT	0,25	633	0													

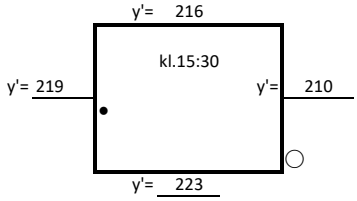

Vann stand

Ave. (y')=	217	[mm]
H=	950	[mm]
h=	733	[mm]
yB=	133	[mm]
yM=	433	[mm]
yT=	633	[mm]

Valve opening full [turns]

Water flow

Bucket & Stopclock (20 l) finished kl. 16:06

Nr.	T (+10s)	T	
1	39,98	29,98	[s]
2	38,6	28,6	[s]
3	37,39	27,39	[s]
4	38,4	28,4	[s]
5	37,36	27,36	[s]

Ave. Time	28,346	[s]
Flow	42,334	[l/min]

Outlet meter [l/min] kl.15:41-15:42

Min	51	[l/min]
Max	59	[l/min]
Median	55	[l/min]

Notes:

*Samples in l/hr, using l/min to work with the spreadsheet

*At 2VB changed from (i think it was) 39,96 to 26,64 (hard to focus immediately), changed back to 39,96, then changed back to 26,64 as in previous similar situations was done (first sure reading recorded)

Appendix 9: Goal tables from simulations

7m CDT.SLDPRT [1,34 mps - correct position of PG - equal refine test as walls [Default]]

Sampling position name	Goal Name	Unit	Value	Averaged Value	Minimum Value	Maximum Value	Progress [%]	Use In Convergence	Delta	Criteria
A1	PG Velocity (X) 7	[cm/s]	25,80806423	25,74579232	25,68092504	25,80806423	100	Yes	0,127139194	0,446680245
	PG Velocity (Z) 7	[cm/s]	0,036215467	0,045690337	0,034823766	0,055060912	100	Yes	0,020237147	0,025307931
A2	PG Velocity (X) 8	[cm/s]	25,74542043	25,68802749	25,62468048	25,74542043	100	Yes	0,120739955	0,450144826
	PG Velocity (Z) 8	[cm/s]	-0,08331078	-0,074890737	-0,083503181	-0,065567052	100	Yes	0,01793613	0,018420821
A3	PG Velocity (X) 9	[cm/s]	25,91532984	25,86250922	25,80081859	25,91532984	100	Yes	0,114511252	0,448275079
	PG Velocity (Z) 9	[cm/s]	-0,08492272	-0,085022664	-0,086633136	-0,083804718	100	Yes	0,002828417	0,023721735
B1	PG Velocity (X) 10	[cm/s]	-26,9960537	-26,9401676	-26,99605372	-26,87669483	100	Yes	0,119358885	0,507067333
	PG Velocity (Z) 10	[cm/s]	-0,74259183	-0,745657752	-0,748924011	-0,742489009	100	Yes	0,001518692	0,080778194
B2	PG Velocity (X) 11	[cm/s]	-26,7941887	-26,73537663	-26,7941887	-26,66662126	100	Yes	0,127567441	0,463160083
	PG Velocity (Z) 11	[cm/s]	-0,25172439	-0,256184931	-0,266094322	-0,249091235	100	Yes	0,007880858	0,041919561
B3	PG Velocity (X) 12	[cm/s]	-26,3231984	-26,25856528	-26,32319842	-26,17989881	100	Yes	0,143299616	0,43544717
	PG Velocity (Z) 12	[cm/s]	0,292750568	0,290786532	0,283705797	0,296192488	100	Yes	0,007424536	0,050369291

Iterations [ ]: 1077
Analysis interval: 88

7m CDT.SLDPRT [1,34 mps - correct position of PG - test of walls [Default]]

Sampling position name	Goal Name	Unit	Value	Averaged Value	Minimum Value	Maximum Value	Progress [%]	Use In Convergence	Delta	Criteria
A1	PG Velocity (X) 7	[cm/s]	25,79605103	25,74043522	25,67637943	25,79605103	100	Yes	0,119671601	0,447864252
	PG Velocity (Z) 7	[cm/s]	0,044899217	0,055124158	0,04427226	0,067784099	100	Yes	0,02351184	0,025309633
A2	PG Velocity (X) 8	[cm/s]	25,73028087	25,67479362	25,61172323	25,73028087	100	Yes	0,118557638	0,451132712
	PG Velocity (Z) 8	[cm/s]	-0,07597298	-0,068938002	-0,076276927	-0,059456375	100	Yes	0,016820552	0,017049238
A3	PG Velocity (X) 9	[cm/s]	25,90629577	25,84922307	25,78562114	25,90629577	100	Yes	0,120674632	0,448716545
	PG Velocity (Z) 9	[cm/s]	-0,08819485	-0,089146324	-0,091697774	-0,088189368	100	Yes	0,002841694	0,023726547
B1	PG Velocity (X) 10	[cm/s]	-27,0029117	-26,95006241	-27,00291168	-26,88438959	100	Yes	0,118522096	0,508040768
	PG Velocity (Z) 10	[cm/s]	-0,75007318	-0,750677718	-0,75331992	-0,74541716	100	Yes	0,00154208	0,081057191
B2	PG Velocity (X) 11	[cm/s]	-26,78885	-26,73059854	-26,78885004	-26,65800305	100	Yes	0,130846992	0,463515674
	PG Velocity (Z) 11	[cm/s]	-0,26756812	-0,272933452	-0,280746631	-0,267199704	100	Yes	0,013546927	0,041919341
B3	PG Velocity (X) 12	[cm/s]	-26,299214	-26,23530653	-26,299214	-26,1562261	100	Yes	0,142987899	0,435447168
	PG Velocity (Z) 12	[cm/s]	0,303668568	0,297351552	0,287322226	0,303957068	100	Yes	0,016634841	0,050369089
A1	PG Turbulence Length 1	[m]	0,010103117	0,009777795	0,009420359	0,010103117	0	No	0,000682758	
	PG Turbulence Intensity 1	[%]	1,665457428	1,635490273	1,602576738	1,665457428	0	No	0,06288069	
A2	PG Turbulence Length 2	[m]	0,009627892	0,009328745	0,008999031	0,009627892	0	No	0,000628861	
	PG Turbulence Intensity 2	[%]	1,587301788	1,560079781	1,529974535	1,587301788	0	No	0,057327253	
A3	PG Turbulence Length 3	[m]	0,008640577	0,008405235	0,008144471	0,008640577	0	No	0,000496106	
	PG Turbulence Intensity 3	[%]	1,487322248	1,464889844	1,439952687	1,487322248	0	No	0,047369561	
B1	PG Turbulence Length 4	[m]	0,008241013	0,008032093	0,007802497	0,008241013	0	No	0,000438516	
	PG Turbulence Intensity 4	[%]	1,59718713	1,575103173	1,551079277	1,59718713	0	No	0,046107852	
B2	PG Turbulence Length 5	[m]	0,008569969	0,00833712	0,008080852	0,008569969	0	No	0,000489117	
	PG Turbulence Intensity 5	[%]	1,576897427	1,554120248	1,529198778	1,576897427	0	No	0,04769865	
B3	PG Turbulence Length 6	[m]	0,00886282	0,00860668	0,00831994	0,00886282	0	No	0,00054288	
	PG Turbulence Intensity 6	[%]	1,581209785	1,55644653	1,528927424	1,581209785	0	No	0,052282361	

Iterations [ ]: 1075
Analysis interval: 88

Octagonal tank Gorle et al.SLDPRT [Gorle et al. replication [Default]]

Position description	Goal Name	Unit	Value	Averaged Value	Minimum Value	Maximum Value	Progress [%]	Use In Convergence	Delta	Criteria
-0,5 x/R Top	PG Velocity 1	[cm/s]	17,50742493	17,36075044	17,00413412	17,63727391	100	Yes	0,211787387	0,468385307
-0,5 x/R Middle	PG Velocity 2	[cm/s]	18,57940621	18,47480917	18,22806797	18,60126806	100	Yes	0,214343872	0,532537974
-0,5 x/R Bottom	PG Velocity 3	[cm/s]	20,22521528	20,05397997	19,93011605	20,22521528	100	Yes	0,052693767	0,439601632
-0,25 x/R Top	PG Velocity 4	[cm/s]	13,38735293	13,50443017	13,38735293	13,59634436	100	Yes	0,090758382	0,313304699
-0,25 x/R Middle	PG Velocity 5	[cm/s]	14,17248922	14,20689186	14,13819021	14,26733404	100	Yes	0,129143834	0,322984692
-0,25 x/R Bottom	PG Velocity 6	[cm/s]	14,32406795	14,24093721	14,1550164	14,33532241	100	Yes	0,176898901	0,298536175
-0,75 x/R Top	PG Velocity 7	[cm/s]	24,10471261	23,66119764	23,29383392	24,10471261	100	Yes	0,221149196	0,696297734
-0,75 x/R Middle	PG Velocity 8	[cm/s]	26,16374956	25,91552839	25,61672543	26,16374956	100	Yes	0,13388975	0,774612304
-0,75 x/R Bottom	PG Velocity 9	[cm/s]	24,11361375	23,88229912	23,52965482	24,20059599	100	Yes	0,164651753	0,646409036
0,25 x/R Top	PG Velocity 10	[cm/s]	12,93186588	12,58945936	12,24469639	12,93186588	100	Yes	0,298747596	0,303735016
0,25 x/R Middle	PG Velocity 11	[cm/s]	13,18233625	12,92548164	12,79522979	13,18233625	100	Yes	0,299353835	0,32486678
0,25 x/R Bottom	PG Velocity 12	[cm/s]	13,77981367	13,65877926	13,50017942	13,77981367	100	Yes	0,138450022	0,313001054
0,5 x/R Top	PG Velocity 13	[cm/s]	18,89344633	18,92410198	18,65851325	19,09132417	100	Yes	0,371269381	0,466675674
0,5 x/R Middle	PG Velocity 14	[cm/s]	19,20551468	19,07626485	18,86175933	19,20551468	100	Yes	0,28940614	0,520829195
0,5 x/R Bottom	PG Velocity 15	[cm/s]	19,82559243	19,73819614	19,64697577	19,82559243	100	Yes	0,049036052	0,449842111
0,75 x/R Top	PG Velocity 16	[cm/s]	23,94643233	23,79858555	23,55763572	24,04092701	100	Yes	0,334233318	0,714232885
0,75 x/R Middle	PG Velocity 17	[cm/s]	26,33477739	26,24396861	25,49260931	26,92417448	100	Yes	0,588656633	0,79065896
0,75 x/R Bottom	PG Velocity 18	[cm/s]	23,76252117	23,74521517	23,56813024	23,99858454	100	Yes	0,17877744	0,627540005

Iterations [ ]: 349
Analysis interval: 63

Octagonal tank Gorle et al.SLDPRT [case 29 - Gorle et al. replication 2 [Default]]

Position description	Goal Name	Unit	Value	Averaged Value	Minimum Value	Maximum Value	Progress [%]	Use In Convergence	Delta	Criteria
-0,5 x/R Top	PG Velocity 1	[cm/s]	17,0043145	17,20410469	16,99277368	17,44171369	100	Yes	0,116012813	0,462065269
-0,5 x/R Middle	PG Velocity 2	[cm/s]	18,32548157	18,15426757	18,00899623	18,32548157	100	Yes	0,248621299	0,529447158
-0,5 x/R Bottom	PG Velocity 3	[cm/s]	20,24341211	19,80200321	19,49204104	20,24341211	100	Yes	0,253413605	0,448405284
-0,25 x/R Top	PG Velocity 4	[cm/s]	13,56660035	13,40497313	13,08696463	13,61268435	100	Yes	0,094977845	0,304353147
-0,25 x/R Middle	PG Velocity 5	[cm/s]	14,08303172	13,85823133	13,72821239	14,08303172	100	Yes	0,154404937	0,326175842
-0,25 x/R Bottom	PG Velocity 6	[cm/s]	13,9107755	13,98825419	13,82831268	14,1372669	100	Yes	0,252364906	0,304751994
-0,75 x/R Top	PG Velocity 7	[cm/s]	23,00454899	23,11531209	22,9435511	23,3868718	100	Yes	0,443320699	0,680687711
-0,75 x/R Middle	PG Velocity 8	[cm/s]	25,80300667	25,44819432	25,23046345	25,80300667	100	Yes	0,572543213	0,773784686
-0,75 x/R Bottom	PG Velocity 9	[cm/s]	23,69728072	23,74100818	23,54327061	23,94329959	100	Yes	0,153088882	0,639115056
0,25 x/R Top	PG Velocity 10	[cm/s]	12,23133649	12,749971	12,23133649	12,99665577	100	Yes	0,225168624	0,312550488
0,25 x/R Middle	PG Velocity 11	[cm/s]	12,71136636	13,05503817	12,71136636	13,30028104	100	Yes	0,166637409	0,32321179
0,25 x/R Bottom	PG Velocity 12	[cm/s]	13,55955926	13,66220479	13,53943	13,79171508	100	Yes	0,065033229	0,306036938
0,5 x/R Top	PG Velocity 13	[cm/s]	18,88878637	18,31849292	17,99828092	18,88878637	100	Yes	0,199586503	0,466960304
0,5 x/R Middle	PG Velocity 14	[cm/s]	18,9799007	18,54724557	18,32131884	18,9799007	100	Yes	0,17796524	0,523022808
0,5 x/R Bottom	PG Velocity 15	[cm/s]	19,50347967	19,46509893	19,17248926	19,74399617	100	Yes	0,361371698	0,449066413
0,75 x/R Top	PG Velocity 16	[cm/s]	23,86805268	23,56875445	23,16075848	23,89625573	100	Yes	0,692928995	0,712698824
0,75 x/R Middle	PG Velocity 17	[cm/s]	25,31209442	25,45816217	24,97222927	25,85475911	100	Yes	0,275973219	0,786007988
0,75 x/R Bottom	PG Velocity 18	[cm/s]	23,37025871	23,62428888	23,29251114	23,91859514	100	Yes	0,416117526	0,627461666

Iterations [ ]: 310
Analysis interval: 63

Octagonal tank Gorle et al.SLDPRT [case 33 - Gorle et al. replication 3 [Default]]

Position description	Goal Name	Unit	Value	Averaged Value	Minimum Value	Maximum Value	Progress [%]	Use In Convergence	Delta	Criteria
-0,5 x/R Top	PG Velocity 1	[cm/s]	18,05536122	17,95176033	17,63249681	18,16057613	100	Yes	0,21121151	0,468124494
-0,5 x/R Middle	PG Velocity 2	[cm/s]	18,92502132	18,78101077	18,55288335	18,92943905	100	Yes	0,265617963	0,52517609
-0,5 x/R Bottom	PG Velocity 3	[cm/s]	20,7786615	20,62027729	20,30731759	21,0490956	100	Yes	0,140839698	0,434768705
-0,25 x/R Top	PG Velocity 4	[cm/s]	14,05694164	14,02706815	13,76236362	14,46290949	100	Yes	0,094801795	0,31913992
-0,25 x/R Middle	PG Velocity 5	[cm/s]	14,68472754	14,66676409	14,58305634	14,7289517	100	Yes	0,145895362	0,320050164
-0,25 x/R Bottom	PG Velocity 6	[cm/s]	14,71021414	14,74074982	14,54662025	14,87904998	100	Yes	0,291530721	0,292533141
-0,75 x/R Top	PG Velocity 7	[cm/s]	23,95366617	23,66247169	23,01269124	24,12585605	100	Yes	0,462573716	0,716776971
-0,75 x/R Middle	PG Velocity 8	[cm/s]	26,11843522	25,77747535	25,57659173	26,11843522	100	Yes	0,54184349	0,770816283
-0,75 x/R Bottom	PG Velocity 9	[cm/s]	24,22149319	24,41809384	24,20807649	24,64701713	100	Yes	0,299136069	0,633798045
0,25 x/R Top	PG Velocity 10	[cm/s]	13,24469424	13,22463237	12,97548414	13,35055752	100	Yes	0,231213774	0,298039989
0,25 x/R Middle	PG Velocity 11	[cm/s]	13,5344279	13,48369248	13,40546198	13,64329176	100	Yes	0,237829784	0,324253192
0,25 x/R Bottom	PG Velocity 12	[cm/s]	14,28005363	14,23579259	14,06359289	14,42775987	100	Yes	0,226179254	0,31564282
0,5 x/R Top	PG Velocity 13	[cm/s]	19,4116489	19,4334505	19,18775007	19,51244825	100	Yes	0,324698181	0,464458789
0,5 x/R Middle	PG Velocity 14	[cm/s]	19,4920974	19,48274696	19,18169196	19,59540265	100	Yes	0,281463286	0,519879705
0,5 x/R Bottom	PG Velocity 15	[cm/s]	20,01602024	20,19613506	20,00011382	20,38347729	100	Yes	0,149345419	0,453471636
0,75 x/R Top	PG Velocity 16	[cm/s]	24,29739846	23,86671447	23,51717731	24,30262902	100	Yes	0,517135694	0,691779887
0,75 x/R Middle	PG Velocity 17	[cm/s]	26,49005816	26,11167757	25,573194	26,74916188	100	Yes	0,500316634	0,780402437
0,75 x/R Bottom	PG Velocity 18	[cm/s]	24,15500304	24,17384436	23,93552379	24,53648751	100	Yes	0,144908129	0,632148573

Iterations [ ]: 389
Analysis interval: 63

Tank_fishlab_assy_Case24.SLDASM [Fish Lab Tank - Case 24 [1HT]]

Goal Name	Unit	Value	Averaged Value	Minimum Value	Maximum Value	Progress [%]	Use In Convergence	Delta	Criteria
PG Velocity 1	[cm/s]	11,20470599	11,57105877	11,18328059	12,04002711	100	Yes	0,338866642	0,34515974
PG Velocity (Z) 1	[cm/s]	11,20000649	11,5657726	11,17820932	12,03514409	100	Yes	0,338090797	0,345075735

Iterations [ ]: 483
Analysis interval: 143

Tank_fishlab_assy_Case24.SLDASM [Fish Lab Tank - Case 25 = 24 laminar & turbulent [1HT]]

Goal Name	Unit	Value	Averaged Value	Minimum Value	Maximum Value	Progress [%]	Use In Convergence	Delta	Criteria
PG Velocity 1	[cm/s]	11,39379886	11,80755216	11,37909093	12,3280846	100	Yes	0,347648915	0,352154653
PG Velocity (Z) 1	[cm/s]	11,38996677	11,80333233	11,37512491	12,32383603	100	Yes	0,34700932	0,352089066

Iterations [ ]: 481
Analysis interval: 143

Tank_fishlab_assy_Case24.SLDASM [Fish Lab Tank - Case 26 = 24 with roughness [1HT]]

Goal Name	Unit	Value	Averaged Value	Minimum Value	Maximum Value	Progress [%]	Use In Convergence	Delta	Criteria
PG Velocity 1	[cm/s]	11,19267686	11,57644825	11,18275438	12,04495583	100	Yes	0,34038503	0,345850734
PG Velocity (Z) 1	[cm/s]	11,18796054	11,57114627	11,17788028	12,04021148	100	Yes	0,339618403	0,345766733

Iterations [ ]: 482
Analysis interval: 143

Tank_fishlab_assy_Case27.SLDASM [Fish Lab Tank - Case 27 [1HT]]

Goal Name	Unit	Value	Averaged Value	Minimum Value	Maximum Value	Progress [%]	Use In Convergence	Delta	Criteria
PG Velocity 1	[cm/s]	10,74578997	10,98281171	10,74578997	11,21366754	100	Yes	0,338615098	0,340700459
PG Velocity (Z) 1	[cm/s]	10,74233801	10,97946328	10,74233801	11,21045481	100	Yes	0,339237192	0,34063252

Iterations [ ]: 474
Analysis interval: 167

Tank_fishlab_assy_Case30_correct_nozzle.SLDASM [Fish Lab Tank - Case 30 - 1HT [1HT]]

Goal Name	Unit	Value	Averaged Value	Minimum Value	Maximum Value	Progress [%]	Use In Convergence	Delta	Criteria
PG Velocity 1HT	[cm/s]	11,8210233	11,82675108	11,65126157	12,04661488	100	Yes	0,395353308	0,397334916
PG Velocity (Z) 1HT	[cm/s]	11,81837755	11,82431132	11,64937232	12,04440796	100	Yes	0,395035648	0,397350455
PG Velocity 1HB	[cm/s]	10,01389535	10,0302032	9,802022325	10,21214652	0	No	0,410124198	
PG Velocity (Z) 1HB	[cm/s]	8,856061757	8,820550602	8,554966619	9,004217533	0	No	0,242730758	
PG Velocity 2HT	[cm/s]	5,33897069	5,306063222	4,569999814	5,833673195	0	No	0,110951606	
PG Velocity (Z) 2HT	[cm/s]	5,010560458	4,904806367	4,189347495	5,281213113	0	No	0,110716603	
PG Velocity 2HB	[cm/s]	6,735718903	6,987809573	6,336638106	7,593913807	0	No	0,130310169	
PG Velocity (Z) 2HB	[cm/s]	6,608109694	6,764671431	6,260794675	7,183618374	0	No	0,172750323	
PG Velocity 3HT	[cm/s]	0,984458462	0,837601629	0,65113124	0,984458462	0	No	0,204346725	
PG Velocity (Z) 3HT	[cm/s]	0,915570891	0,643516319	0,455054852	0,915570891	0	No	0,172482326	
PG Velocity 3HB	[cm/s]	4,101411796	4,42689095	3,942265584	4,844429426	0	No	0,151660891	
PG Velocity (Z) 3HB	[cm/s]	3,804986377	4,023400259	3,639428925	4,325670559	0	No	0,054545631	
PG Velocity Outlet	[cm/s]	22,14392289	21,00537354	18,51034243	22,29271411	0	No	1,772850725	
PG Velocity (X) Outlet	[cm/s]	22,103783	20,96073624	18,4407188	22,25557314	0	No	1,77592696	
PG Turbulence Length 1	[m]	0,004654416	0,004697451	0,004595188	0,004809162	0	No	0,00017581	
PG Turbulence Intensity 1	[%]	16,15587716	15,8525165	15,37434916	16,28220614	0	No	0,907856986	
PG Turbulence Length 2	[m]	0,020660638	0,020876851	0,020231618	0,021723755	0	No	0,001492137	
PG Turbulence Intensity 2	[%]	16,69872408	16,9153972	16,63830257	17,67590038	0	No	0,617538735	
PG Turbulence Length 3	[m]	0,047298712	0,044740949	0,042753136	0,047298712	0	No	0,004545576	
PG Turbulence Intensity 3	[%]	41,8325488	39,74919293	36,78115635	43,156279	0	No	5,744975363	
PG Turbulence Length 4	[m]	0,050950733	0,048608608	0,046206084	0,050950733	0	No	0,000543358	
PG Turbulence Intensity 4	[%]	34,40632885	32,80472314	30,02230871	36,11628628	0	No	4,768273959	
PG Turbulence Length 5	[m]	0,085495961	0,086547892	0,077347336	0,093504435	0	No	0,003699382	
PG Turbulence Intensity 5	[%]	203,8943843	239,4789654	188,8137252	319,2478707	0	No	73,69858623	
PG Turbulence Length 6	[m]	0,065279963	0,062132436	0,05738354	0,066134525	0	No	0,002101443	
PG Turbulence Intensity 6	[%]	43,31242926	39,4542065	35,77028258	43,44472927	0	No	7,67444669	
PG Turbulence Length 7	[m]	0,016474338	0,014011081	0,011043762	0,016474338	0	No	0,001481096	
PG Turbulence Intensity 7	[%]	10,35571127	9,770910664	8,785195573	10,54288618	0	No	1,371729779	
PG Turbulence Length 8	[m]	0,048808674	0,047850302	0,043948335	0,050626051	0	No	0,001705196	
PG Turbulence Intensity 8	[%]	26,0925159	27,50415864	24,41398861	30,0690974	0	No	2,993400489	
PG Turbulence Length 9	[m]	0,083408711	0,082235651	0,073989893	0,086869635	0	No	0,00167278	
PG Turbulence Intensity 9	[%]	55,75840586	61,0541663	49,32474363	70,03733059	0	No	6,794100142	

Iterations [ ]: 567
Analysis interval: 145

Tank_fishlab_assy_Case30_correct_nozzle.SLDASM [Fish Lab Tank - Case 30 [No måler]]

Goal Name	Unit	Value	Averaged Value	Minimum Value	Maximum Value	Progress [%]	Use In Convergence	Delta	Criteria
PG Velocity 1HT	[cm/s]	11,02203359	10,91224687	10,79177212	11,0347692	100	Yes	0,195492987	0,372023253
PG Velocity (Z) 1HT	[cm/s]	10,65042852	10,52109389	10,38383352	10,65689233	100	Yes	0,162830413	0,370923726
PG Velocity 1HB	[cm/s]	10,64895043	10,64987651	10,57986212	10,70308614	100	Yes	0,123224011	0,313260386
PG Velocity (Z) 1HB	[cm/s]	9,456693416	9,432259142	9,394422361	9,456693416	100	Yes	0,062271055	0,301292394
PG Velocity 2HT	[cm/s]	5,782446061	5,814656468	5,671667562	5,897294367	100	Yes	0,225626805	0,309271184
PG Velocity (Z) 2HT	[cm/s]	5,371809823	5,404392659	5,209993813	5,493448872	100	Yes	0,283455059	0,288985312
PG Velocity 2HB	[cm/s]	7,322086076	7,21597511	7,109322824	7,322213246	100	Yes	0,13920666	0,21055203
PG Velocity (Z) 2HB	[cm/s]	7,100863941	7,010934677	6,927417424	7,100863941	100	Yes	0,117793331	0,200002214
PG Velocity 3HT	[cm/s]	1,045158085	1,14006339	1,045158085	1,190062779	100	Yes	0,106081128	0,184553569
PG Velocity (Z) 3HT	[cm/s]	0,952537087	1,057949398	0,952385368	1,12767162	100	Yes	0,109077262	0,179959038
PG Velocity 3HB	[cm/s]	4,399925514	4,28601971	4,186929228	4,40525802	100	Yes	0,096069265	0,165819004
PG Velocity (Z) 3HB	[cm/s]	4,076289346	3,963550249	3,884201109	4,076289346	100	Yes	0,086401944	0,11702428
PG Velocity Outlet	[cm/s]	20,88185962	21,15163992	19,77299489	21,96391427	0	No	0,528710157	
PG Velocity (X) Outlet	[cm/s]	20,86319776	21,13183503	19,7445233	21,94731546	0	No	0,545052873	
PG Turbulence Length 1	[m]	0,035961293	0,036069465	0,035961293	0,03617662	0	No	0,000215327	
PG Turbulence Intensity 1	[%]	22,17483181	22,57164011	22,17483181	22,78711969	0	No	0,198983592	
PG Turbulence Length 2	[m]	0,020078843	0,020295547	0,019923899	0,02079235	0	No	0,00086845	
PG Turbulence Intensity 2	[%]	15,47766337	15,71906064	15,47766337	15,96031278	0	No	0,482649408	
PG Turbulence Length 3	[m]	0,046913038	0,047377799	0,046913038	0,048107623	0	No	0,001194585	
PG Turbulence Intensity 3	[%]	38,91797917	39,09734198	38,56371863	39,51274005	0	No	0,949021416	
PG Turbulence Length 4	[m]	0,052217693	0,052101033	0,050533312	0,053064091	0	No	0,000394647	
PG Turbulence Intensity 4	[%]	30,76062636	31,75626373	30,76062636	32,48778849	0	No	1,129892027	
PG Turbulence Length 5	[m]	0,092063027	0,091128176	0,089611752	0,093797749	0	No	0,001485693	
PG Turbulence Intensity 5	[%]	191,1087708	173,6539994	165,9226461	191,1087708	0	No	20,69269304	
PG Turbulence Length 6	[m]	0,069482414	0,069173957	0,068809616	0,069510359	0	No	0,000700743	
PG Turbulence Intensity 6	[%]	40,06049293	41,61832986	40,05993566	42,78253978	0	No	0,653701466	
PG Turbulence Length 7	[m]	0,01816157	0,018239885	0,017934126	0,018879963	0	No	0,000336495	
PG Turbulence Intensity 7	[%]	10,37976094	10,68657405	10,37976094	10,81233998	0	No	0,192930563	
PG Turbulence Length 8	[m]	0,052361182	0,052020736	0,051020093	0,053758621	0	No	0,000530917	
PG Turbulence Intensity 8	[%]	28,18249066	28,2434626	27,8947593	28,88787359	0	No	0,363181301	
PG Turbulence Length 9	[m]	0,089752315	0,088936522	0,087964227	0,090595423	0	No	0,001521804	
PG Turbulence Intensity 9	[%]	61,89880696	60,73315225	58,93022436	63,78788303	0	No	1,539267172	

Iterations [ ]: 800
Analysis interval: 144

Tank_fishlab_assy_Cases_Comb30-32.SLDASM [Fish Lab Tank - Cases_Comb 30-32 [No måler]]

Goal Name	Unit	Value	Averaged Value	Minimum Value	Maximum Value	Progress [%]	Use In Convergence	Delta	Criteria
PG Velocity - 1HB	[cm/s]	10,46105397	10,4646044	10,33742165	10,5542443	100	Yes	0,082664366	0,313686884
PG Velocity (Z) - 1HB	[cm/s]	9,130769532	9,118108202	9,003181697	9,205777028	0	No	0,088138071	
PG Velocity -1HM	[cm/s]	14,94785506	14,96585071	14,78986883	15,05526834	100	Yes	0,171819518	0,458679794
PG Velocity (Z) - 1HM	[cm/s]	14,39864229	14,41704483	14,24557297	14,50861235	0	No	0,171243324	
PG Velocity - 1HT	[cm/s]	11,04571516	11,0061934	10,87366636	11,16223442	100	Yes	0,052954724	0,340361968
PG Velocity (Z) - 1HT	[cm/s]	10,78276533	10,75841041	10,62309281	10,91347598	0	No	0,041568569	
PG Velocity - 2HB	[cm/s]	7,44576152	7,36855562	7,212416155	7,533024098	100	Yes	0,088450664	0,20119017
PG Velocity (Z) - 2HB	[cm/s]	7,107054108	7,047512212	6,957580118	7,134921237	0	No	0,072025903	
PG Velocity - 2HM	[cm/s]	8,121144029	8,234132878	7,957787515	8,43904612	100	Yes	0,063983206	0,260100018
PG Velocity (Z) - 2HM	[cm/s]	7,867656884	7,940310337	7,754308712	8,077607515	0	No	0,043226639	
PG Velocity - 2HT	[cm/s]	5,465645696	5,575946483	5,310034209	5,850142797	100	Yes	0,196562199	0,289031555
PG Velocity (Z) - 2HT	[cm/s]	5,182867209	5,31867453	5,079762071	5,534473573	0	No	0,219768248	
PG Velocity - 3HB	[cm/s]	4,631550989	4,59462332	4,466473859	4,737513273	100	Yes	0,061882259	0,180350792
PG Velocity (Z) - 3HB	[cm/s]	4,193117088	4,167012151	4,063624628	4,281503722	0	No	0,051210506	
PG Velocity - 3HM	[cm/s]	2,615845074	2,704715398	2,534748609	2,855861056	100	Yes	0,128851038	0,221432193
PG Velocity (Z) - 3HM	[cm/s]	2,59697336	2,671495365	2,515675419	2,800445733	0	No	0,121984849	
PG Velocity - 3HT	[cm/s]	0,770289729	0,721496482	0,63432233	0,863120526	100	Yes	0,090701528	0,191545372
PG Velocity (Z) - 3HT	[cm/s]	0,491110975	0,460159917	0,423804729	0,491110975	0	No	0,067306246	
PG Velocity - 1VB	[cm/s]	13,05496346	13,05470925	12,68560565	13,53097945	100	Yes	0,437746679	0,438461001
PG Velocity (Z) - 1VB	[cm/s]	-12,9854956	-12,99446207	-13,47156262	-12,62458132	0	No	0,437893817	
PG Velocity - 1VM	[cm/s]	12,0798842	11,80344761	11,39396068	12,1928269	100	Yes	0,055564649	0,482684179
PG Velocity (Z) - 1VM	[cm/s]	-11,7755227	-11,47350513	-11,91053588	-11,08117212	0	No	0,077950904	
PG Velocity - 1VT	[cm/s]	8,657819321	8,706760803	8,551258928	8,854192532	100	Yes	0,079113099	0,232939423
PG Velocity (Z) - 1VT	[cm/s]	-8,38686156	-8,420030424	-8,56830059	-8,279951996	0	No	0,056131563	
PG Velocity - 2VB	[cm/s]	7,404088882	7,541123343	7,40007182	7,67751019	100	Yes	0,030576352	0,2682387
PG Velocity (Z) - 2VB	[cm/s]	-6,98352802	-7,072002801	-7,159362235	-6,981912848	0	No	0,032065004	
PG Velocity - 2VM	[cm/s]	6,127211636	6,192918287	6,067035734	6,327420535	100	Yes	0,021724925	0,172105642
PG Velocity (Z) - 2VM	[cm/s]	-5,99846832	-6,053355066	-6,1905166	-5,93001092	0	No	0,037148252	
PG Velocity - 2VT	[cm/s]	5,375976114	5,46000317	5,294799439	5,656357874	100	Yes	0,102491004	0,175411926
PG Velocity (Z) - 2VT	[cm/s]	-5,19922854	-5,279444349	-5,465204882	-5,13037859	0	No	0,102176345	
PG Velocity - 3VB	[cm/s]	3,920338687	3,686003654	2,999302037	4,341668653	100	Yes	0,133553831	0,194345657
PG Velocity (Z) - 3VB	[cm/s]	-2,66702468	-2,443506782	-3,010496052	-1,852536995	0	No	0,169057853	
PG Velocity - 3VM	[cm/s]	3,853919482	3,888784972	3,824824843	3,944830184	100	Yes	0,015660585	0,193835559
PG Velocity (Z) - 3VM	[cm/s]	-3,71915383	-3,765433818	-3,840954102	-3,682428283	0	No	0,011146659	
PG Velocity - 3VT	[cm/s]	3,617388089	3,733174678	3,569343474	3,923543116	100	Yes	0,03380239	0,163877563
PG Velocity (Z) - 3VT	[cm/s]	-3,59755988	-3,710115895	-3,895337409	-3,547850448	0	No	0,03494903	
PG Velocity - Outlet pipe	[cm/s]	21,42738961	21,52865101	21,32977424	21,64422807	0	No	0,314453831	
PG Velocity (X) - Outlet pipe	[cm/s]	21,40193669	21,5035304	21,29971128	21,62785319	0	No	0,328141912	
PG Velocity - 0VT	[cm/s]	8,105673575	8,450896465	7,890582469	8,863599084	0	No	0,43890244	

PG Velocity - 0VM	[cm/s]	6,636567435	6,714027795	6,623015525	6,782949813	0	No	0,138524277	
PG Velocity - 0VB	[cm/s]	4,442481021	4,636343705	4,422832053	4,806620058	0	No	0,318860785	
PG Velocity - 1V0	[cm/s]	6,660947473	6,792290312	6,649618889	6,965253746	0	No	0,095296648	
PG Velocity - 2V0	[cm/s]	8,257121818	8,300324202	8,233561162	8,375597707	0	No	0,142036544	
PG Velocity - 3V0	[cm/s]	6,230656331	5,866271759	5,597216576	6,259593049	0	No	0,242381212	
PG Velocity - 3H0	[cm/s]	1,937067082	1,985413612	1,817854797	2,100266956	0	No	0,100067292	
PG Velocity - 2H0	[cm/s]	3,004562085	2,604667739	2,29510241	3,004562085	0	No	0,055111637	
PG Velocity - 1H0	[cm/s]	8,926401782	9,156597583	8,886277435	9,487662354	0	No	0,315190971	
PG Velocity - 0HB	[cm/s]	12,03193852	12,21575595	12,00365312	12,37610184	0	No	0,06869895	
PG Velocity - 0HM	[cm/s]	8,997775694	8,971326028	8,6998728	9,144418279	0	No	0,210216286	
PG Velocity - 0HT	[cm/s]	13,6079245	13,6116599	13,55123611	13,65680166	0	No	0,105565556	
PG Turbulence Length - 1HB	[m]	0,020280047	0,020280022	0,020045771	0,020506362	0	No	0,000334181	
PG Turbulence Intensity - 1HB	[%]	16,8111426	16,90430114	16,65959751	17,00121174	0	No	0,282267787	
PG Turbulence Length - 1HM	[m]	0,013189731	0,012470593	0,011192478	0,013189731	0	No	0,00100617	
PG Turbulence Intensity - 1HM	[%]	9,555405279	9,437328562	8,743288056	9,648124825	0	No	0,404526876	
PG Turbulence Length - 1HT	[m]	0,036394745	0,036285328	0,036192685	0,036394745	0	No	7,55883E-05	
PG Turbulence Intensity - 1HT	[%]	20,9462406	20,92962408	20,46903437	21,22983624	0	No	0,281572623	
PG Turbulence Length - 2HB	[m]	0,051731745	0,051952883	0,051439275	0,05259953	0	No	0,000843273	
PG Turbulence Intensity - 2HB	[%]	29,7355572	30,22158778	29,0443637	31,25624848	0	No	0,29389195	
PG Turbulence Length - 2HM	[m]	0,052880687	0,052078228	0,051709454	0,052880687	0	No	0,000339644	
PG Turbulence Intensity - 2HM	[%]	29,47272482	29,25868963	28,78048115	29,73421941	0	No	0,334050456	
PG Turbulence Length - 2HT	[m]	0,04997435	0,049662009	0,048005342	0,050881417	0	No	0,000345661	
PG Turbulence Intensity - 2HT	[%]	38,59277869	38,38063063	36,40999322	40,01478092	0	No	1,253049099	
PG Turbulence Length - 3HB	[m]	0,066938755	0,066700584	0,066237107	0,067749362	0	No	0,000864368	
PG Turbulence Intensity - 3HB	[%]	36,41983378	36,71351218	35,05787584	38,05034393	0	No	0,527274748	
PG Turbulence Length - 3HM	[m]	0,090120315	0,088958045	0,087621522	0,09175799	0	No	0,001038717	
PG Turbulence Intensity - 3HM	[%]	71,26555338	69,24061507	66,47060046	71,92758229	0	No	2,892319958	
PG Turbulence Length - 3HT	[m]	0,096374953	0,094767022	0,092668239	0,097535301	0	No	0,000806621	
PG Turbulence Intensity - 3HT	[%]	245,1519979	273,0531564	205,5098424	323,9901431	0	No	27,68476171	
PG Turbulence Length - 1VB	[m]	0,004191341	0,004274429	0,004183097	0,004330757	0	No	4,41576E-05	
PG Turbulence Intensity - 1VB	[%]	13,17522634	13,26887441	12,99290742	13,52029667	0	No	0,390236584	
PG Turbulence Length - 1VM	[m]	0,005936446	0,005975218	0,005804193	0,006120704	0	No	6,63138E-05	
PG Turbulence Intensity - 1VM	[%]	19,77498913	20,31914854	18,32595884	22,03596573	0	No	1,500465971	
PG Turbulence Length - 1VT	[m]	0,010859667	0,010771687	0,010703839	0,010859667	0	No	4,18649E-05	
PG Turbulence Intensity - 1VT	[%]	17,74251974	17,65979257	17,51740468	17,88248403	0	No	0,078608115	
PG Turbulence Length - 2VB	[m]	0,045256646	0,043430286	0,041114474	0,045482674	0	No	0,000544997	
PG Turbulence Intensity - 2VB	[%]	26,65927493	25,77632792	24,77689478	26,70239011	0	No	0,227453768	
PG Turbulence Length - 2VM	[m]	0,082133828	0,080786518	0,079131916	0,082133828	0	No	0,001342374	
PG Turbulence Intensity - 2VM	[%]	32,77736483	32,18149658	31,57244286	32,89614941	0	No	0,230015719	
PG Turbulence Length - 2VT	[m]	0,088286773	0,087838229	0,085912943	0,089705806	0	No	0,001269192	
PG Turbulence Intensity - 2VT	[%]	37,58332169	36,73827387	35,33143667	37,94597881	0	No	0,75256759	
PG Turbulence Length - 3VB	[m]	0,032728939	0,032739395	0,03214728	0,033807583	0	No	0,001422203	
PG Turbulence Intensity - 3VB	[%]	40,02365426	40,9058292	36,64418549	45,96761199	0	No	1,354413508	

PG Turbulence Length - 3VM	[m]	0,083709939	0,083034555	0,08132966	0,084626569	0	No	0,002303859	
PG Turbulence Intensity - 3VM	[%]	46,80865426	45,5336421	44,470538	46,90074625	0	No	0,497978863	
PG Turbulence Length - 3VT	[m]	0,092701977	0,092080565	0,089532225	0,094830842	0	No	0,002088252	
PG Turbulence Intensity - 3VT	[%]	52,48067225	50,09690229	47,12163313	52,86572759	0	No	0,416846338	

Iterations [ ]: 1268
Analysis interval: 144

Tank_fishlab_assy_Cases_Comb34-37-Correct_Inlet.SLDASM [Fish Lab Tank - Cases_Comb 34-37 [No måler]]

Goal Name	Unit	Value	Averaged Value	Minimum Value	Maximum Value	Progress [%]	Use In Convergence	Delta	Criteria
PG Velocity - 1HB	[cm/s]	10,46394403	10,61324549	10,45955759	10,7918819	100	Yes	0,174400263	0,343062322
PG Velocity (Z) - 1HB	[cm/s]	9,737635282	9,872985982	9,728911038	10,04432767	0	No	0,179147336	
PG Velocity -1HM	[cm/s]	18,33234277	18,24395152	18,12549329	18,35262581	100	Yes	0,064598059	0,545404439
PG Velocity (Z) - 1HM	[cm/s]	17,90425547	17,82310921	17,69258226	17,94635211	0	No	0,077859765	
PG Velocity - 1HT	[cm/s]	13,21178502	13,12103219	13,05714872	13,21178502	100	Yes	0,154636299	0,371606123
PG Velocity (Z) - 1HT	[cm/s]	13,05338523	12,95120175	12,87560544	13,05338523	0	No	0,177779794	
PG Velocity - 2HB	[cm/s]	6,604944065	6,633379453	6,599954189	6,669215712	100	Yes	0,069261523	0,193612924
PG Velocity (Z) - 2HB	[cm/s]	6,477955005	6,505964565	6,4733809	6,539191079	0	No	0,065810179	
PG Velocity - 2HM	[cm/s]	6,863287994	6,888093557	6,863287994	6,9511511	100	Yes	0,07036672	0,226946588
PG Velocity (Z) - 2HM	[cm/s]	6,81713016	6,840660407	6,81713016	6,89767091	0	No	0,063007809	
PG Velocity - 2HT	[cm/s]	5,161352303	5,190402332	5,161352303	5,225181402	100	Yes	0,063829099	0,220867096
PG Velocity (Z) - 2HT	[cm/s]	5,096294247	5,120991054	5,087262412	5,158522416	0	No	0,061167475	
PG Velocity - 3HB	[cm/s]	3,925548996	3,931202217	3,905983778	3,9479862	100	Yes	0,042002422	0,131373531
PG Velocity (Z) - 3HB	[cm/s]	3,646126038	3,664136314	3,637511506	3,689284604	0	No	0,026079906	
PG Velocity - 3HM	[cm/s]	2,228041834	2,285662453	2,228041834	2,375802962	100	Yes	0,147761127	0,157208095
PG Velocity (Z) - 3HM	[cm/s]	2,215251119	2,272091059	2,215251119	2,358186654	0	No	0,142935535	
PG Velocity - 3HT	[cm/s]	1,312652701	1,37009922	1,312652701	1,429721166	100	Yes	0,117068465	0,128602528
PG Velocity (Z) - 3HT	[cm/s]	1,220764101	1,288080877	1,220764101	1,364489042	0	No	0,143724941	
PG Velocity - 1VB	[cm/s]	10,78459595	10,67526359	10,59110607	10,78563199	100	Yes	0,194525927	0,434625975
PG Velocity (Z) - 1VB	[cm/s]	-10,4518256	-10,30915933	-10,45182563	-10,2097651	0	No	0,24206053	
PG Velocity - 1VM	[cm/s]	11,5825584	11,5228462	11,37876725	11,65150499	100	Yes	0,272737738	0,334147843
PG Velocity (Z) - 1VM	[cm/s]	-10,8236736	-10,77180785	-10,9146914	-10,61569581	0	No	0,272123996	
PG Velocity - 1VT	[cm/s]	11,05116373	11,05164608	10,96547533	11,10690924	100	Yes	0,14143391	0,272460804
PG Velocity (Z) - 1VT	[cm/s]	-10,5337585	-10,52758979	-10,58001715	-10,44202497	0	No	0,137992185	
PG Velocity - 2VB	[cm/s]	7,995776662	7,957000049	7,903015784	8,013403997	100	Yes	0,110388213	0,221405599
PG Velocity (Z) - 2VB	[cm/s]	-7,65873486	-7,64358222	-7,687126948	-7,604055321	0	No	0,083071627	
PG Velocity - 2VM	[cm/s]	7,151370207	7,191928776	7,151370207	7,225675047	100	Yes	0,061905249	0,188412805
PG Velocity (Z) - 2VM	[cm/s]	-6,93750508	-6,994036453	-7,032731207	-6,937505081	0	No	0,085267604	
PG Velocity - 2VT	[cm/s]	5,206470919	5,31117698	5,206470919	5,35678383	100	Yes	0,150312912	0,249180076
PG Velocity (Z) - 2VT	[cm/s]	-4,99093515	-5,078276325	-5,117652266	-4,990935153	0	No	0,126717113	
PG Velocity - 3VB	[cm/s]	3,520048852	3,505941821	3,40072521	3,680867914	100	Yes	0,190293319	0,190564447
PG Velocity (Z) - 3VB	[cm/s]	-3,07363128	-3,129246622	-3,310908561	-3,041225987	0	No	0,269682574	
PG Velocity - 3VM	[cm/s]	4,322261341	4,34606774	4,319497171	4,367949729	100	Yes	0,048452559	0,142734868
PG Velocity (Z) - 3VM	[cm/s]	-4,23260234	-4,261134873	-4,27778369	-4,232561425	0	No	0,045222265	
PG Velocity - 3VT	[cm/s]	3,38844257	3,389601531	3,35484045	3,400106812	100	Yes	0,023118934	0,155309229
PG Velocity (Z) - 3VT	[cm/s]	-3,36700824	-3,368109964	-3,378717704	-3,331911482	0	No	0,015956495	
PG Velocity - Outlet pipe	[cm/s]	17,52425704	18,21929088	17,52425704	18,54113378	0	No	0,852356795	
PG Velocity (X) - Outlet pipe	[cm/s]	17,27629477	17,98962531	17,27629477	18,30607125	0	No	0,823068256	
PG Velocity - 0VT	[cm/s]	8,593793319	8,59118541	8,35963586	8,916054466	0	No	0,556418606	
PG Velocity - 0VM	[cm/s]	9,577574218	9,187453518	8,965531343	9,577574218	0	No	0,27367548	
PG Velocity - 0VB	[cm/s]	77,47960669	77,93324615	77,07189582	79,58880976	0	No	2,257378988	
PG Velocity - 1V0	[cm/s]	2,169169191	2,362698731	2,127034454	2,585895068	0	No	0,113476285	
PG Velocity - 2V0	[cm/s]	7,565781568	7,464440195	7,368680204	7,62798798	0	No	0,052343878	
PG Velocity - 3V0	[cm/s]	5,212026708	5,273639396	5,096370714	5,455141288	0	No	0,210520185	

PG Velocity - 3H0	[cm/s]	2,590959361	2,966931236	2,580198312	3,269864919	0	No	0,217865847	
PG Velocity - 2H0	[cm/s]	3,110800851	3,09458949	2,99258949	3,268950617	0	No	0,06654619	
PG Velocity - 1H0	[cm/s]	14,60266389	14,19030245	13,58302208	14,88305567	0	No	0,243551296	
PG Velocity - 0HB	[cm/s]	14,85672889	14,83622582	14,69064613	14,98499542	0	No	0,220762316	
PG Velocity - 0HM	[cm/s]	11,14353686	10,98108228	10,82185508	11,23058443	0	No	0,097198766	
PG Velocity - 0HT	[cm/s]	15,88556145	15,89968684	15,85024238	15,94231163	0	No	0,09206925	
PG Turbulence Length - 1HB	[m]	0,020956177	0,020498998	0,019659823	0,020956177	0	No	0,000689	
PG Turbulence Intensity - 1HB	[%]	17,41204208	16,89929562	16,05477267	17,41204208	0	No	0,893603931	
PG Turbulence Length - 1HM	[m]	0,006950969	0,007490695	0,006950969	0,007790253	0	No	0,000341642	
PG Turbulence Intensity - 1HM	[%]	5,044894256	5,279365146	5,044894256	5,390088736	0	No	0,092979462	
PG Turbulence Length - 1HT	[m]	0,033909938	0,034154596	0,033909938	0,034291205	0	No	0,000381267	
PG Turbulence Intensity - 1HT	[%]	17,06491703	17,2505202	17,06491703	17,46366107	0	No	0,398744032	
PG Turbulence Length - 2HB	[m]	0,066531064	0,066403731	0,066117065	0,066563656	0	No	0,000446591	
PG Turbulence Intensity - 2HB	[%]	30,49780711	30,26290535	30,06278889	30,51524039	0	No	0,452451506	
PG Turbulence Length - 2HM	[m]	0,087790178	0,087243898	0,085786319	0,087967466	0	No	0,002181147	
PG Turbulence Intensity - 2HM	[%]	33,43375853	33,12535563	32,59905619	33,43375853	0	No	0,834702334	
PG Turbulence Length - 2HT	[m]	0,099500202	0,098090853	0,0956982	0,099500202	0	No	0,003802002	
PG Turbulence Intensity - 2HT	[%]	38,59463234	38,0894857	37,63891292	38,59463234	0	No	0,955719429	
PG Turbulence Length - 3HB	[m]	0,075424236	0,075407402	0,075241192	0,075472281	0	No	0,00023109	
PG Turbulence Intensity - 3HB	[%]	38,12781094	37,90600984	37,71385798	38,14812041	0	No	0,434262422	
PG Turbulence Length - 3HM	[m]	0,125818826	0,124396012	0,122110098	0,125818826	0	No	0,003708728	
PG Turbulence Intensity - 3HM	[%]	82,70022707	79,90479001	75,98934751	82,70022707	0	No	6,710879556	
PG Turbulence Length - 3HT	[m]	0,134909469	0,132787446	0,130222059	0,134909469	0	No	0,00468741	
PG Turbulence Intensity - 3HT	[%]	139,2763271	131,9523096	124,1161152	139,2763271	0	No	15,16021192	
PG Turbulence Length - 1VB	[m]	0,010570353	0,01063165	0,010570353	0,010651403	0	No	7,9094E-05	
PG Turbulence Intensity - 1VB	[%]	18,25020991	18,61726842	18,25020991	18,79583959	0	No	0,54562968	
PG Turbulence Length - 1VM	[m]	0,016151489	0,016076764	0,015998888	0,016156092	0	No	0,000157204	
PG Turbulence Intensity - 1VM	[%]	21,09919161	21,13354446	20,94541913	21,36005615	0	No	0,275188272	
PG Turbulence Length - 1VT	[m]	0,028882368	0,029049622	0,028853849	0,029244084	0	No	0,000390235	
PG Turbulence Intensity - 1VT	[%]	21,80870103	21,77567083	21,69642382	21,90523505	0	No	0,208811232	
PG Turbulence Length - 2VB	[m]	0,044320409	0,044844626	0,044240129	0,045734796	0	No	0,001494666	
PG Turbulence Intensity - 2VB	[%]	26,93009085	27,16263432	26,82972586	27,47302953	0	No	0,643303665	
PG Turbulence Length - 2VM	[m]	0,084314351	0,084323449	0,08408602	0,084504141	0	No	0,000418121	
PG Turbulence Intensity - 2VM	[%]	32,86172458	32,89231393	32,85581462	32,96735787	0	No	0,111543256	
PG Turbulence Length - 2VT	[m]	0,090765903	0,089715859	0,0884142	0,09086108	0	No	0,002446879	
PG Turbulence Intensity - 2VT	[%]	44,76968415	43,97239026	43,65471282	44,76968415	0	No	1,114971334	
PG Turbulence Length - 3VB	[m]	0,040542453	0,042490202	0,040542453	0,043465443	0	No	0,002922989	
PG Turbulence Intensity - 3VB	[%]	40,92960241	41,12568558	39,29892173	42,16612509	0	No	1,98059119	
PG Turbulence Length - 3VM	[m]	0,092850147	0,093170663	0,092505964	0,093791141	0	No	0,001285177	
PG Turbulence Intensity - 3VM	[%]	44,91396829	44,98292544	44,78726202	45,17947742	0	No	0,392215406	
PG Turbulence Length - 3VT	[m]	0,105412062	0,104303922	0,10302229	0,105772812	0	No	0,002750523	
PG Turbulence Intensity - 3VT	[%]	59,18984031	59,05218534	58,7422455	59,2646581	0	No	0,522412602	

Iterations [ ]: 826
Analysis interval: 145

TAKK!

THANK YOU!

¡GRACIAS!

=)

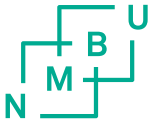

Norges miljø- og biovitenskapelige universitet
Noregs miljø- og biovitskapelege universitet
Norwegian University of Life Sciences

Postboks 5003
NO-1432 Ås
Norway